Table of Contents

List of abbreviations

AA	Acrylic Acid
ACN	Acetonitrile
AIBN	Azobisisobutyronitrile
AMN	Artificial Metallonuclease
BAC	N,N'-Bis(acryloyl)cystamine
CD	Circular Dichroism
CLSM	Confocal Laser Scanning Microscopy
Cu-TPMA-Phen	[Cu(TPMA)(Phenanthroline)](ClO4)2
DDS	Drug Delivery System
DLS	Dynamic Light Scattering
DMAEMA	N,N-dimethylaminoethyl methacrylate
DNR	Daunorubicin
DPP	Distillation-precipitation polymerization
DVB	Divinylbenzene
EE%	Encapsulation Efficiency %
EPR	Electron Paramagnetic Resonance
EPR effect	Enhanced Penetration and Retention effect
EtOH	Ethanol
FT-IR	Fourier Transform Infrared Spectroscopy
GSH	Glutathione
KPS	Potassium Peroxide
LC%	Loading Capacity %
LCST	Lower Critical Solution Temperature
MAA	Methacrylic acid
MBA	N,N'-Methylenebisacrylamide
MMA	Methyl Methacrylate
MTT	3-(4,5-dimethylthiazol-2-yl)-2,5-diphenyltetrazolium bromide
NCs	Nanocontainers
NPs	Nanoparticles
ON	Oligonucleotide

PBS	Phosphate saline buffer, pH 7.4
PEGMA	Poly(ethylene glycol) methyl ether methacrylate (Mn 475)
PLGA	poly (D, L-lactide-co-glycolide)
ROS	Reactive Oxygen Species
SEM	Scanning Electron Microscope
SPION	Superparamagnetic Iron Nanoparticle
SST	Somatostatin
UCST	Upper Critical Solution Temperature
UV	Ultraviolet–visible spectroscopy

Introduction

1.1 ClickGene

ClickGene is a Horizon 2020 Innovative Training Network (ITN) funded by the European Union and focused on gene therapy and click chemistry. The main research goal of the project is to develop new materials and methodologies for site-selective genetic engineering and create a strong multi-disciplinary network between academic and industrial partners in the areas of chemical synthesis, nanotechnology and molecular cell biology.

Gene therapy is expected to play a key role in next-generation medicine by correcting the underlying genetic causes of disease, thereby facilitating a personalized approach to medicine. As this technology can address a wide range of medical conditions, above all cancer, the field is growing fast and drawing more and more attention. Current gene therapy methods possess undesirable side effects, including insertional mutagenesis, toxicity, low efficiency and off target cutting. Questions also remain regarding the optimal methods for delivering these drugs to target cells. The ClickGene network was ideated to overcome these limitations through an original and innovative multi-disciplinary approach.

The core of the project is the development of a new library of artificial metallonucleases (AMNs). These AMNs are original Cu(II)-based complexes capable of inducing oxidative DNA strand breaks through reactive oxygen species (ROS) generated catalytically. After the synthesis, AMNs are to be conjugated via click chemistry with specifically-designed sequence-selective nucleic acid targeting molecules such as zinc finger proteins and triplex forming oligonucleotides. This modification will provide the AMNs with the capability of selecting a specific sequence to cut and therefore allowing highly selective therapy.

Appropriate drug delivery systems (DDSs) will be designed and synthesized to carry AMNs to their intended target, the nucleus of human cells. The properties of these DDSs will be optimized in terms of composition in order to protect the drug and to favor the selective release in the target area, facilitating the activity and cell-selective uptake. The selected delivery system were liposomes and polymeric hollow nanocontainers, two of the most promising options in the field. The composition of fatty acids for the liposomes and the choice of monomers for the polymeric nanocarriers will be crucial to create efficient DDS and give the best interaction possible with the target cells. The resulting selective targeting will allow to deliver the therapy to specific cell types, reducing the toxicity linked with the non-targeted activity of drugs.

Another important element of the network is the detection of biomarkers of disease for diagnostic applications. The production of a new family of reagents that can monitor the presence of epigenetic base modification in a given DNA sequence is one of the target of the project, along with the development of arrays for rapid detection of epigenetic bases at certain loci.

The Ph.D. candidate was involved in the formulation and the synthesis of new polymeric nanocontainers for the selective release of the innovative AMNs in tumoral environment.

1.2 Cancer

Despite many advancements in diagnostic and treatment, cancer is still one of the leading cause of death worldwide. Cancer incidence and mortality are actually growing, the reasons are complex but reflect both aging and growth of the population, as well as changes in the prevalence and distribution of the main risk factors, which are mostly associated with socioeconomic development. Also, the rising prominence of cancer as a leading cause of death partly reflects marked declines in mortality rates of stroke and coronary heart disease, relative to cancer, in many countries. GLOBOCAN 2018 estimates of cancer incidence and mortality produced by the International Agency for Research on Cancer show that at the end of 2018 there will be 18.1 million new cases and 9.6 million cancer deaths worldwide. Nearly one-half of the cases and over one-half of the cancer deaths in the world will occur in Asia, in part because close to 60% of the global population resides there. Europe accounts for 23.4% of the total cancer cases and 20.3% of the cancer deaths, although it represents only 10% of the global population, followed by the Americas' 21% of incidence and 14.4% of mortality worldwide (13% of the population). In both sexes combined, lung cancer is the most commonly diagnosed cancer (11.6% of the total cases) and the leading cause of cancer death (18.4% of the total cancer deaths), closely followed by female breast cancer (11.6%), prostate cancer (7.1%), and colorectal cancer (6.1%) for incidence and colorectal cancer (9.2%), stomach cancer (8.2%), and liver cancer (8.2%) for mortality.[1]

Treating cancer is always complicated and depends on tumor type and development stage. In general, there are three main approaches: surgical excision, irradiation therapy and chemotherapy. In case of localized and metastasized cancer, the approach generally relies on chemotherapy, which is used alone or in combination with other form of therapy. Despite many advancements, conventional chemotherapeutic agents present some crucial limitations. For a start, most anti-cancer drugs have a limited water solubility, they are hydrophobic and require organic solvents in the formulation, which greatly contribute to their toxicity.[2] Another important factor is multidrug resistance or MDR, which is a cancer cell mechanism that transport various drugs out of cells due to increased synthesis of efflux

pumps, such as P-glycoprotein, in the cell membrane.[3] Conventional chemotherapeutic agents also lack in specificity and selectivity, causing severe adverse non-specific effects on healthy cells and rapidly proliferating normal cells, which translates into significant morbidity and mortality.[4] It appears evident that a new approach, based on more specific and targeted delivery of drugs is necessary to effectively tackle the burden of cancer. In all cases, the effectiveness of the treatment is directly related to the ability to target and kill the cancer cells while affecting as few healthy cells as possible. Since their ideation, nanoscale drug delivery systems represent a revolutionary approach and a promising option to overcome the limitations of the current therapies and maybe, eventually, defeat cancer.

1.3 Nanomedicine

Significant achievements have been recently witnessed in the field of nanotechnology, which has been a crucial impulse to the development of nanoscale DDS to serve as efficient diagnostic and/or therapeutic tools against cancer. The field of drug delivery is now a very hot research area as it affects the life of millions of patients every year. The current annual global pharmaceutical market is valued $980 billion.[5] Nanomedicine is a rapidly-progressing field focused on solving the limitations of conventional chemotherapy such as nonspecific biodistribution, lack of targeting, lack of aqueous solubility and low therapeutic indices.[2,4,6,7] Ideal DDS are expected to have the following features: (1) localize the therapeutic to the site of action to reduce the systemic side effects; (2) maintain the drug concentration within the effective therapeutic window for a prolonged amount of time; (3) improved adherence by reducing the number of required doses; and (4) ability to be cleared or degraded when administrated on their own.[8]

Generally speaking, DDS are colloidal nanoparticles (NPs) attractive for cancer treatment because their drug release properties can be influenced by the composition, structure, size and surface characteristics. The vast choice of materials and their organization allow the systems to be fine-tuned for specific applications and targets, such as controlled release of the payload at a predetermined rate and for a definite period of time.[9] Regarding the size, by definition NPs refers to materials with sizes between 1 to 100 nm, but the term has become commonly used to describe particulate with a size range of 10-1000 nm.[8] The first DDS to be mentioned in literature were liposomes, described in the early 1960s and closely followed by the first polymeric systems, reported before the end of the decade. The first protein-based DDS (human serum albumin) was described in 1972 and numerous other breakthroughs were made during the ‘70s, such as the employment of emulsion polymerization as a synthesis procedure for polymeric NPs and the preparation of micelles as drug delivery systems. Also, in 1979 the first biodegradable acrylic DDS was reported.[8]

Nevertheless, these primitive DDSs were largely ineffective due to interactions with the blood components, such as macrophages and opsonins. One of the most important discoveries for the advancements of the field was the employment of hydrophilic polyethylene glycol chains (PEG) for coating the NPs. PEGylation, as the coting process is named, was shown to increase stability and half-life time of the DDSs and provided them with invisibility in the bloodstream for the so-called “stealth effect”.[10,11]

The ability of DDSs to target cancer, regardless the structure of the system, relies on two different approaches. The first is the so-called passive targeting: this is the common ground for the nanoscale systems and the underlying mechanism for the employment of DDSs as amelioration for cancer therapy, since it takes advantages of the unique features of tumoral tissues. Specifically, NPs and nanosized DDSs accumulate in tumors because of the enhanced penetration and retention (EPR) effect.[12] This phenomenon relies on the pathophysiological differences between tumors and healthy tissues. Due to overstimulated and defective angiogenesis, tumors have leaky vessels allowing the penetration of DDSs with compatible size. It is reported that the size threshold to take advantage of the EPR effect is roughly 400nm, but some studied showed that NPs with a diameter < 200 nm are more effective.[2,13] Also, the inefficient lymphatic drainage guarantees the retention of the delivery agents and the released drug in the area.[14,15] Whereas the free drug diffuse nonspecifically after conventional administration, nanoscale DDSs are designed to specifically enter the tumor tissues because of the EPR effect and release selectively there their payload (Figure 1).

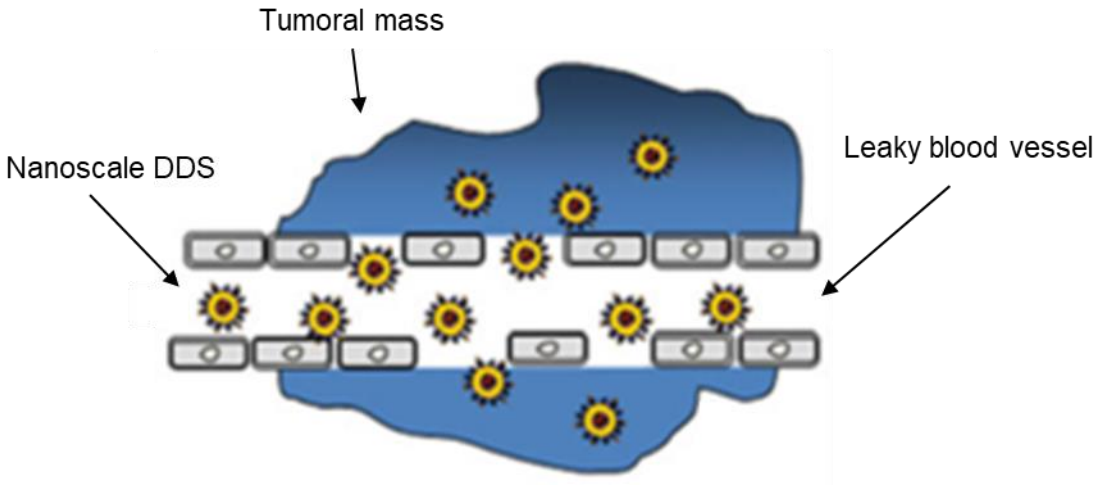

Figure 1: *Schematic representation of the consequence of the EPR effect.*[16]

The second approach is active targeting, achieved by conjugating tumor-specific ligands to the surface of the nanosystems to promote the internalization into responsive cells. Active targeting takes advantage of the overexpression of receptors, such as folate or transferrin

on the tumor cell surface, favoring the internalization of the DDSs. Among the targeting agents, the folate receptor (FR) has been probably the most exploited since it is highly expressed on epithelial malignancies such as ovarian, colorectal, and breast cancer (100–300 times more than in normal tissues).[17] It is also known that folic acid linked cargos are efficiently bound and internalized by FR expressing cells, presumably via receptor-mediated endocytosis.[18]

DDSs are generally classified into lipid-based and polymer-based systems. Although several different NPs have been described in literature, the most used are liposomes and nanoemulsion as lipid-based systems, and micelles and polymeric NPs as polymer-based systems.

1.3.1 Liposomes

Liposomes are spherical lipid vesicles with at least one lipid bilayer delimiting the hydrophilic core. Liposomal structures are mainly made of amphiphilic lipids such as phospholipid, glycolipids and sphingolipids (Figure 2).

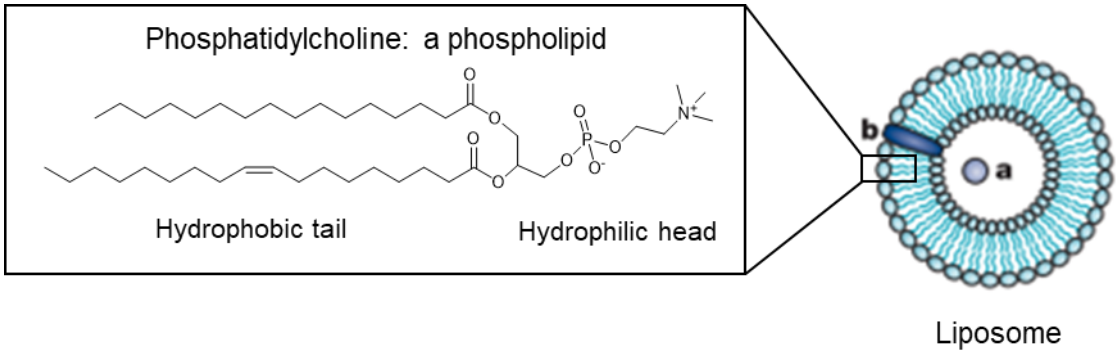

Figure 2: *Structure of a phospholipid (1-palmitoyl,2-oleyl phospatidylcholine) and organization of a unilamellar liposome, where* ***a*** *is an hydrophilic drug and* ***b*** *is a hydrophobic drug.*[19]

Composition is a key factors for the stability of bilayers, drug encapsulation and the in vivo fate of the final DDS. Cholesterol is a fundamental component in the preparation, since it improves the characteristics of the system in terms of fluidity, stability and permeability. Phospholipids are widely used as components for liposome and consist of two hydrophobic fatty acids “tails” and a hydrophilic “head” represented by the anionic phosphate group, which are hold together by a glycerol molecule. In liposomes the polar heads of phospholipids are exposed to the surrounding aqueous environment, whereas the apolar tails interact one another. Liposomes are advantageous DDSs because of their biocompatibility and their capability of encapsulating both lipophilic and hydrophilic drugs: the first ones locate in the bilayer, the latter in the inner aqueous core.

1.3.2 Nanoemulsions

Emulsions are mixtures of two or more liquids that are normally immiscible. An emulsion is a two-phase system where one liquid (dispersed phase) is dispersed in the other (continuous phase). Emulsions are instable systems that can undergo phenomena such as flocculation, creaming and coalescence. Their kinetic stability can be improved with the addition of a surfactant, which is always needed as a component in the formulation (generally about 20-25% of the components).[20]

Nanoemulsions (NEs), on the contrary, are kinetically-stable emulsion where the lipid dispersed phase size ranges between 20–200 nm. The small size of the droplets causes the translucent appearance and the characteristic stability against coalescence, flocculation and creaming, which has been demonstrated to be advantageous for drug delivery.[21,22] As a consequence, NE formulations require lower amount of surfactant compared to conventional emulsion, generally only 5-10% of the components.[23] By using NEs as a delivery system the drug half-life and the bioavailability of lipophilic drugs can be improved.[24] Nowadays this pharmaceutical form is frequently used for the delivery of various biopharmaceuticals as peptides, vaccines, DNA encoded drugs and antibiotics. NE formulations can be delivered by various routes including oral, ocular and transdermal and they are also widely used as a topical preparation formulation and cosmetics.[23]

1.3.3 Micelles

The fundamental unit constituting a polymeric micelle is the unimer, which is an amphiphilic di-block copolymer, made of two separate blocks with opposite characteristics: one is hydrophilic, the other is hydrophobic. Above a specific threshold concentration in water – the critical micelle concentration (CMC) - and a specific temperature – the critical micelle temperature (CMT) – unimers aggregate, exposing the hydrophilic block and hiding the hydrophobic one inside to avid interactions with water (Figure 3).

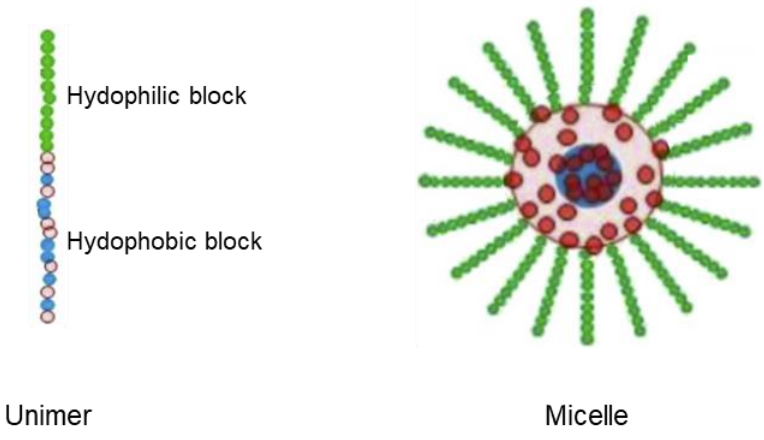

Figure 3: *Schematic structures of unimers and micelles with an hydrophobic drug loaded in the core.*[25]

The resulting aggregates of amphiphilic polymers assemble to form the so-called micelles, usually 10–80 nm in diameter, consisting of a hydrophobic core for drug loading and a hydrophilic shell that acts as a physical (“steric”) barrier to prevent both micelle aggregation and opsonization during systemic administration.[26] Micelles are designed to delivery hydrophobic drugs, which can be loaded into the core of the micellar structure and protected by the hydrophilic corona during transport to the tumor site.[27]

1.3.4 Polymeric Nanoparticles

Nanoparticles (NPs) are defined as nanoparticulate dispersions or solid particles with a size in the range of 10-1000 nm. Several different polymeric NPs have been proposed as DDSs to date, with different characteristics and surface properties. These systems are reported to be advantageous over most other DDSs: for instance, particle size and surface characteristics of NPs can be easily manipulated to achieve both passive and active targeting and to favor the interaction NP-drug. Also, they have higher stability in blood fluids after administration and higher drug loading compared to other colloidal systems. Drugs can be incorporated into the systems without any chemical reaction, which is important for preserving the drug activity. Furthermore, the virtually unlimited choice of components allows the synthesis of DDSs with different properties that can be tuned to respond to environmental, chemical, thermal, or biological triggers.[8]

NPs can be prepared from a variety of materials such as proteins, polysaccharides and synthetic polymers. The preparation method plays a crucial role to give the final system the wanted characteristics and the there are two main synthesis approaches: (1) Preparation of nanoparticles by dispersion of preformed polymers (physical method) and (2) preparation of nanoparticles by polymerization of monomers (chemical method). Dispersion of preformed polymers is a common technique used to prepare biodegradable nanoparticles from natural polymers such as poly (lactic acid) and poly (D, L-lactide-co-glycolide) (PLGA). The chemical polymerization methods, on the other hand, are used to form NPs starting from monomers, where the drug can be incorporated either by being dissolved in the polymerization medium or by adsorption onto the nanoparticles after polymerization is completed.[28]

Two among the most exploited polymeric NPs are nanospheres and nanocapsules (Figure 4). Nanospheres consist of a seamless spherical polymeric matrix within which the drug is loaded. The drug is typically distributed evenly throughout this matrix and the release into the environment takes place via diffusion. Nanocapsules, often referred to as reservoir systems, contain the drug in the core, separated from the environment by a polymeric membrane and released in a diffusion-driven manner. Polymeric NPs are attractive for drug

delivery applications since by modifying the composition of the system, the payload can be release with different kinetics. These systems have been widely explored for their release properties, which allow the release at feasible and clinically relevant time scales.[4]

Recently, the breakthroughs in the field have allowed the design of advanced nanoparticle, able to respond to environmental, chemical, thermal, or biological triggers. These so-called 'smart materials' release their therapeutic payload only when triggered.

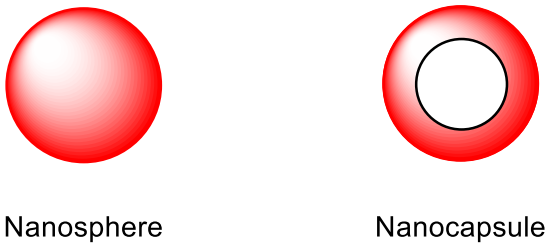

Figure 4: *Schematic representation of nanospheres (spherical polymer matrix) and nanocapsules (hollow polymeric capsule)*

1.4 Stimuli-responsive polymeric nanoparticles

As mentioned above, the effectiveness of nanoscale polymeric DDSs can be improved by producing a responsive or "smart" system, that is, a structure designed to respond to pre-set conditions by altering its properties. These conditions, the so-called stimuli, can be physical (e.g. temperature, pH or light), chemical (presence of signaling molecules, reducing agents, etc.) or biological (enzymes). Stimuli are basically triggers that promote modifications in the structure of the DDS, such as formation/breakage of secondary forces (hydrogen bonding, hydrophobic effects or electrostatic interactions), changes in solubility or variations in the hydrophilic/hydrophobic balance of the system. Stimuli-responsive DDSs can be developed to respond to both external stimuli (such as magnetic fields, ultrasound, light and heat sources) and internal pathological conditions. Sensitive DDSs triggered by internal stimuli can respond both at cellular or tissue level and are currently employed in the treatment of pathological conditions such as cancer and inflammatory diseases, characterized by well-defined characteristics associated with the pathology.[29] This approach is extremely advantageous, since these smart system can be designed to release the drug only when in contact with a pre-set stimulus, characteristic of the target pathological area. These stimuli include difference in temperature between tumoral and healthy tissues, variation between physiological and pathological pH, and other biological factors (glucose, inflammation-responsive, and glutathione concentration).[8] The most advanced systems can respond to more than one stimulus simultaneously, often causing a synergic effect on the drug release profile.[30–35]

1.4.1 Drug delivery systems triggered by internal stimuli

pH sensitivity

pH is arguably the most exploited stimulus for smart drug release since there is a clear difference between healthy tissues (pH 7.4) and diseased tissues (pH 6.0 - 6.5 in tumors).[36–38] Also, intracellular differences between normal and cancer cells have been highlighted and can be used to facilitate the dug release in these conditions. At a tissue level, tumors have lower extracellular pH due to their faster metabolism. As there is a rapid proliferation of tumoral cells, local vascularization is often disorganized and insufficient to meet nutritional and oxygen requirements of cancer cells. Oxygen insufficiency causes hypoxia, leading to the production of lactic acid, which in turn decreases the pH in the tissue.[39] Similarly, during inflammation and infection states, the local pH shifts from neutral to acid because leukocytes, which are involved in inflammation and actively transport lactic acid to the exudate.[29] At a cellular level, the most significant pH variation occurs during endocytosis, the most used internalization pathways for DDSs. In this process, the cell membrane forms an endosome containing the internalized NPs, which migrates in the cell to fuse with a lysosome. The NPs in the endosome-lysosome system encounter much lower pH than the neutral extracellular environment, such as the endosome pH 5.0 – 6.0 and lysosomes pH 4.5. – 5.0. Also, lysosomal pH in cancer has been reported to be as low as 4.0.[8]

Ionizable polymers are optimal candidates for pH-responsive systems. Weak acids and bases like carboxylic acids and amines exhibit a change in the ionization state depending variation of the pH. This leads to a conformational change or a change in the swelling behavior when these ionizable groups are part of the polymer structure. Also, charged moieties on the drug delivery systems can interact with oppositely charged drugs, and pH variations can result in breakage of these interaction favoring the release of the loaded drugs. Classical monomers used to prepare pH-sensitive NPs are acrylic acid (AA), methacrylic acid (MAA) and N,N-dimethylaminoethyl methacrylate (DMAEMA).[40]

Temperature sensitivity

Our body temperature is roughly 37°C, whereas in pathological states this value can be higher than 41°C. Furthermore, the application of an external heat source in the so-called hyperthermia treatments can trigger the drug release from temperature-responsive systems. This application differs from the internally modulated temperature-responsive delivery as it requires an externally applied heat source and does not target physiological changes in temperature.[41,42] Temperature can be therefore considered as both an internal and an external stimulus and, as such, has been largely used as a mechanism for smart

drug delivery.[40,43,44] Specifically, temperature triggers the expansion or collapse of suitable polymeric networks (hydrogel) by affecting the aqueous solubility of the system in the medium. Thermo-responsive systems are characterized by either an upper critical solution temperature (UCST) or a lower critical solution temperature (LCST). The UCST is the critical temperature above which the polymer and solvent are miscible in all proportions, whereas LCST is the below which they are miscible in all proportions. The LCST behavior, by large the most exploited in drug delivery systems,[8] is an entropy-driven process in which the polymer tends to shrink at temperatures above the critic temperature. These transitions are fully reversible and can be fine-tuned by adjusting the ratio between the hydrophobic and hydrophilic monomers used to form the polymer.[40]

There is a wide range of synthetic and natural polymers exhibiting LCST around the physiological temperature. Most of the studies about LCST-based systems focus on *poly* N-isopropylacrylamide composite hydrogels (PNIPAAM) and their copolymers. PNIPAAM displays an LCST between 30°C and 34°C, making it an interesting material for biomedical applications. The addition of hydrophilic monomers in the copolymerization increases the critical temperature, while hydrophobic monomers cause the opposite effect.[40] Another monomer known for its temperature responsiveness is DMAEMA. Poly DMAEMA has a LCST around 50°C in water, however the copolymerization with AA and crosslinking agents has been shown to shift the transition temperature around 40°C, optimal for drug delivery purposes.[45]

Redox sensitivity

It is known that there is a considerable difference in the redox potential between the extracellular and intracellular media.[39] In the extracellular matrix and on cell surface proteins are rich in stabilizing disulfide bonds as a result of high redox potential, due to a low concentration of glutathione (GSH), approximately 2–20 μM. On the contrary, the cytosol is a highly-reducing environment, where the concentration of reduced GSH is between 0.5 and 10 mM.[46,47] In addition, the difference is even more remarkable in case of cancer. Specifically, the concentration of GSH in tumoral cells is at least four-fold higher than in normal cells.[46–49] This large difference between tumor-associated GSH concentration and very low extracellular levels constitutes a strong, specific and exploitable signal, which renders the redox-responsive systems very promising candidates for specific drug release.[50] Although diselenide linkage have recently started to be investigated,[51] the redox sensitivity of DDSs relies on cross-linking agents presenting a disulfide moiety, which translates into having polymeric network held together solely by reduction-sensitive bonds. In presence of high concentration of GSH, the network composing the DDS will break and the payload will be quickly and easily released, at a time scale from minutes to few hours.[52]

One of the most employed disulfide-bearing cross-linking agent is the commercially available N,N-bis(acryloyl)cystamine (BAC).

1.4.2 Drug delivery systems triggered by external stimuli

Photo responsivity

Photo-responsive polymers have the ability to deliver drugs in response to light, with drug release occurring almost instantaneously with high accuracy due to photoinduced structural modifications of the DDSs. This is a fully noninvasive method of delivery, which responds to only a specific wavelength and can be activated either once or repeatedly, in an on-off manner.[53] The release is obtained by three main mechanisms which can be reversible or irreversible: (1) photoinduced transition of hydrophobicity-hydrophilicity, (2) photo-cleavage reaction, and (3) photoinduced heating to trigger temperature-responsive systems.[54] The UV-vis (10-400 nm) or near infrared (650-900 nm) regions of the light spectrum can be used to trigger the drug release for a photo-sensitive DDS. However, in general wavelengths below 650 nm are considered to be the most useful to trigger the drug release.[8] The introduction of photochromic moieties in the polymer network cause the system, upon photoreaction due to light illumination, to modify the hydrophobic-hydrophobic balance causing the disruption of the system. Irreversible photo-disruption and reversible photo-isomerization reactions have been also used to fabricate photo-responsive materials.[55,56] In this case, photocaging groups are used, such as coumarin-4-yl-methyl, o-nitrobenzyl, p-hydroxyphenacyl, and 7-nitroindoline derivatives.

Magnetic responsivity

Colloidal iron oxide nanoparticles, typically composed of nanocrystalline magnetite (Fe_3O_4) or maghemite (γFe_2O_3), have been extensively investigated for biomedical applications due to their excellent biocompatibility and ease of synthesis. These particles display magnetic properties that, in the case of Fe_3O_4, arise from electron hopping between the Fe_2+ and Fe_3+ ions that coexist in the octahedral crystal habit.[57]

The main advantages of these superparamagnetic iron nanoparticles (SPIONs) are that they can be: visualized (SPIONs are used as negative contrast agents in MRI); guided or held in place by means of a magnetic field; and heated in a magnetic field to trigger the drug release or to produce hyperthermia/ablation of tissue.[58] These exploitable characteristics have opened up a very wide range of biomedical applications for drug delivery.[59] Furthermore, a DDS grafted with SPIONs would be a so-called theranostic system: not only would it be able to be selectively driven to and treat the diseased cells, but also it would be possible to monitor the drug delivery process, the therapeutic efficacy and the progresses of the therapy by visualizing the area of interest.[60] SPION-grafted DDSs can be roughly

divided in two classes, depending on the process used for obtaining them: i) nanocapsules with SPIONs in the core and ii) nanospheres harboring precipitated SPIONs in the pores.

Scope of the Thesis

The main research topic of this Ph.D. was the synthesis and characterization of new polymeric nanocontainers (NCs) for the targeted release of chemotherapy drugs. During the three years, the candidate was given different classes of compounds to be selectively delivered to tumoral cells and tissues by taking advantage of the unique stimuli present in these areas.

The first goal was the synthesis, characterization and study of drug release profile of hollow pH-sensitive NCs for the release of daunorubicin. Secondly, an innovative system was then designed for the release of daunorubicin, a three-stimuli sensitive NC, more complex and capable of responding more specifically to the pathological conditions of pH, temperature and redox activity associated with tumoral tissues and cells.

In the framework of a collaboration with CNR Bologna, the first pH-sensitive system was also tested for the encapsulation of the cyclic peptide somatostatin, due to the compatibility of its characteristics. A key point of this project was to monitor the structure of the peptide, highly susceptible to degradation, during the entire encapsulation and release experiments, which was done through circular dichroism. The collaboration was extended for the study of the release profile of somatostatin from nanoemulsions, where the candidate set up a HPLC/MS analytical methodology to follow up the fate of the peptide when the nanoemulsions were placed in buffer and plasma.

Once the Cu(II)-based complexes were developed, they were given to the candidate who had to create a formulation capable of loading and releasing the molecule specifically in tumoral environment. The pH-sensitive NCs, thanks to its versatility, was tested in loading and release experiments of Cu-TPMA-Phen. It was crucial to ideate a methodology to investigate whether the loading/release processes would affect the structure of the Cu complex, fundamental to the activity of the compound. This was achieved by using continuous wave electron paramagnetic resonance.

The last objective was the synthesis of a novel DDS for the release of ONs and derivatives. The final goal of the network ClickGene was the delivery of Cu(II)-based complexes with metallonuclease activity conjugated with DNA fragments as targeting agents. To achieve this goal, the fundamental characteristic of DDSs for oligonucleotides were studied and a strategy for the synthesis of a novel system was designed. This task required a suitable system that could strongly interact with large polyanionic molecules and, at the same time, to easily release them under pre-set conditions.

Anthracyclines

3.1 Introduction

Chemotherapeutic agents are usually small molecules that disrupt the normal functioning of a cell by inhibiting replication or inducing apoptosis. Due to their capability at provoking cytotoxicity, chemotherapeutic agents have been almost exclusively utilized in the treatment of cancer, where they exhibit the most deleterious effects to rapidly proliferating cells. Prominent chemotherapeutic agents include paclitaxel, doxorubicin, daunorubicin, cisplatin, and docetaxel. In particular, doxorubicin (DOX) and daunorubicin (DNR) belong to a class of chemotherapeutics known as the anthracyclines antibiotics, originally isolated from fermentation products of *Streptomyces peucetus*, which were found to have antineoplastic activity in 1984[61]. These molecules are among the most effective drugs available, inducing the greatest degree of cytotoxicity and used to treat the widest variety of tumor types. DOX is the most common one and it is used to treat aggressive lymphoma, breast cancer, and sarcomas. On the other hand, DNR is the first option for patients with myeloblastic leukemia (Figure 5).[62] Anthracyclines have been shown to induce protein-associated strand breaks by trapping topoisomerase II in the topoisomerase-II-DNA complex, resulting in disrupting the DNA and preventing cellular replication.[63] Apart from the topoisomerase inhibition, anthracyclines are responsible for several other biological reactions. First, the aglycone moiety can insert between base pairs of DNA (intercalation) with consequent inhibition of macromolecular biosynthesis.[61] Second, these molecules interfere with nuclear helicases hindering the process of strand separation. Third, anthracyclines are anthraquinones and all quinones undergo one and two electron reductions producing reactive species capable of damaging macromolecules and membranes.[61,64,65]

The primary concern with utilizing chemotherapeutic agents is their inability to differentiate between healthy and tumor tissue.[12] The drugs will attack all cells without discrimination, being particularly harmful to any rapidly proliferating cells in the body such as hair, intestinal epithelial cells, and bone marrow. The most cytotoxic agents are the most effective but these often result in severe side effects. Doxorubicin and daunorubicin are widely considered to be the best anti-cancer drug available nowadays but they result in side effects such as, nausea, fatigue, and extensive cardiotoxicity.[62] Therefore, therapies must be optimized considering the balance between the effectiveness of the drug and a patient's ability to tolerate the side effects.[4]

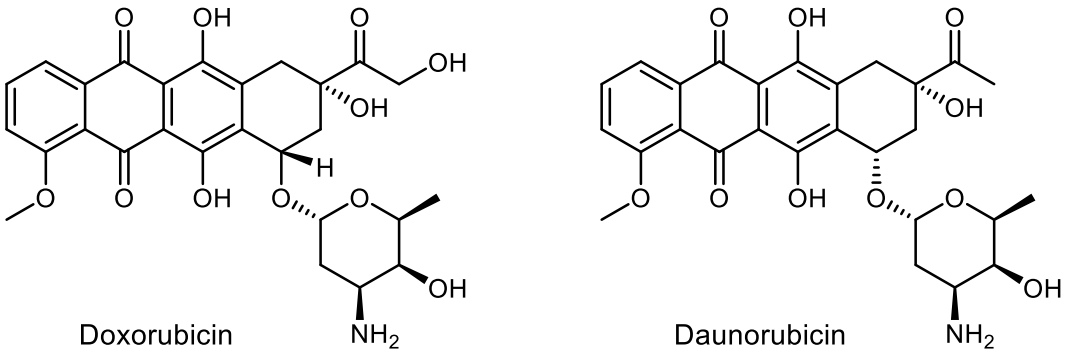

Figure 5: *Structure of Doxorubicin (DOX) and Daunorubicin (DNR).*

Nanoscale drug delivery systems (DDS), designed to target specifically tumors, could be utilized to alleviate some, if not all, of these cytotoxic effects to healthy cells. Among the various nanoparticles studied for DOX and DNR delivery, some liposomal formulations have been approved and are currently in use. Liposomes consist of one or more bilayers of natural or synthetic lipids entrapping an aqueous core. Due to their natural composition, liposomes are weakly immunogenic, biologically inert and have overall low intrinsic toxicity. Myocet® (Elan Pharmaceuticals Inc., Princeton, NJ, USA) and and Daunoxome® (Gilead Sciences), encapsulating DOX and DNR respectively, are examples of liposomes composed of neutral and/or negatively charged lipids and cholesterol prescribed for metastatic breast cancer and Kaposi's sarcoma. Another noticeable example is Doxil®, the first FDA-approved nano-drug (1995), which consists DOX encapsulated in PEGylated "stealth" liposomes. This slow-release form of doxorubicin is approved in USA and Europe for treatment of Kaposi's sarcoma and recurrent ovarian cancer.[11,66]

The recent advances in polymeric nanotechnology have drawn attention to new biocompatible and design-controlled delivery systems. They could release the encapsulated drug specifically in presence of pre-set conditions, the so-called stimuli, that could be found exclusively in tumors (e.g. pH variations, enzyme concentration, redox, or temperature gradient). Being anthracyclines very effective but scarcely tolerable, many different polymeric systems have been designed to encapsulate and release DOX and DNR in an effort to increase the tolerability of these drugs. Among the cutting-edge strategies applied nowadays, hollow polymeric nanocontainers (NCs) are considered as one of the most promising.[67] An appropriate choice of components allows the synthesis of different of stimuli-responsive nanoparticles and the central cavity has been proved to facilitate the accommodation of larger amount of drug compared to other systems.[68]

During the doctorate, the student was involved in the design and synthesis of two different stimuli-responsive NCs, which were then tested for their ability of loading and releasing DNR.

3.2 Experimental

3.2.1 Materials and Method

Materials

N,N′- methylenebisacrylamide (MBA, 96%) and 2,2′-Azobisisobutyronitrile (AIBN, 98%) were purchased from Acros. Methacrylic acid (MAA, 99%) was bought form Sigma-Adrich and distilled prior use. N,N-dimetilaminoethylethacrylate (DMAEMA), Poly(ethyleneglycol) methylethermethacrylate (PEGMA; Mn = 475) and acetonitrile (ACN) were obtained from Sigma-Aldrich. N′-bis(acryloyl)cystamine (BAC, 98%) was purchased from Alfa Aesar. Daunorubicin HCl (DNR) was provided by Pharmacia & Upjohn.

Scanning electron Microscopy (SEM)

SEM images were obtained with FEI Inspect microscope with tungsten filament operating at 25 kV. The dried NPs (powders) were placed on a thin layer of carbon tape holder on the specimen stub. Prior the analysis, the samples were sputter coated with a thin layer of gold to prevent charging of a specimen with the electron beam in conventional SEM mode.

Dynamic Light Scattering (DLS)

The hydrodynamic diameter and ζ-potential of the NPs were measured with Malvern Instruments Zetasizer Nano Series at an angle of 173°. All the measurements were run at 25°C. In the data presented, each measurement represents the average value of 5 measurements, with 11–15 runs for each measurement. The polydispersity of the sample, a parameter used to describe the homogeneity of the sample, is reported as polydispersity index (PDI). The samples were usually prepared by suspending 1 mg of sample in 100 ml of distilled water with the aid of ultrasonic bathing (at least 30 minutes). When needed, the pH was adjusted by addition of HCl 1M or NaOH 1M solutions.

Fourier transform infrared Spectroscopy (FT-IR)

FT-IR was used to characterize the chemical structure of the NPs and confirm their successful modification. The spectra were obtained with Perkin-Elmer Spectrum 100 spectrometer by directly analyzing the powders.

UV-visible Spectroscopy

Jasco V-650 Spectrophotometer was used to measure the concentration of the samples during the encapsulation and release experiments. All calculations were based on a standard curve recorded in each media.

3.2.2 pH-sensitive Nanocontainers

The system was obtained via a three-step process, namely the formation of the PMAA cores, the synthesis of the pH-sensitive shell and finally the core removal.

Synthesis of PMAA cores

MAA (2.1 g; 24.4 mmol) was dissolved in 200 ml of ACN and stirred at 75°C for 30 minutes under nitrogen atmosphere before adding AIBN (0.3 g; 1.8 mmol). After 30 minutes the flask content turned milky and the temperature was increased to 95-100°C to start the distillation. The reaction was stopped after collecting 20 ml of distilled ACN. The product was purified by three cycles of centrifugation and resuspension in ACN with ultrasonic bathing for three times (5 min x 8000 rpm). After drying in an oven at 50°C overnight, the product was collected as white powder.

Synthesis of the pH-sensitive shell - PMAA@P(MAA-co-PEGMA-co-MBA)

PMAA cores (0.15 g) were suspended with ultrasonic bathing in 200 ml of ACN and stirred at 75°C for 30 minutes under nitrogen atmosphere. The monomers for the formation of the shell were then added: MAA (0.53 g; 6.1 mmol) and after 10 minutes PEGMA (0.16 g; 0.3 mmol; 5% mol of MAA) and MBA (0.15 g; 0.97 mmol; 16% mol of MAA). AIBN (0.09 g; 0.5 mmol; 8% mol of MAA) was added after 30 minutes and the reaction medium was stirred for 10 minutes before increasing the temperature to 95-100°C to start the distillation. The reaction was stopped after collecting 30 ml of distilled ACN. The product was purified by three cycles of centrifugation and resuspension in ACN with ultrasonic bathing (5 min x 5000 rpm). After drying in an oven at 50°C for 24h, the product was collected as white powder.

Core removal - Hollow P(MAA-co-PEGMA-co-BAC) NCs

250 mg of PMAA@P(MAA-co-PEGMA-co-MBA) were suspended with ultrasonic bathing in 200 ml of a mixture of EtOH/H_2O dist. (1:1). The reaction medium was stirred over night at r.t. to obtain the hollow nanocontainers. The product was purified by three cycles of centrifugation and resuspension in ACN with ultrasonic bathing (5 min x 5000 rpm). After drying in an oven at 50°C overnight, the product was collected as white/transparent powder.

Loading of DNR

5 mg of hollow NCs were suspended in 5 ml of phosphate buffer saline (PBS, pH 7.4) with the aid of ultrasonic bathing. 5 mg of daunorubicin hydrochloride (DNR HCl) were then dissolved in the medium. The suspension was covered with foil and maintained under gentle agitation for 72h at r.t.. The non-encapsulated DNR was then removed with 15 cycles of centrifugation/resuspension (5 min x 9000 rpm). The encapsulated amount of DNR was

indirectly determined by UV spectroscopy: the total amount of loaded DNR was calculated by the difference between the amount of DNR in feeding and in the supernatant fractions. These calculations were based on a standard curve of DNR in PBS and the concentration was determined with absorbance measurements at λ484 nm.

The success of the process was evaluated by the parameters encapsulation efficiency (EE%) and loading capacity (LC%).

$$\mathrm{EE\%} = \frac{\text{Encapsulated drug (mg)}}{\text{Drug in feeding (mg)}} \text{x } 100$$

$$\mathrm{LC\%} = \frac{\text{Encspsulated drug (mg)}}{\text{Loaded NCs (mg)}} \text{x } 100$$

The experiments were carried out three times for statistical analysis.

In-vitro release experiment

1 mg of DNR-loaded NCs were suspended in 0.5 ml of buffer and loaded into MWCO 140 kDa dialysis tube and incubated in 50 ml each buffer solution: citrate buffer 0.1M pH4.0; citrate buffer 0.1M pH 6.0 and PBS 1x. At different time points (30 min, 1h, 2h, 5h, 8h, 10h, 24h, 48h, 72h), 1 ml of the solutions was withdrawn and analyzed. The concentration of each sample, and therefore of the release medium at each time point was determined with UV spectroscopy by using the standard curve method (λmax 484 nm). A standard curve of DNR was recorded in each buffer used as release medium. The experiment was carried out three times for statistical analysis.

3.2.3 Three-stimuli-sensitive Nanocontainers

The system was obtained with four subsequent DPP, followed by the core removal to give the hollow NCs. The formation of PMAA cores and of the pH-sensitive shell are very similar to the ones described for the pH-sensitive NCs, reported in 3.2.2. The monomer concentration was adjusted to yield smaller particles**.**

Synthesis of PMAA cores

MAA (1.1 g; 12.2 mmol) was dissolved in 200 ml of ACN and stirred at 75°C for 30 minutes under nitrogen atmosphere before adding AIBN (0.3 g; 1.8 mmol). After 30 minutes the flask content turned milky and the temperature was increased to 95-100°C to start the distillation. The reaction was stopped after collecting 20 ml of distilled ACN. The product was purified by three cycles of centrifugation and resuspension in ACN with ultrasonic bathing for three times (5 min x 18000 rpm). After drying in an oven at 50°C overnight, the product was collected as white powder.

Synthesis of the pH-sensitive shell - PMAA@P(MAA-co-PEGMA-co-MBA)

PMAA cores (0.15 g) were suspended with ultrasonic bathing in 200 ml of ACN and stirred at 75°C for 30 minutes under nitrogen atmosphere. The monomers for the formation of the shell were then added: MAA (0.53 g; 6.1 mmol) and after 10 minutes PEGMA (0.16 g; 0.3 mmol; 5% mol of MAA) and MBA (0.15 g; 0.97 mmol; 16% mol of MAA). AIBN (0.09 g; 0.5 mmol; 8% mol of MAA) was added after 30 minutes and the reaction medium was stirred for 10 minutes before increasing the temperature to 95-100°C to start the distillation. The reaction was stopped after collecting 30 ml of distilled ACN. The product was purified by three cycles of centrifugation and resuspension in ACN with ultrasonic bathing (5 min x 15000 rpm). After drying in an oven at 50°C overnight, the product was collected as white powder.

Synthesis of the temperature-sensitive shell - PMAA@P(MAA-co-PEGMA-co-MBA) @P(DMAEMA-co-MAA-co-PEGMA-co-MBA)

PMAA@P(MAA-co-PEGMA-co-MBA) (0.2 g) were suspended with ultrasonic bathing in 1 l of ACN and stirred at 75°C for 30 minutes under nitrogen atmosphere. DMAEMA (0.79 g; 5 mmol) was added over 30 minutes. After 10 minutes, MAA (0.43 g; 5 mmol), PEGMA (0.24 g; 0.5 mmol; 10% mol of MAA) and MBA (0.25 g; 1.6 mmol; 32% mol of MAA) were added as well. AIBN (0.13 g; 0.8 mmol; 16% mol of MAA) was added after 30 minutes and the reaction medium was stirred for 10 minutes before increasing the temperature to 95-100°C to start the distillation. The reaction was stopped after collecting 200 ml of distilled ACN. The product was purified by centrifugation (5 minutes x 12000 rpm) and resuspension in ACN with ultrasonic bathing for three times. After drying in an oven at 50°C overnight, the product was collected as white/yellowish powder.

Synthesis of the redox-sensitive shell - PMAA@P(MAA-co-PEGMA-co-MBA) @P(DMAEMA-co-MAA-co-PEGMA-coMBA)@P(MAA-co-PEGMA-co-BAC)

PMAA@P(MAA-co-PEGMA-co-MBA)@P(DMAEMA-co-MAA-co-PEGMA-co-MBA) (0.15 g) were suspended with ultrasonic bathing in 750 ml of ACN and stirred at 75°C for 30 minutes under nitrogen atmosphere. MAA (0.39 g; 4.5 mmol), PEGMA (0.11 g; 0.22 mmol; 5% mol of MAA) and BAC (0.19 g; 0.72 mmol; 16% mol of MAA) were added as well. AIBN (0.06 g; 0.4 mmol; 8% mol of MAA) was added after 30 minutes and the reaction medium was stirred for 10 minutes before increasing the temperature to 95-100°C to start the distillation. The reaction was stopped after collecting 150 ml of distilled ACN. The product was purified by centrifugation (5 min x 10000 rpm) and resuspension in ACN with ultrasonic bathing for three times. After drying in an oven at 50°C overnight, the product was collected as white powder.

Core removal - Hollow P(MAA-co-PEGMA-co-MBA)@P(DMAEMA-co-MAA-co-PEGMA -co-MBA)@P(MAA-co-PEGMA-co-BAC) NCs

100 mg of three shells/core NPs were suspended with ultrasonic bathing in 200 ml of a mixture of EtOH/H_2O dist. (1:1). The reaction medium was stirred for 48 at r.t. to obtain the hollow nanocontainers. The product was purified by centrifugation and resuspension (5 min x 12000 rpm) with ultrasonic bathing for three times. After drying in an oven at 50°C overnight, the product was collected as transparent/white powder.

Loading experiment

5 mg of hollow NCs were suspended in 5 ml of phosphate buffer saline (PBS, pH 7.4) and 5 mg of DNR were then added. The suspension was covered with aluminium foil and gently stirred for 72 hours at room temperature. The non-encapsulated drug was removed by centrifugation and resuspension cycles in fresh PBS (5 min x 10000 rpm). Generally, 15 cycles were necessary. The amount of loaded DNR was indirectly determined via UV-vis according to a standard curve (λmax 484 nm). The concentration of the loaded drug was calculated by the difference in concentration between the original DNR solution and the supernatants collected after the loading process. The parameters used to evaluate the loading were Encapsulation Efficiency % (EE%) and Loading Capacity % (LC%) (see 3.2.2, loading of DNR).

In-vitro release experiment

The release behavior of the DNR-loaded NCs was investigated in different pH (pH 4.0, 6.0 and 7.4), at different temperatures (room temperature and 40°C) and in presence/absence of reducing agents (10 mM glutathione, GSH). The buffers were: citrate buffer pH 4.0 0.1M, citrate buffer pH 6.0 0.1M and PBS (pH 7.4). The release profile of DNR was determined with the dialysis bag method. Typically, 0.5 mg of DNR-loaded NCs were suspended in 0.2 ml of buffer, loaded into MWCO 140 kDa dialysis tube and incubated in 30 ml of each buffer solution. At different time points (30 min, 1h, 2h, 5h, 8h, 10h, 24h, 48h), 1 ml of the solution was withdrawn and analyzed. The concentration of each sample was determined with UV spectroscopy by using the standard curve method (λmax 484 nm). A standard curve of DNR was recorded in each buffer used as release medium. The experiment was carried out three times for statistical analysis.

In vitro cytotoxicity studies

The cytotoxicity of the formulation was evaluated via MTT assay.[69] In particular, MCF-7 (human breast adenocarcinoma cell) and HEK-293 (Human Embryonic kidney 293 cells) cells (0.1 ml, 8×10^3 cells per well) were seeded in 96-well flat-bottomed microplates and let reach 70% confluence in a controlled atmosphere (37°C, 5% CO_2 and 95% relative

humidity). 100 µl of suspension of the appropriate concentrations of free DNR, loaded DNR(0.01 - 60µM) or free NCs (0.006 – 35.2 µg/ml) were added to each well. After an incubation period of 24 h, the aliquots of treatment were removed and replaced with 100 µl of MTT solution (1 mg/ml diluted in PBS) and the cells were incubated again for 4 h. The solution was then removed and the formed formazan crystals were dissolved in DMSO. The absorbance was measured at 540 nm (reference filter 620 nm) using a microplate reader (Sirio S, SEAC Radim group). The measurements were then converted to percent viability. Cytotoxicity experiments were repeated three times for statistical analysis.

Intracellular localization - Confocal Laser Scanning Microscopy

Cellular uptake of DNR-loaded NCs was studied with confocal laser scanner microscopy, or CLSM (Leica TCS SP8 MP, inverted confocal microscope with Acousto-Optical Beam Splitter, for the excitation and multiband spectral detector Argon - excitation at 458, 476, 488, 496 & 514 DPSS 561 - excitation at 561nm (RED). Multiphoton IR laser MaiTai DeepSee from Spectral Physics, excitation at 780nm. MCF-7 cells were grown on 22mm cover slips placed into six-well culture plates (5 *10^6) for 24h in 1.5 mL of culture medium. Afterwards, the cells were treated with free DNR and DNR-loaded NCs (10 µM). After 2h incubation, the cover slips were recovered and washed twice with PBS, 10% formaldehyde in PBS and PBS again, before placing them onto microscope slides.

3.3 pH-sensitive Hollow Nanocontainers

The first DDS to be studied was a pH-sensitive hollow NC. The extracellular and intracellular pH profile of biological system is greatly affected by diseases and this difference is, arguably, the most exploited pathological stimulus for drug release[36–38]. In tumors the extracellular pH is generally more acidic (roughly 6.0) than the pH of the blood or normal extracellular tissues (7.4) and, in lysosomes, which are involved in the internalization of the NCs into cells,[4] pH values are significantly lower than the cytosolic pH (pH 4-4.5 in tumoral cells). When opportunely synthesized, the nanocarriers can take advantage of these pH differences and selectively release the encapsulated drug in the target area.[39]

In this context, the pH-sensitive hollow nanocontainer was designed by using methacrylic acid (MAA) as the main monomer: the resulting poly-methacrylic acid (PMAA) polymer presents carboxylic groups that can be protonated or deprotonated depending on the pH of the medium (pKa ca. 4.5) and therefore differently interact with the surrounding environment.[70,71] Other components were used in the synthesis, such as N,N-methylenebis(acrylamide) (MBA), used as a cross-linking agents in order to maintain the structure of the hollow NCs in water, and poly(ethylene glycol) methyl ether methacrylate

(PEGMA), which is an hydrophilic, nontoxic component known to show resistance against nonspecific protein adsorption and prolong *in vivo* circulation time of drug delivery systems (Figure 6).[72]

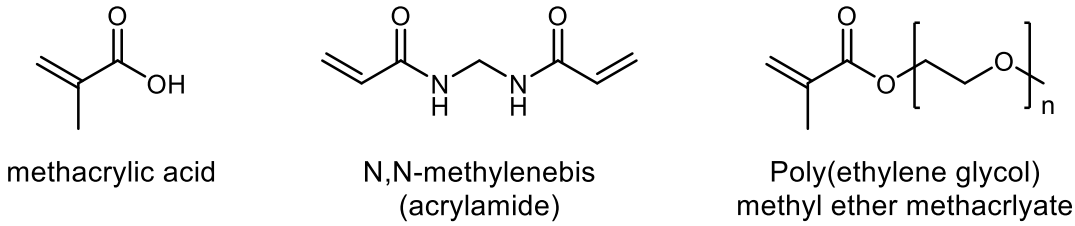

Figure 6: *Monomers used for the synthesis of the pH-sensitive NCs. Methacrylic acid (MAA); N,N-methylenebis(acrylamide) (MBA); Poly (ethyleneglycol) methyl ether methacrylate (PEGMA).*

3.3.1 Synthesis

The hollow pH-sensitive nanocontainers (NCs) were synthetized with a three-step process (Figure 7). The first step was the formation of PMAA cores, which were obtained with the distillation-precipitation polymerization method (DPP). These were sacrificial templates on which the real DDS were to be formed. The pH-sensitive shell was fabricated on the core surface with a second DPP, yielding a core-shell structure. Finally, the core removal gave the pH-sensitive hollow NCs.

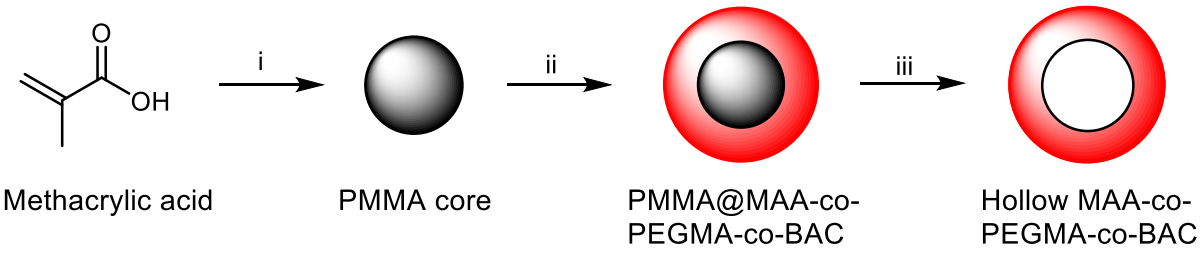

Figure 7: *Synthesis scheme of pH-sensitive hollow NCs. (i) Distillation-precipitation polymerization: MAA, AIBN, nitrogen bubbling in ACN 80°C → 100°C; (ii) Distillation-precipitation polymerization: MAA, PEGMA, BAC AIBN, nitrogen bubbling in ACN 80°C → 100°C; (iii) Core removal in a mixture of water/EtOH (1:1).*

The polymerization technique was DPP, a free radical chain polymerization used to synthesize spherical and monodisperse particles by taking advantage of the insolubility of the oligomers compared to the solubility of monomers. DPP allows facile and straightforward syntheses of monodispersed systems, and its versatility permits to use several different monomers, resulting in final nanoparticle with different characteristics. The first step was the synthesis of the monodisperse cores. The formation of the PMAA cores via DPP can be chemically described as a two-sage process. The first one is *nucleation*: the reaction system is homogenous and the oligomers grow in the continuous phase by the subsequent addition of monomers, until they reach the critical chain length, when the resulting oligomers are no longer soluble and precipitate to form nuclei. These particles are unstable and aggregate one another, giving the so-called mature particles. At this point the

reaction medium turns milky white, due to the suspension of the mature particles. The second phase is *growth*: the mature particles capture residual monomers and oligomers in the medium through hydrogen-bonds, while the solvent (acetonitrile) is distilled out of the system. At this stage only few double bounds are displayed on the surface of the particles, but the reactive vinyl groups needed for the growth are provided with the absorption of residual MAA monomers. The absorption of oligomers or their reactions with the adsorbed reactive vinyl groups on the PMAA particles is responsible for the size increase of the particles in this phase.[73]

In the second-stage DPP, needed for the formation of the pH-sensitive shell, the PMAA cores acted as the previously-described mature particles. The monomers and the oligomers in the suspension were absorbed on their surface and the phase of *growth* resulted in the formation of the cross-linked shell (Figure 8).[74]

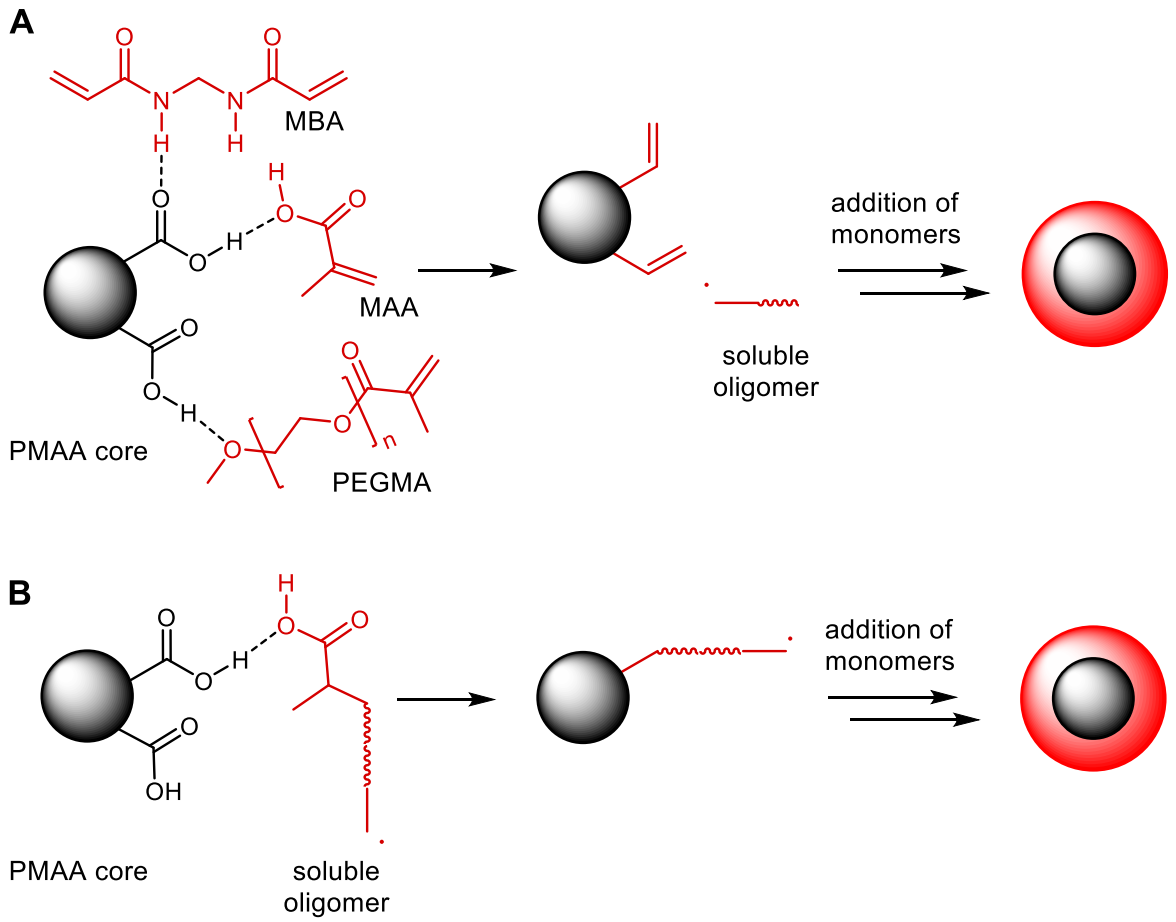

Figure 8: *Mechanism of formation of pH-sensitive shells.* ***A****) hydrogen-bonding interactions between the PMAA core and the monomers lead to displaying reactive double bonds on the surface of the cores. The double bonds react with radical oligomers to form the shell.* ***B****) direct hydrogen-bonding interactions between the PMAA cores and oligomers, which gives reactive PMAA cores surfaces.*[35]

The last step was the removal of the cores. These sacrificial templates were made without cross-linking agents, which means that their formation exclusively relies on aggregation of oligomers (mature particles) and the adsorption via hydrogen bonds of other small polymer chains and residual monomers. In an aqueous environment, such as the mixture of water and ethanol (1:1) used for the core removal process, these interactions break in favor of new interactions with the solvent, resulting in the dissolution of the core.

3.3.2 Characterization

Scanning Electron Microscopy

SEM is an extremely useful tool to evaluate the size, the shape and the monodispersity of NPs. Figure 9 shows the images collected with SEM of the synthesis intermediates and the final hollow NCs. In each case, the NPs are spherical and monodisperse; their size (diameter) and standard deviations are reported in Table 1.

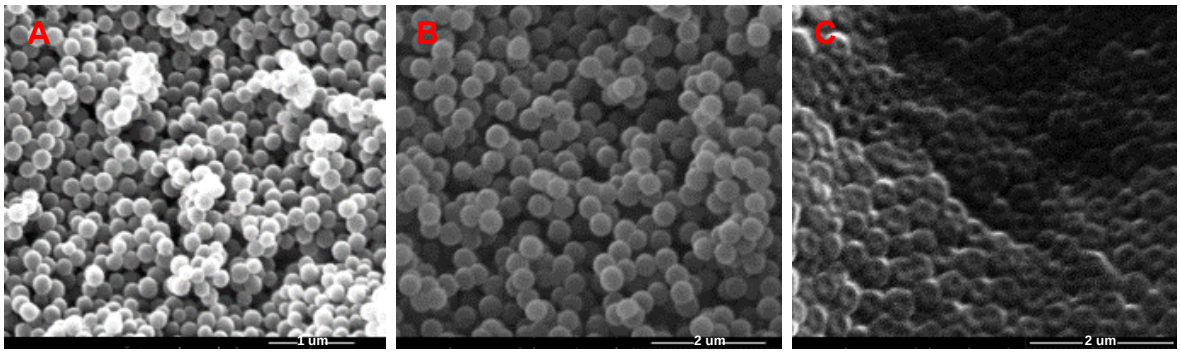

Figure 9: *SEM images of:* ***A.*** *PMAA cores;* ***B.*** *core-shell structures;* ***C.*** *Hollow NCs with the central cavity.*

Figure 9A shows the PMAA cores with an average size of 190 nm. The successful formation of the shell on the PMAA cores (Figure 9B) was confirmed by the increase to 350 nm (+160 nm). Lastly, the central cavity and the peculiar shape of the NPs in Figure 9C proved the success of the core removal procedure to give the pH-sensitive NCs.

Table 1: *Size of the intermediates for the synthesis of pH-sensitive hollow NCs. The values represent means ± standard deviation (n=50).*

Synthesis step	**Size standard ± deviation**
PMAA cores	190±15 nm
PMAA@P(MAA-*co*-PEGMA-*co*-MBA)	350±15 nm
Hollow NCs P(MAA-*co*-PEGMA-*co*-MBA)	350±15 nm

Fourier Transform Infrared Spectroscopy

The Fourier Transform Infrared Spectroscopy (FT-IR) was used to investigate the chemical structure of the intermediates and the final hollow NCs (Figure 10). The black line represents

the spectrum of the PMAA cores, where the most characteristic peaks are: 1701 cm^{-1} C=O stretching of the carboxylic group; 1487 cm^{-1} C-H asymmetrical bending; 1393 cm^{-1} C-H symmetrical bending; 1261 cm^{-1} O-H bending; 1168 cm^{-1} C-O bending. The synthesis of the pH-sensitive shell (red line) scarcely modified the spectrum of the system. The sole noticeable difference is the presence of the peak at 1531 cm^{-1}, the N-H amide bending (amide II band) of MBA. After the core removal process (blue line), the intensity of the peaks of MAA was decreased and some previously hidden peaks, belonging to the other components of the shell, became visible: 1640 cm^{-1} C=O amide stretching (amide I band) of MBA; 1110 cm^{-1} C-O-C ether asymmetrical stretching of PEGMA. The bands in the range 2800–3000 cm^{-1} present in each spectrum are attributed to the stretching vibrations of the CH_2 and CH_3 groups.

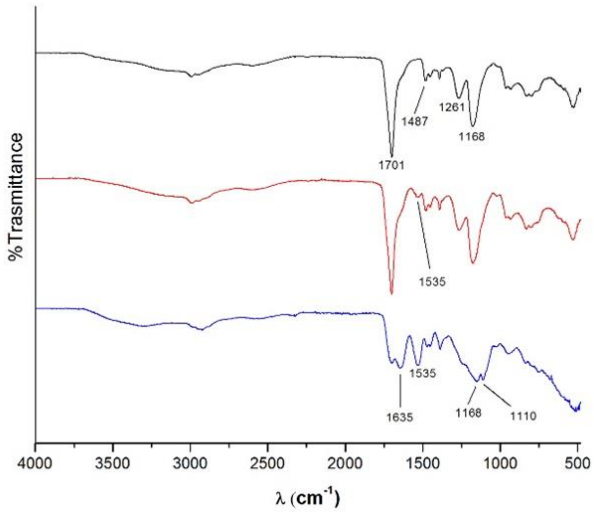

Figure 10: *FT-IR spectra of PMAA cores (black), core-shell structures (red) and hollow NCs (blue).*

Dynamic Light Scattering

DLS was used to acquire information about the size distribution, degree of polydispersity and aggregation of the particles dispersed in water. For a spherical particle like the hollow NCs, the hydrodynamic diameter is essentially the same as the geometric particle diameter plus any possible solvation layers.

The DLS hydrodynamic diameter in distilled water of the hollow NCs was found to be 554.4±16.23 nm and the sample resulted narrowly-moderately polydisperse (PDI 0.163±0.035). The ζ potential was negative as expected (-43.1±0.436 mV) due to the negative charges of the carboxylate anions of PMAA in distilled water. It was not possible to measure the synthesis intermediates because the cores are water soluble.

3.3.3 Drug loading

Daunorubicin was loaded into the NCs using a well-established procedure[31,72,75]. The success of the process was evaluated by the parameters encapsulation efficiency (EE%) and loading capacity (LC%), which were respectively 87.1±2.9 and 47.2±0.1 (Table 2). The system exhibited remarkable encapsulation ability under the described experimental conditions.

Table 2: *Results of the drug loading experiments. The values represent means ± standard deviation (n=3).*

EE%	LC%	mg DNR/mg NCs	µmol DNR/mg NCs
87.1 ± 2.9	47.2 ± 0.1	893	1.69

The loading process of DNR into the hollow NCs entirely depends on the interactions between the functional groups of the dissolved drug and the delivery system. The key interactions in this context are electrostatic interactions between the negatively charged NCs and the positively charged drug molecules. In pH 7.4, where the experiments were run, the PMAA carboxylic groups are mainly negative (pKa ca. 4.5; $-COO^-$) and the DNR amino groups are partially positive (pKa 8.6;[76] $-NH_3^+$), resulting in the formation electrostatic interactions promoting the encapsulation. Also hydrogen bonds plays a fundamental role involving other non-ionized functional groups: for example protonated carboxylic groups, amide group of the cross-linking agent and PEG chains can interact through hydrogen bonding with the functional groups of DNR, such as its carbonyl and hydroxyl groups.[75]

3.3.4 Drug release

The capability of the system to release the drug under the stimulus pH was tested with the drug release experiment. The loaded NCs were put into dialysis bags and incubated in the release media at different pH, that is pH 4, 5.5 and 7.4. At the designed time point, 1 ml of each medium was analyzed to determine the concentration of the drug in the medium and therefore the percentage of drug released along the time (Figure 11).

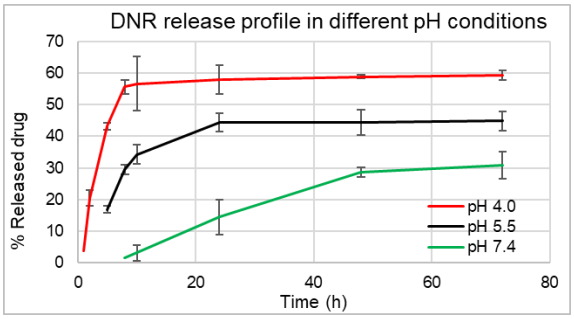

Figure 11: *Drug release profiles of the hollow NCs at pH 7.4 (green), pH 5.5 (black) and pH 4.0 (red). Error bars are based on mean ± SD of three experiments.*

This result shows that the system is pH-sensitive since the amount of released drug varies depending on the pH of the environment. After 72 hours, the amount of drug released was roughly 60% in pH 4.0, 45% in pH 5.5 and 30% in pH 7.4. Also, the plateaus (no drug, or very little amount, is released) are reached at different time points depending on the pH, that is 5h in pH 4.0, 24h in pH 5.5 and 48h in pH 7.4. In other words, the hollow pH-sensitive NCs respond to different pH conditions by releasing different amount of drug with different kinetics: the more acidic the release medium is, the faster and the larger the amount of drug released.

The behavior shown in Figure 8 can be explained by considering the interaction between DNR and the carboxylic groups of the NCs. At slightly basic pH levels (7.4) the carboxylic groups of PMAA are deprotonated and can interact electrostatically with the protonated amino group of DNR (pKa 8.6) favoring the retention of the drug in the NCs, as explained for the encapsulation process. In pH 5.5, a lower percentage of carboxylic groups is protonated, which causes a decrease in the number of interactions shell-drug and consequently a larger amount of drug is released in these conditions. At pH 4.0 the carboxylic groups are mainly protonated, therefore there will be only few electrostatic interactions and the drug will be more easily released than in the previously-described conditions.

3.4 Three-stimuli-sensitive Nanocontainers

A second DDS was designed and synthesized for the loading and release of DNR. This system is a hollow three-stimuli sensitive NCs, responsive to pH, redox condition and temperature variations. The results presented below were also published in the journal Scientific Report.[35]

The rationale behind the design of a three-stimuli sensitive system is that tumors present several pathological alterations that cannot be found in healthy tissues. Multi-responsive materials combine multiple sensitivities, resulting in a stricter control on the drug release. Multi-sensitive DDS response can be optimized for each independent stimulus of interest, but also the overall system can be fine-tuned in terms of composition and properties to respond opportunely when exposed to the combined effect of multiple stimuli.[77] In light of these considerations, many multistimuli-sensitive or “smart” drug delivery systems have been recently proposed[30–34]. Among the exploited pathological alterations, the best known and the most used are: the lower pH compared to normal tissues [36–38], the difference in temperature[40,43,44], higher in tumoral areas, and the concentration of glutathione[78–80], which is at least four-fold higher in tumoral cells[46].

The proposed system consists of three different shells, each one responsible for one specific sensitivity. Multi-sensitive drug delivery agents usually concentrate all the sensitivities in a single layer, where the units responsible for the sensitivities are mixed together. In this case, the system was designed with three different shells, aiming at gaining even more control on the sensitivities by optimizing each synthesis step. The DDS was synthesized in a layer-by-layer manner, obtained with a sequence of DPPs. The first shell wes responsible for the pH-sensitivity of the drug delivery system. It was synthesized by using MAA as the main monomer as reported for the hollow pH-senstive NCs (3.3.1). The second shell is temperature responsive: it senses the variations in temperature because of the presence of N,N'-dimethylaminoethyl methacrylate (DMAEMA) as the main monomer of the shell.[45,81] Its polymer, PDMAEMA, exhibits the so-called lower critical solution temperature (LCST). Above this temperature, the polymer turns insoluble and changes its hydrogen-bonding properties: intra- and inter-molecular hydrogen bonds become favored compared to the interactions with the surrounding environment, such as the solvent and the encapsulated drug.[40,45,82] In this condition, the second shell is no longer available for interacting with DNR, which is consequently released. The third shell is redox sensitive, due to the crosslinking agent N,N-Bis(acryloyl)cystamine (BAC): this monomer has a disulfide bond and it is easily broken in presence of reducing agents.[42,46] The monomers responsible for the temperature and redox sensitivities are shown in Figure 12.

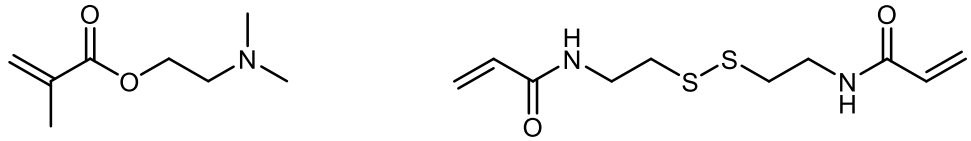

2-(dimethylamino)ethyl methacrylate N,N'-bis(acryloyl)cystamine

Figure 12*: Monomers responsible for the temperature and redox responsivity of the second and third shell, respectively. N,N'-dimethylaminoethyl methacrylate (DMAEMA) and N,N-Bis(acryloyl)cystamine (BAC).*

3.4.1 Synthesis

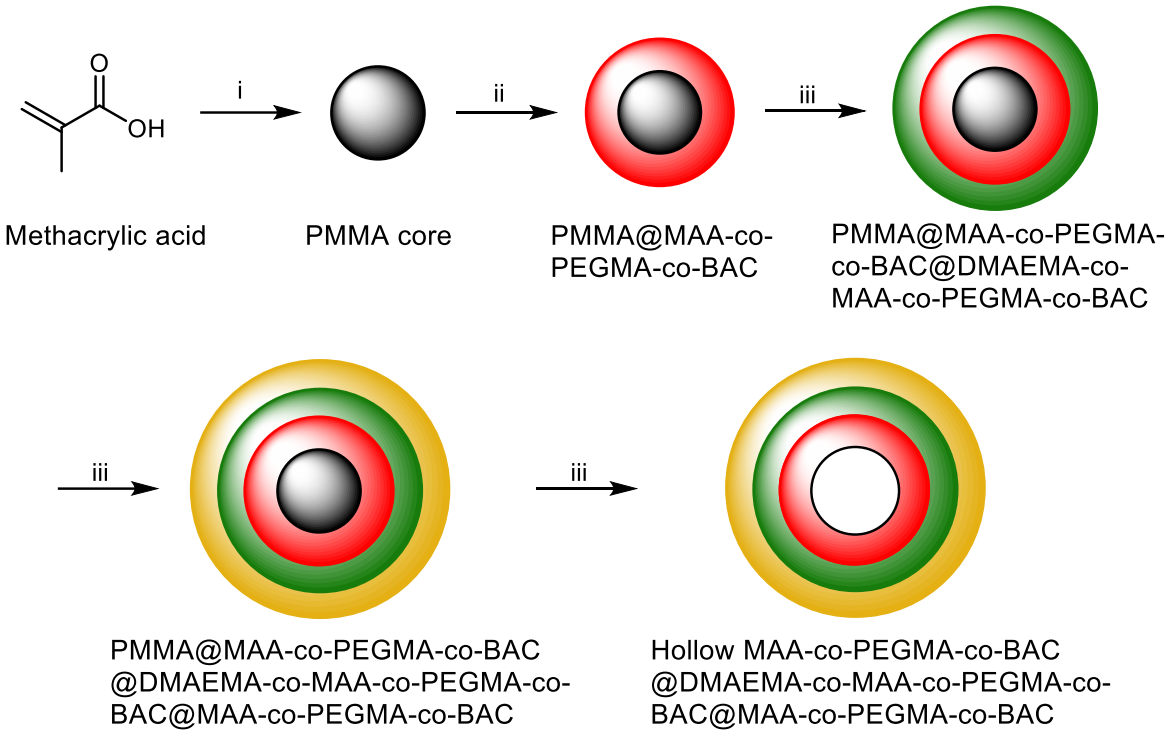

Figure 13: *Synthesis scheme of the three-stimuli-sensitive hollow NCs. (i) Distillation-precipitation polymerization: MAA, AIBN, nitrogen bubbling in ACN 80°C → 100°C; (ii) Distillation-precipitation polymerization: MAA, PEGMA, BAC, AIBN, nitrogen bubbling in ACN 80°C → 100°C; (iii) Distillation-precipitation polymerization: DMAEMA, MAA, PEGMA, BAC, AIBN, nitrogen bubbling in ACN 80°C → 100°C; (iv) Distillation-precipitation polymerization: MAA, PEGMA, DMAEMA, AIBN, nitrogen bubbling in ACN 80°C → 100°C; (v) Core removal in a mixture of water/EtOH (1:1).*[35]

The multi-responsive NCs were obtained with a sequence of four DPPs followed by the core removal. After the formation of the sacrificial cores, the three shells were synthesized in this order: pH-, temperature and redox-sensitive. Lastly, the core removal gave the three-stimuli-sensitive hollow NCs (Figure 13). The first two step of the synthesis, the formation of the cores and first shell, are identical to what was reported for the pH-sensitive NCs and were prepared by following a very similar procedure. Also, the chemical explanation of the core and shell formation mechanism shown in Figure 8 is representative for this DDS as well.

3.4.2 Characterization

Scanning Electron Microscopy

Figure 14 shows the synthesis intermediates and the hollow three-stimuli-sensitive NCs where the NPs are spherical and monodisperse. In Figure 14E are the hollow NCs, the visible central cavity in the NPs prove the successful core removal. Table 3 reports the size of the NPs; from the increase in diameter of the NPs after each modification (a single shell

increased the diameter of roughly 30 nm), it is possible to conclude that each DPP produced a shell.

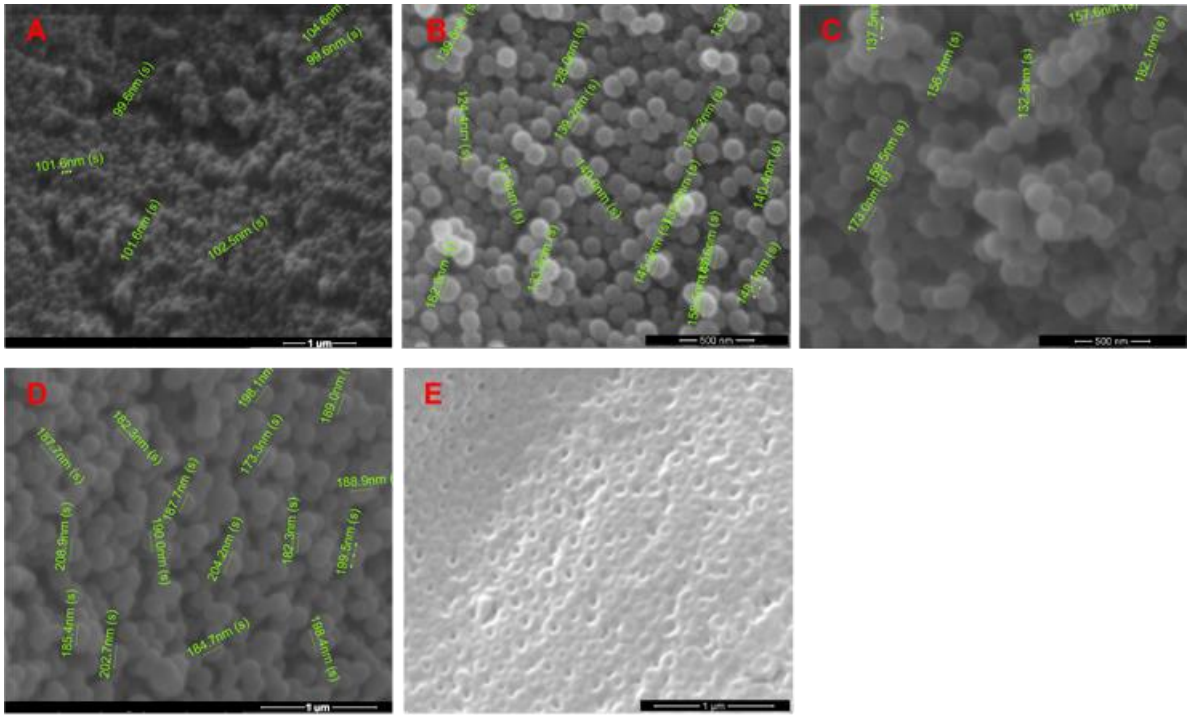

Figure 14: *SEM images of:* ***A.*** *PMAA cores;* ***B.*** *PMAA@P(MAA-co-PEGMA-co-MBA);* ***C.*** *PMAA@P(MAA-co-PEGMA-co-MBA)@P(DMAEMA-co-MAA-co-PEGMA-co-MBA);* ***D.*** *PMAA@P(MAA-co-PEGMA-co-MBA)@P(DMAEMA-co-MAA-co-PEGMA-co-MBA)@P(MAA-co-PEGMA-co-BAC);* ***E.*** *Hollow P(MAA-co-PEGMA-co-MBA)@P(DMAEMA-co-MAA-co-PEGMA-co-MBA)@P(MAA-co-PEGMA-co-BAC).*[35]

Table 3: *Size of the intermediates for the synthesis of three-stimuli-sensitive hollow NCs. The values represent means ± standard deviation (n=50).*

Synthesis step	**Size standard ± deviation**
PMAA cores	100±10 nm
PMAA@P(MAA-*co*-PEGMA-*co*-MBA)	130±10 nm
PMAA@P(MAA-*co*-PEGMA-*co*-MBA)@P(DMAEMA-co-MAA-co-PEGMA-co-MBA)	160±15 nm
PMAA@P(MAA-*co*-PEGMA-*co*-MBA)@P(DMAEMA-co-MAA-co-PEGMA-co-MBA)@P(MAA-*co*-PEGMA-*co*-BAC)	190±15 nm
Hollow P(MAA-*co*-PEGMA-*co*-MBA)@P(DMAEMA-co-MAA-co-PEGMA-co-MBA)@P(MAA-*co*-PEGMA-*co*-BAC)	190±15 nm

Fourier Transform Infrared Spectroscopy

Fourier transform infrared (FT-IR) was used to characterize the chemical structure of the system and confirm the synthesis of the shells (Figure 15). The spectra of the PMAA cores and the first shell are identical to what reported for the pH-sensitive NCs. The monomers used for the formation of the three shell are all fairly similar and therefore it was not possible

to notice new peaks corresponding to new functional group due to the formation of the second and third shells. The success of the DPPs could only be confirmed by some variations in intensity of the pre-existing peaks due to signal overlaps. Specifically, the formation of the second shell was proved by the increase in intensity of the peak at 1261 cm^{-1} (highlighted with the dotted line in Figure 15c), due to the overlap between the C-0-C ester stretching of DMAEMA and the O-H bending of MAA. After the formation of the third shell, the intensity of the peak at 1531 cm^{-1} in Figure 15d increased because of the overlap of the N-H amide bending peaks belonging to BAC and MBA. The core removal affected the overall configuration of the spectrum: the intensity of the PMAA characteristic peaks (1701 cm^{-1} and 1168 cm^{-1}) decreased, showing some previously-covered peaks such as the C=O amide stretching of MBA and BAC (1640 cm^{-1}) and the C-O-C ether asymmetrical stretching at of PEGMA (1110 cm^{-1}).

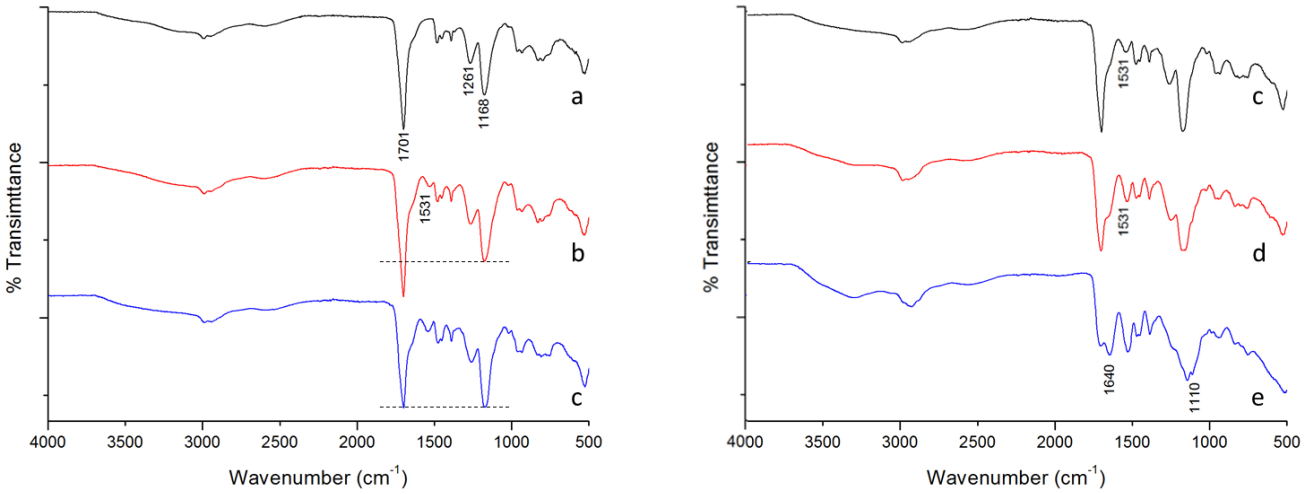

Figure 15: *FT-IR spectra of:* ***a.*** *PMAA cores;* ***b.*** *PMAA@P(MAA-co-PEGMA-co-MBA);* ***c.*** *PMAA@P(MAA-co-PEGMA-co-MBA)@P(DMAEMA-co-MAA-co-PEGMA-co-MBA);* ***d.*** *PMAA@P(MAA-co-PEGMA-co-MBA)@P(DMAEMA-co-MAA-co-PEGMA-co-MBA)@P(MAA-co-PEGMA-co-BAC);* ***e.*** *Hollow P(MAA-co-PEGMA-co-MBA)@P(DMAEMA-co-MAA-co-PEGMA-co-MBA)@P(MAA-co-PEGMA-co-BAC).*[35]

Dynamic Light Scattering

The hydrodynamic diameter of the three-stimuli sensitive NCs was measured with DLS. The experiments were run in different pH conditions to see whether the pH affects the hydrodynamic diameter of the NCs (the experiment was run in pH 2, 4, 7 and 10). The results are reported in Table 4. Firstly, it must be noticed that the diameter obtained with DLS is much larger than the one obtained with SEM (190 nm). This effect is due to the interaction between the hydrophilic NCs and the aqueous environment, where the NCs assumed a “swollen state”, in contrast to the dry state in SEM samples.[83] In pH 7 the hydrodynamic diameter was found to be 408±45.3 nm. When the pH was decreased to 2,

the NCs showed the tendency to aggregate, as seen by the extremely large results of 1840 nm.

Table 4: *Hydrodynamic diameter (D_h) of the hollow NCs in different pH conditions. The values represent means ± standard deviation.*

	pH 2	**pH 4**	**pH 7**	**pH 10**
D_h (nm)	1840±140.2	813.8±70.1	408±45.3	514.0±51.7
PDI	0.609±0.085	0.625±0.045	0.367±0.059	0.559±0.122

This phenomenon can be explained by considering that the carboxylic groups of PMAA were completely protonated in such conditions and tended to associate one another via hydrogen bonds. In pH 4 the hydrodynamic diameter was found to be 813 nm, which describes a situation where aggregates and single NCs coexist, giving an intermediate result. Here the fraction of protonated carboxylic group decreased, but –COOH was still the preponderant form. The diameter in pH 10 was 514 nm because in this conditions the carboxylic groups of PMAA were completely dissociated, resulting in the Donnan osmotic swelling of the polymeric network.

3.4.3 Drug loading

The three-stimuli-sensitive NCs were loaded with the anticancer drug DNR and the results in terms of EE% and LC% are summarized in Table 5.

Table 5: *Results of the drug loading experiments. The values represent means ± standard deviation (n=3).*

EE%	**LC%**	**mg DNR/mg NCs**	**µmol DNR/mg NCs**
85.3 ± 1.4	63.0 ± 0.4	1.71 ± 0.03	3.24 ± 0.05

These results depend on the formation of electrostatic and hydrogen-bonding interactions between DNR and the NCs, as described for the pH-sensitive NCs (3.3.3). The LC% and the amount of DNR loaded per mg of polymer here are higher because the amount of DNR in feeding was higher as well, as reported in the Experimental section (3.2.2). Specifically, the ratio DNR/polymer (mg/mg) here was 2:1 and for the pH-sensitive NCs was 1:1.

3.4.4 Drug release

The DNR release profile of the three-stimuli-sensitive NCs was investigated with *in vitro* drug release experiments under different conditions of pH, temperature and in presence or absence of reducing agents (Figure 16). Each graph (A, B and C) represents a different pH condition: the black lines show the effect of pH without any other stimulus, the green lines show the effect of the presence of 10mM of GSH and the red lines of increased temperature (40°C). Considering the black line first, the amount of released drug in pH 7.4, 6 and 4 were

respectively 40%, 68% and 98% after 48h. This behavior depends on the difference in strength of the interaction between the NCs and the DNR molecules. In pH 4.0 the protonated carboxylic groups of PMAA were incapable of forming electrostatic interactions with the positive amino group of DNR. Furthermore, hydrogen-bonding interactions are known to be weaker in low pH, favoring the release. [36] In pH 6 and 7.4 the carboxylic groups are protonated to a larger extent and therefore capable of interacting with the DNR through electrostatic interactions, which justifies the results of 68% and 40% respectively after 48h.

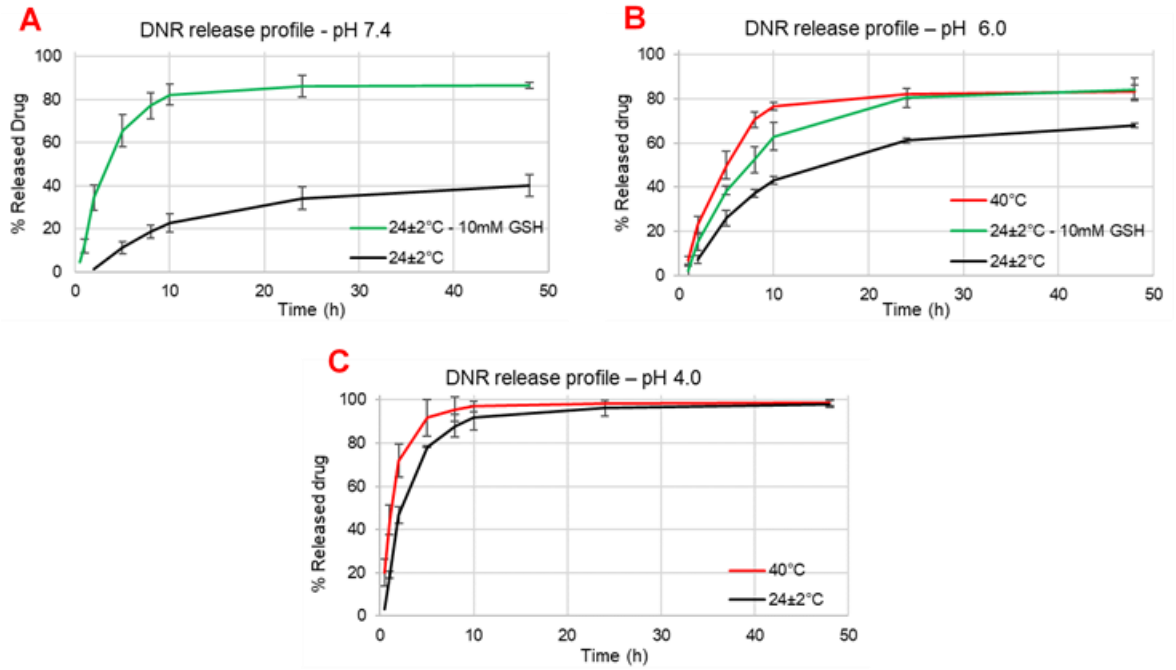

Figure 16: *In vitro drug release experiments under different conditions.* ***A****) results obtained in pH 7.4;* ***B****) results obtained in pH 6.0;* ***C****) results obtained in pH 4.0. Error bars are based on mean ± SD of three experiments.* [35]

The temperature responsivity of the system, given by the second shell, is shown by the red lines in the graphs. Considering pH 6.0 (Figure 16B), the amounts of released drug after 48 at room temperature and at 40°C were respectively 67% and 83%. Also the release kinetic was different, after only 2h at 40°C the system released 23%, which corresponds to an increase by 16% compared to the sole pH stimulus (7%). When the system was exposed to pH 4.0 (Figure 16C), after 48h all the payload was released regardless the temperature, but after 2h 71% of the drug was released at 40°C and only 46% at 24±2°C. These results confirm that the system responds to increased temperature by releasing an increased amount of drug.

In green are shown the experiments in presence of glutathione (GSH) 10 mM. In Figure 16A (pH 7.4) the system released 87% of drug in presence of GSH and 40% without reducing agents. In pH 6.0, shown in Figure 16B, in presence and absence of GSH the system released 84% and 68% respectively. This behavior is due to BAC, the cross-linking

agent used for the synthesis of the third shell, which has a disulfide bond that is rapidly broken in presence of reducing agents. Also, the effect of GSH is known to be pH dependent and at pH 7.4 it is more effective than in pH 6.0, which agrees with what was found here.[84]

The *in vitro* drug release experiments run in simulated tumor conditions showed the system capable of quickly releasing a larger amount of drug in presence of the three selected stimuli, therefore proving the hollow NCs three stimuli sensitive.

3.4.5 Cytotoxicity

The cytotoxicity of the DNR-loaded NCs and free NCs was tested with the MTT assay on MCF-7 (human breast carcinoma cells) and HEK-293 (human embryonic kidney cells). The cells were treated for 24 h with free DNR, DNR-loaded NCs (DNR in the range of 0.01 - 60 μM) and free NCs (0.006 - 35.2 μg/ml) and the results were expressed as percentages of cell viability (Figure 17).

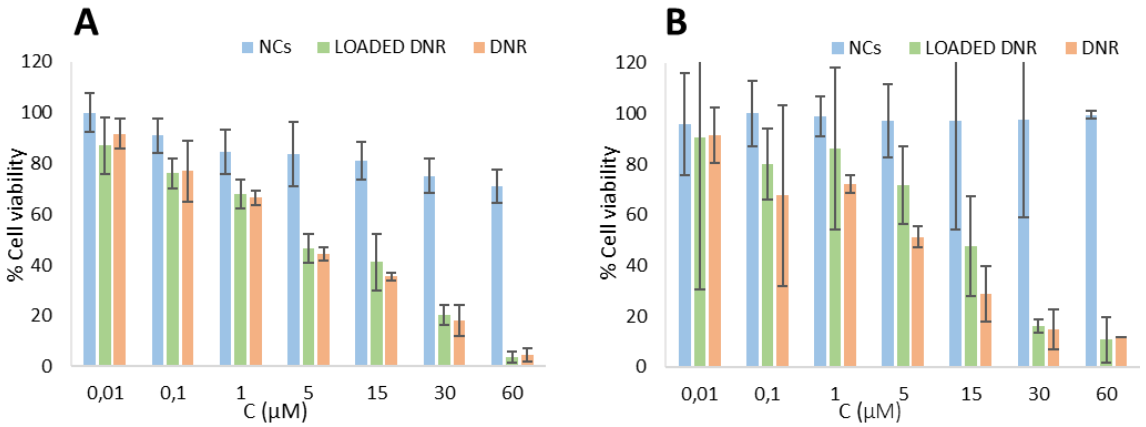

Figure 17: *Evaluation of cell viability via MTT assay. Cytotoxicity in MCF-7 (A) and HEK-293 (B). Error bars are based on mean ± SD of three experiments run in triplicates.*[35]

The cytotoxicity of free DNR and DNR-loaded NCs was statistically identical regardless the concentration and the free NCs exerted only marginal toxicity, even at high concentrations. The MTT assay confirmed that the NCs were non-toxic and capable of releasing almost 100% of the encapsulated drug in tumor environment without affecting its activity. Even though the toxicity of free and loaded DNR is identical, it has to be taken into consideration that the encapsulated DNR has the advantage of being selectively carried to the cancer cells by virtue of the NCs and their passive targeting, while free DNR also distributes to healthy tissues causing the severe side effects mentioned above.

3.4.6 Intracellular localization

As explained before, the target of DNR is DNA and therefore the drug released from the NCs has to be delivered into the nuclei of the treated cells. Confocal laser scanning

microscopy was used to investigate the intracellular localization of the released drug. As shown in Figure 18, both free and encapsulated DNR were localized in the nuclei of the cells, where they could exert their functions and stop the cell proliferation.

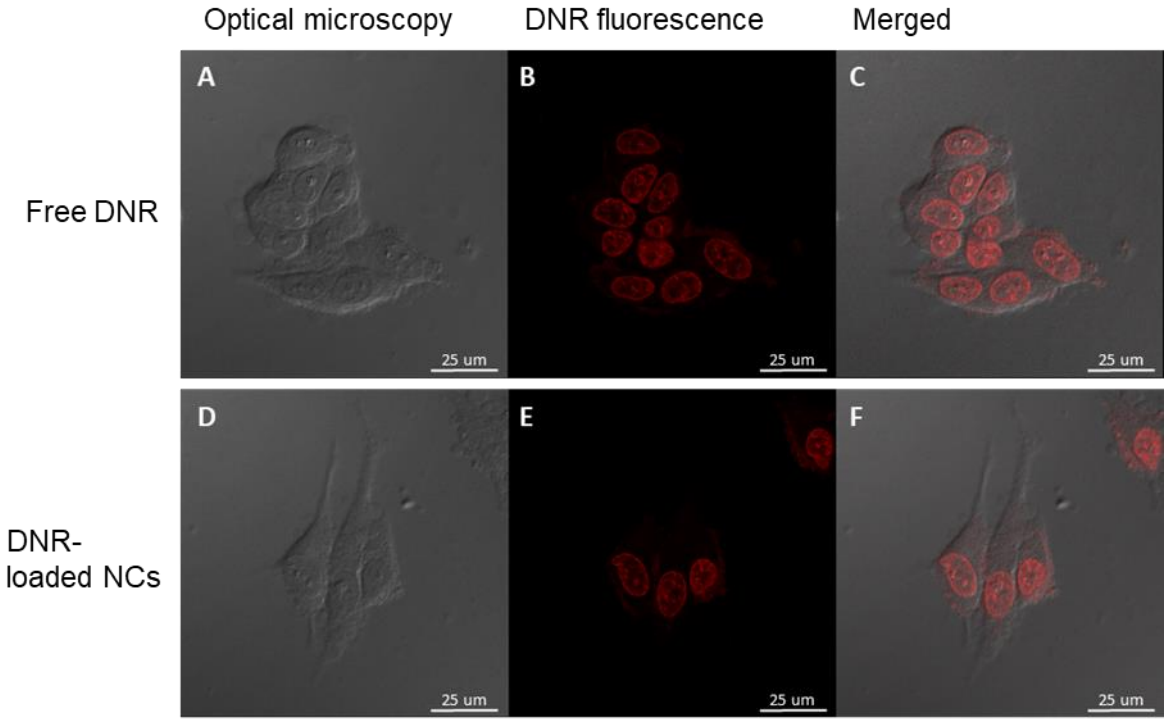

Figure 18: *Intracellular localization of free DNR (A-C) and DNR-loaded NCs (D-F) in MCF-7 cells after 2h incubation.*[35]

It is worth mentioning that this experiment was not meant to prove that the NCs preferentially localize into cancer cells after systemic administration, which could be done only by means of *in vivo* experiments, beyond the scope of this work. The goal of this experiment was to demonstrate that the encapsulated DNR eventually localizes into the nuclei of the cells, and therefore the encapsulation does not interfere with the final localization of the drug.

3.5 Conclusion

Both systems showed promising results in terms of stimuli-dependent and sustained release. The pH-sensitive system showed excellent loading ability and the pH-sensitivity was confirmed with *in vitro* drug release experiments. The release kinetics of this system are being currently analyzed with a mathematical model. This study will give a more detailed insight into the roles of the bounds between polymer and drug and how they behave in different pH conditions. The DNR-loaded three-stimuli-sensitive NCs showed remarkable anti-cancer activity and, by virtue of their capability of preferentially accumulate into tumors due to passive targeting, they can be considered a promising platform to develop injectable

DDSs for the controlled release of anthracyclines. The results obtained with the three-stimuli-sensitive DDS have been published in Scientific Reports.

Somatostatin

4.1 Introduction

Somatostatin (also known as somatotropin release-inhibiting factor or growth hormone release-inhibiting factor, SST) is an endogenously-produced cyclic peptide of 14 amino acids that has recently attracted attention because of its high therapeutic potential (Figure 19). SST is physiologically involved in the inhibition of the secretion of multiple hormones (e.g. growth hormone, insulin, glucagon, gastrin), gastric acid and pancreatic enzymes. In the central nervous system, this peptide acts as a neurotransmitter and affects locomotor activity and cognitive functions.[85] SST exerts its activity by binding to at least five different subtypes of specific receptors (SSTR 1-5) located on the target cells. The involvement of the peptide in such a wide range of biological activities can be exploited for the treatment of a variety of human diseases.[86,87]

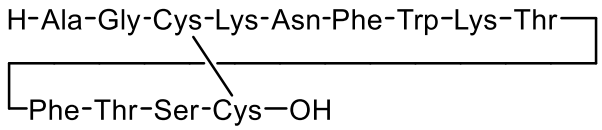

Somatostatin

Figure 19: *Amino acid sequence of the peptide somatostatin (SST).*

Several clinical trials demonstrated impressive efficacy of somatostatin and its analogues in hypersecretory disorders such as acromegaly, pancreatic ascites and pancreatic cholera.[88] In addition, the antineoplastic and anti-proliferative activity of SST was confirmed in several experimental model, both *in vitro* and *in vivo.* SST proved to be useful in the treatment of gastrointestinal neoplasms of endocrine origin, including Zollinger-Ellison syndrome, insulinoma, glucagonoma, and carcinoid tumors. Clinical experience with SST and analogs has also shown that they are well tolerated compared to other antineoplastic therapies currently in use.[88–90]

Despite such therapeutic potential, the peptide displays a very short biological half-life (in plasma roughly 1 minute) and therefore the treatments generally require continuous infusion regimen[85]. To date, many delivery systems have been studied and tested to overcome this problem. Among those, both lipid[91] and polymeric[92] carriers have been used, but this field of research still remains very active.

In collaboration with the group of dr. Chatgilialoglu and dr. Ferreri in CNR, Bologna, part of the Ph.D. involved in the study of two different drug carriers for SST. The aim of this project was to identify a DDS acting as a long-circulating depot of SST, capable of releasing the peptide in a prolonged manner and simultaneously protecting it from degradation. Some preliminary experiments on the peptide, such as the time- and pH-dependent stability, were run in Bologna and used by the student as a starting point for the design of the encapsulation/release experiments.

In this framework, the polymeric pH-sensitive NCs described for DNR were used for encapsulation and pH-dependent release studies of SST. The conformation of the peptide was monitored by circular dichroism (CD) to assess whether the native-like structure of SST was retained and to identify any possible degradation phenomenon. In addition, a formulation of SST-containing nanoemulsion (NE) was prepared by the group in CNR and its release profile and protecting activity were analyzed with LC/MS.

4.2 Experimental

4.2.1 Materials and Method

Somatostatin (SST) was received form Bachem and used with no further purification. Formic acid and ammonium formate were purchased from Sigma-Aldrich and used as received.

Materials and instruments used for the synthesis and characterization of the pH-sensitive hollow NCs are reported in section 3.2.1.

4.2.2 pH-sensitive NCs

The procedure for the synthesis of the pH-sensitive NCs is described in 3.2.2.

Loading experiment

Several experimental conditions were tested in order to identify the best option. In particular, the concentration of the citrate buffer pH 5.0 (0.1 M – 0.001M) and the ratio SST(mg): NPs (mg) were studied as variables. The procedure below was considered the most efficient and formulation produced accordingly was used for the drug release experiments.

1 mg of NCs were suspended in 1 ml of citrate buffer pH 5.0 0.005M. Then, 2 mg of SST was added and the final suspension was gently stirred (ca. 320 rpm) for 5h. The non-encapsulated SST was completely removed by centrifugations and resuspensions in fresh citrate buffer (5 min x 13000 rpm), 5 cycles were necessary. The amount of encapsulated SST was determined with by UV spectroscopy and calculated by the difference of SST

concentration between the original SST solution and the resulting supernatant after the loading process. The calculations were based on a standard curve of SST in citrate buffer pH 5.0 (λmax 280 nm). The parameters used to evaluate the encapsulation were Encapsulation Efficiency (EE%) and Loading Capacity (LC%) (see 3.2.2 loading of DNR). The experiment was carried out three times for statistical analysis.

In-vitro release experiment

The release behavior of the NCs was tested with the dialysis bag method (dialysis tube MWCO 140 kDa). In order to study the pH sensitivity of the drug delivery system, the release experiments were run in acidic environment (citrate buffer pH 4.0, 0.005M) and in slightly basic environment (phosphate saline buffer, pH 7.4, 0.005M). In particular, 1.0 mg of NCs were suspended in 0.5 ml of buffer, loaded in the dialysis bags and incubated in 20 ml of the buffer solutions at 37°C. At different time points (30 min, 1h, 2h, 4h, 6h, 9h, 12h, 24h), 1 ml was collected from each solution. The concentration of the samples was measured with UV-vis and the calculations were made upon a standard curve of SST recorded for each buffer (λmax 280 nm). A standard curve of SST was recorded in each buffer used as release medium.

Structural study of somatostatin – Circular Dichroism

Circular dichroism (Jasco J700 spectropolarimeter) was used to evaluate the conformation of SST after the encapsulation and release processes. The spectra of the non-encapsulated and released SST were recorded and compared with the spectrum of fresh SST as a reference. All the samples were prepared in order to have the same concentration (0.015 μmol - measured with UV-vis). For the encapsulation, the supernatant collected after the loading experiment (containing the non-encapsulated fraction of SST) was directly analyzed and the spectrum was compared with the one of a solution of fresh SST. Regarding the possible degradation due to the release process, 3 ml of both release media (pH 4.0 and pH 7.4) were collected at 6h time point, freeze-dried, then dissolved in distilled water, in order to obtain equally concentrated samples. These solutions of released SST were analyzed with CD and compared with a solution of fresh SST as a reference.

4.2.3 Nanoemulsions

Formulation, preparation and characterization of the SST-containing NE were optimized and carried out by the group of dr. Chatgilialoglu and dr. Ferreri in CNR, Bologna.

LC/MS analysis

Agilent 1260 Infinity automated LC/MS purification system was used and the analyses were run with a reverse phase C-18 column (ZORAX SB-C18 Rapid Resolution HT 2.1x50 mm

1.8 micron 600 Bar). A Phenomenox HPLC guard cartridge was used as well. The mobile phases were (A) H_2O + 0.1% formic acid and (B) Acetonitrile + 0.1% formic acid. The samples were eluted with a linear gradient of B from 5% to 90% in 15 min, B was then decreased to 5% in 5 min (20 min) and kept so for 5 min (25 min).

In vitro Release experiments in buffer

The release experiment was designed to analyze not only the directly released SST (in the release medium) but also the amount of non-released SST, still in the lipid droplets (indirect analysis).[91] Two different protocols were followed: (1) the freeze-dried NE was reconstituted to start the release experiment; (2) after reconstitution in water, the NE was immediately centrifuged, the lipid fraction was isolated and re suspended in citrate buffer pH 5.0 0.1M to start the experiment. SST-containing NE were kept in a horizontal shaker at 37°C (stirring rate 100 rpm). Reached the time point (0 min, 1h, 3h, 6h, 24h), three samples for each protocol of 0.2 ml were collected, centrifuged (15000 rpm x 5 min x 4°C) and 50 µl of supernatant were directly analyzed via LC/MS (direct analysis). The remaining lipid pellets were then dissolved in a mixture of hexane/formate buffer pH 3.0 (0.2 ml each, total volume 0.4 ml), vortexed for 5 min and after 10 min 50 µ of aqueous phase were withdrawn and analyzed with LC/MS (indirect analysis). The experiment was carried out three times for statistical analysis.

In vitro release profile in human plasma

Two different protocols were followed: (1) the freeze-dried NE was reconstituted directly in human plasma to start the release experiment; (2) after reconstitution in mq water, the NE was immediately centrifuged, the lipid fraction was isolated and suspended in human plasma to start the experiment. SST-containing NE were kept in a horizontal shaker at 37°C (stirring rate 100 rpm). Reached the time point (0 min, 1h, 3h, 6h, 24h), three samples of 0.2 ml for each protocol were collected and centrifuged (15000 rpm x 5 min x 4°C). To 100 µl of the so-obtained supernatant were added 100 µl of TCA 6% (final concentration of TCA 3%) and the product was put in ice bath for 10 min and centrifuged again (15000 rpm x 5 min x 4°C). 100 µl of the resulting supernatant were collected, quenched with a solution of NaOH 1M (11 µl) and analyzed via LC/MS.[93] The indirect analysis was nor performed due to incompatibility with the HPLC column.

4.3 pH-sensitive Nanocontainers

The pH-sensitive NC described in paragraph 3.3 was employed as drug delivery system for SST. The NCs could encapsulate and release SST in a pH-dependent manner without affecting its structure, proving the NC to be a selective drug delivery system that both

preferentially releases SST in tumor areas and lengthens SST half-life by releasing it in a prolonged and controlled manner.

Being SST extremely unstable, degradation was monitored after the encapsulation and during the release experiments. CD was chosen as the best methodology, since it is regularly used to evaluate the conformation and the secondary structure of proteins and peptides.[94] Besides, CD spectra are the sum of all the structural elements of the analyzed peptide/protein and it is also widely used to study tertiary structures, structural transitions and aggregation phenomena.[95,96]

4.3.1 Loading experiment

The loading experiments of SST into the hollow NCs were run in different conditions to optimize the results. The choice to run the experiment in buffer pH 5.0 for 5 hours was based on the stability studies previously run by the collaborators in Bologna. In particular, SST was reported to be most stable at pH 5.0, where its native-like structure was retained up to 6 hours.

The first critical factor to be considered was the concentration of the buffer. On the one hand, buffered solutions have been reported to increase the stability of SST. On the other hand, CD spectra are affected by salt concentration, resulting in poor quality signals.[95] The concentrations tested for the loading experiments were 0.1 M, 0.01 M, 0.005 M and 0.001 M; the results are shown in Figure 20.

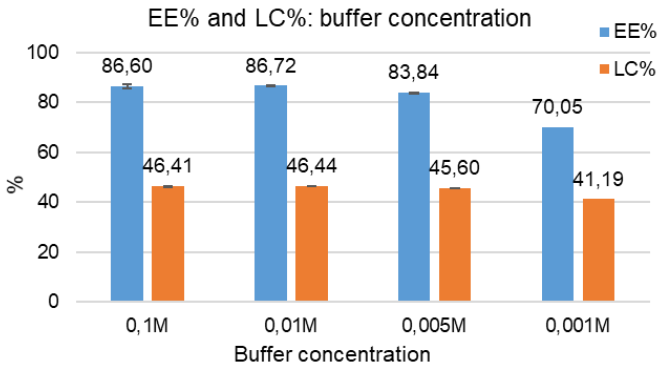

***Figure 20**: Dependence of EE% and LC% on the concentration of the buffer. Error bars are based on mean ± SD of three experiments.*

The best EE% and LC% were obtained by using 0.1M and 0.01M citrate buffer and the results in these conditions were statistically identical. When the buffer concentration was decreased to 0.005M, slightly lower EE% and LC% were obtained (respectively, roughly 3% and 1% decrease). A further reduction in concentration (0.001M) affected more evidently the results: EE% was 70% (decrease by 14 percentage points) and in LC% of was 41% (by 4 percentage points). According to the findings of the group in Bologna, SST is

more stable in buffer than in distilled water, probably because of a stabilizing effect of the salts. In very low concentrated buffers, this stabilizing effect may be less intense, resulting in the formation of interactions among the molecules of SST in solution. Probably the resulting aggregates cannot be encapsulated, which may be the reason for the decrease in EE% and LC%. The concentration chosen for the experiments was 0.005M. Although more concentrated buffers allow the encapsulation of a slightly larger amount of SST, higher concentrations of salts interfere with CD signals, and thus it would not be possible to confirm the native-like structure of the peptide after the encapsulation-release processes.

Once optimized the buffer concentration, the second factor to consider was the ratio SST: NCs. The loading experiment was also run with 2 mg of SST: 1 mg of NCs in 0.005M citrate buffer pH 5.0 and the results are shown in Table 6.

Table 6: *EE% and LC% in 0.005M citrate buffer pH 5.0 obtained with different ratios of the components used for the experiment.*

Ratio SST : NCs	**EE%**	**LC%**	**mg/mg of NCs**	**µmol/mg of NCs**
1 mg SST: 1mg NCs	83.84±0.25	45.60±0.07	0.84	0.51
2 mg SST: 1 mg NCs	87.78±2.42	63.70±0.64	1.75	1.07

2 mg of SST: 1 mg of NCs allowed more efficient encapsulation than 1 mg of SST: 1 mg of NCs. Although these findings may sound obvious, more drug in feeding does not always translate into more encapsulated drug. Specifically, when working with aggregation-prone molecules such as SST, high concentrations can favor this phenomenon, leading to less efficient encapsulation (decreased values of EE% and LC%). In addition, NCs have a finite surface area and a finite number of functional groups capable of interactions with SST. Therefore, after a certain amount any increase in SST will not cause more molecules to be loaded but a decrease in the efficiency of the process.

The driving forces for the encapsulation are the electrostatic and hydrogen-bonding interactions between the peptide and the NC, similarly to what already described for DNR. In regard to the electrostatic interactions, at pH 5.0 SST is positively charged due to the amino groups (isoelectric point 10.2)[97] and the hollow NCs are partially negatively charged because of the carboxylate anions of PMAA. In addition, SST is a peptide and therefore it displays many secondary amide moieties (peptide bonds) and other groups in the -R chains that can act as both hydrogen-bonding donor and acceptor.

4.3.2 In-vitro release experiment

The SST release profile was studied in both acidic (pH 4.0, 0.005M citrate buffer) and slightly basic environment (0.005M phosphate saline buffer pH 7.4,). After 24 hours, the

amount of drug released at pH 4.0 and pH 7.4 was respectively roughly 80% and 60%. The hollow NCs responded to acidic pH conditions by releasing a larger amount of SST than at pH 7.4, which again confirms the pH sensitivity of the system (Figure 21).

This different release behavior can be explained by considering the carboxylic groups of PMAA, which are mostly protonated at pH 4.0, thus they no longer interact with the positively charged amino groups of SST. On the contrary, in slightly basic pH (7.4) the carboxylic groups of PMAA are deprotonated and can interact electrostatically with the peptide, favoring the retention of the drug. In addition, the improved release at pH 4.0 also depends on the strength of the hydrogen-bonding interactions, which are weaker in acidic conditions[36].

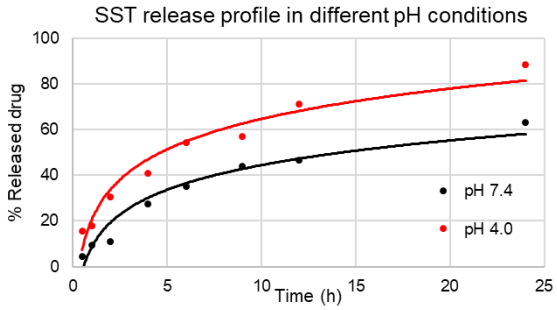

Figure 21: *Drug release profiles of SST-loaded pH-sensitive NCs at pH 7.4 (black) and pH 4.0 (red).*

4.3.3 Structural study of somatostatin – Circular Dichroism

The conformation of SST was studied with CD after the encapsulation and release experiments, in order to investigate whether these processes affect the structure of the peptide[95,96,98]. Figure 22A shows the comparison between the CD spectrum of the supernatant collected after the encapsulation experiment (containing the non-encapsulated fraction of SST) (red line) and the spectrum of a solution of fresh SST (used as a reference - black line). The CD spectra were very similar, which confirmed that the encapsulation process itself does not affect the conformation of SST (the difference between the peaks at 202 nm is 0,24321).

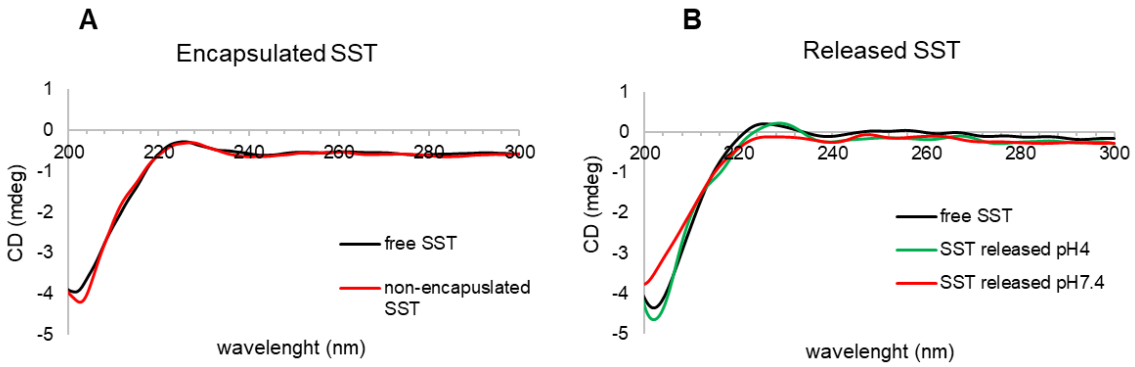

Figure 22: A) *CD spectra of SST collected after the encapsulation experiment (red) and free SST as a reference (black);* ***B)*** *CD spectra of SST released at pH 4.0 (green), pH 7.4 (red) and free SST as a reference (black).*

The conformation of the released peptide was also investigated after the release experiments and the results are shown in Figure 22B. Since CD spectra are concentration-dependent,[95] once the samples were collected (6 h time point) they were freeze-dried and re-solubilized in distilled water, in order to obtain identical concentrations. The solutions of released SST were then analyzed with CD, and compared with a solution of SST as a reference. The CD spectra of the released drug at pH 4.0 and the solution of free SST were very similar (the difference between the peaks at 202 nm is 0,28312). Considering the SST released at pH 7.4, the spectrum was slightly different to the reference (the difference between its peaks and the free SST at 202 nm is 0,81941). CD spectra in Figure 22B show that SST released at pH 4.0 was still in its native-like conformation and therefore the whole processes of encapsulation and release did not affect the structure of SST. On the contrary, when released at pH 7.4 the peptide underwent some structure modification process (e.g. aggregation or degradation). This can be attributed to the low stability of SST in slightly basic conditions, which agrees with the stability experiments reported by the group in Bologna. As a result, the CD spectrum of released SST in pH 7.4 was probably given by a combination of native-like SST (released close to 6h) and aggregates or other degradation products (SST released earlier), due to the low stability in those pH conditions. However, the proven retention in configuration after the release at pH 4.0 confirmed that the encapsulation and release processes do not affect the peptide, but any aggregation/degradation process occurring at pH 7.4 was due to the poor stability of SST in such conditions.

4.4 Nanoemulsion

Lipid-based DDS have proven very promising for the delivery of proteins and peptides.[99–101] The most remarkable advantages of lipids as delivery systems are their biocompatibility and flexibility: lipids can be used for different types of vehicles such as liposomes, lipid microbubbles, inverse lipid micelles, cochlear liposomes, lipid microtubules and nanoemulsions (NEs).[102]

NEs are nano-sized emulsions, which are often employed for improving the delivery profile of active pharmaceutical molecules. Unlike usual emulsions, NEs are thermodynamically stable and the droplet size typically falls in the range 20–200 nm, due to which NEs appear transparent. NE formulations are reported to offer several advantages over other DDS, such as improved biocompatibility, the components are non-toxic and non-irritant and the small-sized droplets, having very large surface area, provide greater absorption.[103,104] Overall, NE formulations can be considered as a safe and completely biocompatible DDS option to increase drug bioavailability[105].

In light of these considerations, NEs were chosen as an advantageous option for delivering SST. The goal of this project was to identify a biocompatible NE-based DDS for SST, guaranteeing prolonged release and improving the stability and the pharmacokinetic of the peptide. The formulation and preparation of the NE were carried out by the group in CNR (Bologna), who also completely characterized it in terms of hydrodynamic diameter, polydispersity index and stability after the freeze-drying procedure. The study of the lyophilization process was fundamental since the formulation was meant to be given as a freeze-dried solid, to be reconstitute prior either oral or intravenous administration. Once optimized all these critical parameters, the NEs were used for the release profile studies with LC/MS as an analytical methodology. Since degradation and aggregation products of SST have different retention times compared to the native peptide, LC/MS is an optimal tool to assess whether the SST is in its native-like structure and there is no need for further conformation analysis with CD.

The release experiments were run in 0.1M citrate buffer pH 5.0 and, in order to test the resistance to the peptidase activity, in human plasma. Citrate buffer pH 5.0 was chosen because it was the buffer used for the preparation of the NEs. Salts cannot be removed by freeze-drying and, when reconstituting the NE in water, the buffered solution would form again. Plasma was used to mimic the release behavior of the system in the blood stream, in order to understand if after administration the system was capable not only of releasing SST in a prolonged manner but also of protecting it from enzymatic degradation.

4.4.1 Preparation and characterization

The best conditions for the preparation of SST-containing NE were studied by dr. A. Larocca in the framework of an industrial Ph.D. project ongoing at the company Lipinutragen (Bologna) in agreement with University of Bologna. In particular, the final NE consisted of 0.5 mg/ml SST, 2mM lecithin and 2% w/v sorbitol in 0.1M citrate buffer pH 5.0. The size of the droplets was estimated by DLS to be below 200nm. The NEs were freeze-dried and the solid was used for the reported release experiments.

4.4.2 Release experiments in buffer citrate pH 5.0

The release experiment was designed to analyze not only the directly released SST (in the aqueous phase of the NE – *direct analysis*) but also the amount of non-released SST, still in the lipid droplets (*indirect analysis*). Since SST is not stable, the determination of the peptide in the lipid phase was meant to collect important additional information for the characterization of the release profile of the NE. The *direct analysis* consisted of measuring the concentration of SST in the aqueous fraction of the emulsion via LC/MS; in the *indirect analysis* the peptide was extracted from the lipid droplets and analyzed by LC/MS.[91]

The release experiments were run following two different protocols. In the first one (Protocol 1 - Figure 23), the freeze-dried NEs were reconstituted in water to recreate the same conditions of the preparation. The second protocol (Protocol 2 - Figure 24) involved a centrifugation after the reconstitution, to remove the aqueous phase of the NE and the fraction of peptide in it; the resulting SST-containing lipid pellet was then suspended in 0.1M citrate buffer pH5.0 to start the release experiment. At the set time points (0, 1h, 3h, 6h, 24h), the samples were collected and analyzed with LC/MS via *direct* and *indirect analysis*. The two protocols were designed to obtain clearer insight into the behavior of SST and release dynamics of the NE. In particular, the first protocol gave information on the behavior of the NE and the variations in repartition of SST between the two phases along the time; the second one on the diffusion of SST from the lipid droplets to the less concentrated aqueous phase. Also, since the experiments were run for 24h the stabilizing effect of NE on SST was evaluated.

The results of the release experiment with protocol 1 (Figure 23) are presented in two ways. In Figure 23A, 100% of released SST refers to the sum of SST found with the *direct analysis* and the *indirect analysis* at each time point. Only the peptide that could be measured (both in the aqueous phase and in the lipid phase of the NE) contributed to this graph, regardless the preparation conditions. In other words, the values in Figure 23A can be considered as the ratio of SST in the two phases (aqueous and lipid) of the NE. In Figure 23B, on the contrary, only the results of the *direct analysis* were used, and 100% was the starting amount of SST used for the preparation of the NEs (0.5 mg/ml).

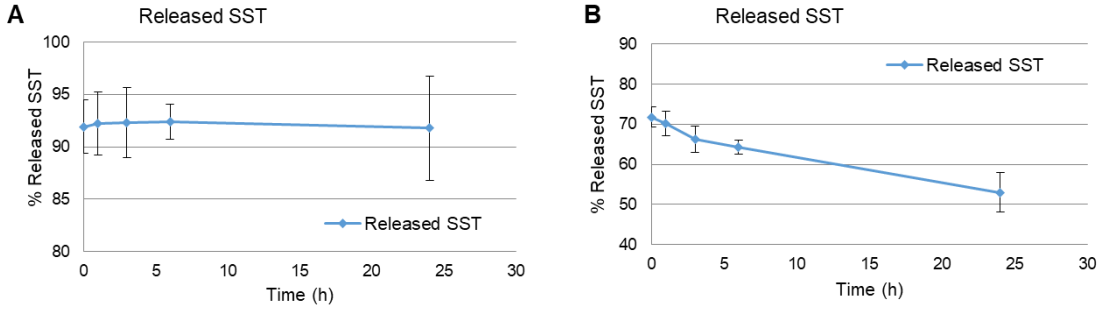

Figure 23: *Released SST form the NEs following protocol 1 in 0.1M buffer citrate pH5.0.* ***A)*** *considering as 100% the sum of the fraction released and the fraction in the lipid droplets at each time point.* ***B)*** *Considering as 100% the amount of SST expected in the samples because of the preparation procedure.*

In Figure 23A the SST in the aqueous phase was 92% at time 0 and the concentration remained steady up to 24h. Figure 23B shows that the SST found in the aqueous phase at time 0 was 72% and decreased to 53% after 24h. Interestingly, at time 0 the amount of released SST was different in the two graphs: part of the SST was already unavailable at time 0 (roughly 22%). The results in Figure 23B also proved that SST underwent some degradation/aggregation processes along the time, since there was a considerable

decrease in the peptide concentration. Nevertheless, when SST was removed from the aqueous phase, part of the SST associated to the lipid phase was released and moved to the aqueous phase, which is shown in Figure 23A, where the ratio free/encapsulated remained constant up to 24h. By comparing the two graphs it is clear that, as some SST was degraded in the aqueous phase, some SST in the lipid droplets was released in order to maintain a constant presence of peptide in the water fraction. Even though a burst-release profile can be ascribed to the formulation, since SST was constantly released into the aqueous phase of the NE for 24h, the system can be considered capable of releasing the peptide in a prolonged manner.

In protocol 2 the freeze-dried NEs were first reconstituted in water and then centrifuged to remove the non-encapsulated fraction of SST, immediately released by the droplets upon reconstitution. The pellet obtained after the centrifugation was suspended in buffer to start the release experiment. Again, the results of protocol 2 (Figure 24) were expressed in two ways. In Figure 24A 100% is represented by the sum of SST found with the *direct analysis* and the *indirect analysis* and in Figure 24B 100% was considered to be amount of SST used for the preparation of the NEs.

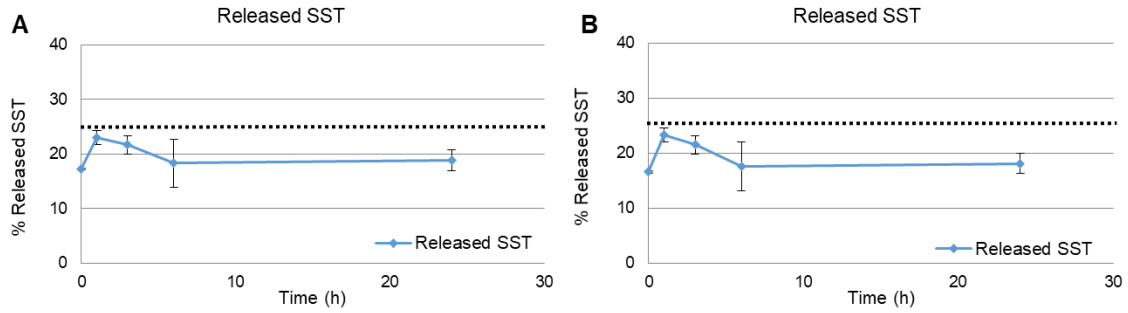

Figure 24: *Released SST form the NEs following method 2.* ***A)*** *considering as 100% the sum of the fraction released, the fraction still encapsulated and the non-encapsulated one at each time point.* ***B)*** *Considering as 100% the amount of SST expected in the samples because of the preparation procedure. The dotted line represents 25%, the amount of SST available after the centrifugation to remove the non-encapsulated fraction of SST.*

The aqueous phase removed by centrifugation contained 75.36±6.75% of the peptide in feeding, therefore only 25% was available for the release experiments (marked with the dotted line in Figure 24). There is no remarkable difference between Figure 24A and 24B: in both cases at time 0 17% of the total amount of SST was in the aqueous phase of the NE. After 1h, the peak of concentration was reached in both conditions (23% of total SST, corresponding to 90% of the available amount). Afterward the concentration starts to decrease and after 24 h it is 19% (85% of the available drug). The similarity between Figure 24A and 24B suggests that no or very little degradation occurred during this experiment. Probably this is due to the overall lower concentration of the peptide, and consequently the stabilizing effect of the NE is more evident. Also, it is clear that upon reconstitution SST

distributes between the two phases immediately and, apart from the peak at 1h, the concentration of SST remains constant in both compartments for the whole experiments.

4.4.3 Release experiments in human plasma

Only the *direct analysis* was used to evaluate the concentration of SST in these experiments, since the *indirect analysis* proved unsuitable for the LC/MS system when working with plasma. Therefore, 100% of released SST corresponds to amount of SST used for the preparation of the NEs.

The experiments were run following two protocols similar to the ones described above. The first procedure consisted of reconstituting the freeze-dried NE directly in plasma to start the release experiment (Figure 25A). In the second one, the NE was first reconstituted in water, then underwent centrifugation to remove the non-encapsulated fraction of SST, and the resulting pellet was suspended in human plasma to start the experiment (Figure 25B).

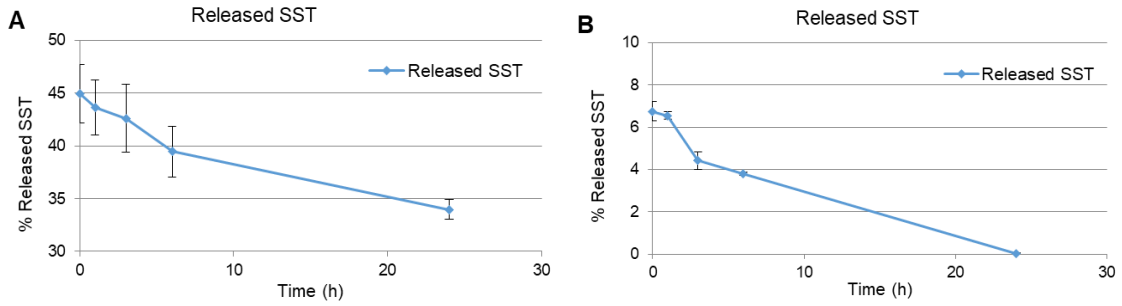

Figure 25: A. *Measurement of SST concentration in plasma after reconstituting the NEs directly in plasma (protocol 1).* ***B.*** *Measurement of SST concentration in plasma after removing the non-encapsulated SST fraction (protocol 2).*

In Figure 25A, the amount of SST measured in the aqueous phase of the NE was 45% at time 0 and decreased to 34% after 24h. When the NE release profile was studied following protocol 2, roughly 7% of the SST was found in plasma at time 0 and after 24h only traces of SST were found (0.03%) (Figure 25A). These results imply that there was a decrease in concentration due to degradation of the peptide. Nevertheless, SST is known to have very short half-life in plasma (roughly 1 minute)[85] and the NE proved efficient in improving the peptide half-life and maintaining a measurable concentration of SST at least for the first 7-8 h.

4.5 Conclusions

Two different systems were studied for the encapsulation and release of SST. The first one was the pH-sensitive NC, which was proven able to release the peptide in a pH-dependent manner. Also, the structure of the peptide, highly susceptible to degradation, was proven to be retained when in the carrier. The second DDS was a NE formulation, studied in

collaboration with the research group of dr. Chatgilialoglu and dr. Ferreri in CNR (Bologna) and founders of the spin-off company Lipinutragen (Bologna). The NE was successful in improving the half-life of the drug by dramatically reducing the degradation rate, as proved both in buffer and in human plasma. Also, under certain conditions the NE was shown to be able to release the peptide in a prolonged manner. In particular, even though a burst-release profile can be ascribed to the NE formulation upon reconstitution in both media, the steady presence of SST in the aqueous phase shown in the release experiment in buffer proved the system capable of releasing SST form the droplets into the aqueous phase in a prolonged manner up to at least 24h.

Both systems gave encouraging results and can be considered as long-circulating depot of SST with promising application for the amelioration of the infusion regimen needed by patients treated with SST.

Polypyridyl-based Copper Phenanthrene Complexes

5.1 Introduction

DNA-cleaving small molecules have recently drawn considerable attention due to their potential for gene editing and cancer therapy. Such molecules mimic natural endonucleases by cutting DNA at or near specific base sequences.[106] Coordination compounds are considered the most promising option in this field. Their artificial metallo-nuclease (AMN) activity relies on the capability of cleaving DNA via oxidation mediated by reactive oxygen species (ROS). The resulting damages on the genome of cancer cells impede the cell replication, therefore representing a valid alternative to conventional chemotherapy.[107,108] The activity of such molecules is due to their shape and charge, which are fundamental to the interaction via groove binding, insertion or intercalation with the requisite site of DNA.[109]

Among the various metal centers, copper compounds are attractive options because of their biologically-accessible redox properties and wide structural variability. Cu is also essential to human body and the physiological copper ion homeostasis probably facilitate biocompatibility and transport of endogenous Cu-based AMNs. The best known example of Cu(II) AMNs is Sigman's reagent $[Cu(1,10\text{-phenanthroline})_2]^{2+}$ (Cu-Phen), which oxidizes DNA in the presence of a reductant and/or oxidant.[110] A limiting factor of Cu-Phen systems is their poor solution stability where speciation, ligand dissociation, and transmetalation may occur. More recently, the addition of appropriate ligands, such as multidentate polypyridyl derivatives (e.g. tris-(2-pyridylmethyl) amine or 2,2',2''-tris-(dipicolylamino)trimethylamine), has been shown to yield complexes with improved stability and excellent DNA cleavage sensitivity.[111,112]

The group of Dr. A. Kellett, partner of the ITN ClickGene based at Dublin City University (Dublin), designed and synthesized a new class of highly original AMNs, obtained by combining the tris-(2-pyridylmethyl) amine (TPMA) polypyridyl ligand scaffold with the Cu(II) phenanthroline nuclease core, in order to combine the stabilization and coordination flexibility of TPMA with the nuclease activity of the Cu-Phen complex. The general formula of this new class of AMNs is $[Cu(TPMA)(N,N')]^{2+}$, where N,N' is either 2,2'-Bipyridine (Bipy), 1,10-phenanthroline-5,6-dione (PD), Phen, dipyridoquinoxaline (DPQ) and dipyridophenazine (DPPZ) (Figure 26).[106]

In this context, the student was involved in the study of the solution conformation and stability of these complexes. Continuous wave EPR (cw-EPR), Hyperfine Sublevel

Correlation (HYSCORE), and Davies Electron Nuclear Double Resonance (ENDOR) spectroscopies were used for the characterization of the complexes in collaboration with dr. G. Mitrikas, coworker in NCSR Demokritos, Athens (GR).

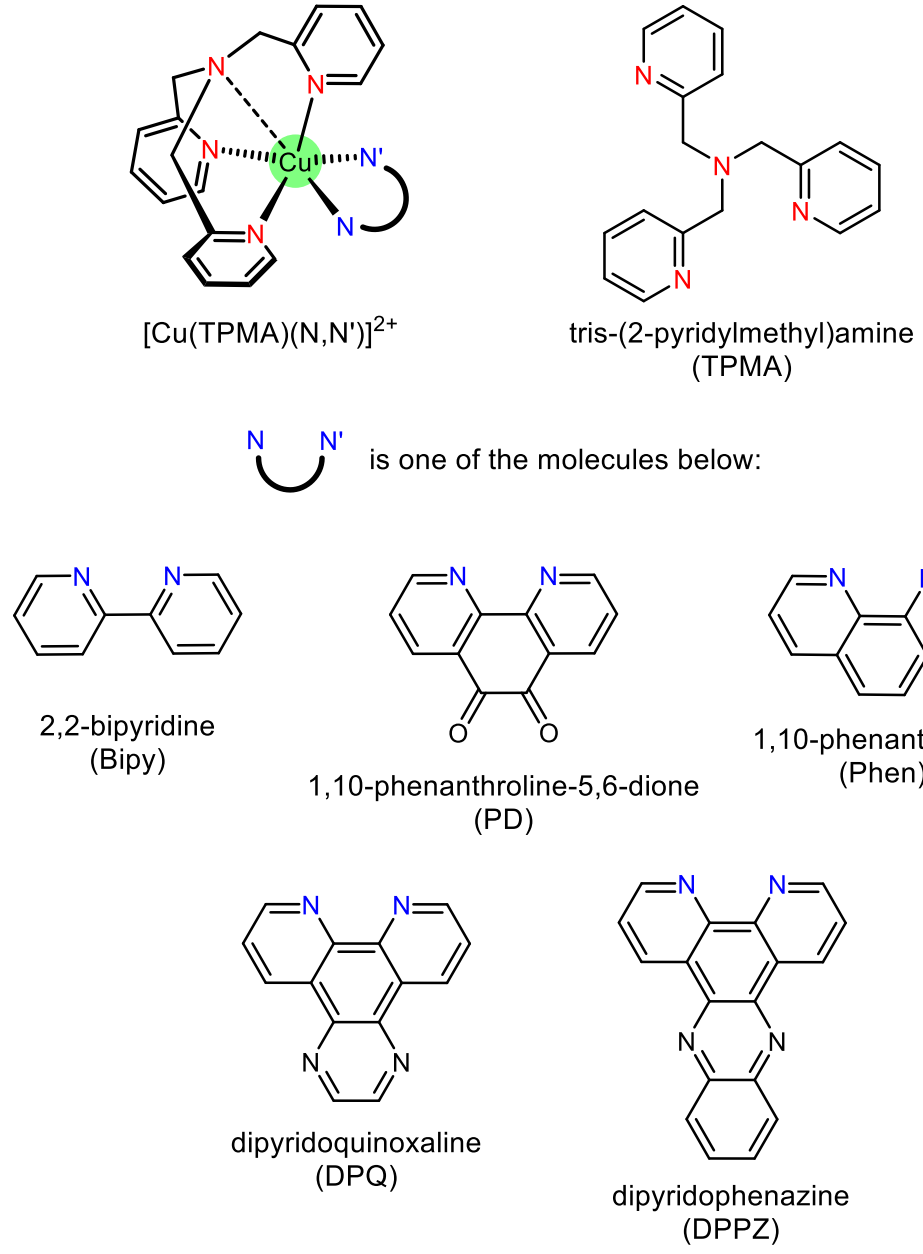

Figure 26: *General structure of the Cu complexes and the ligands employed for the synthesis of the new class of Cu-based AMNs.*

Also, the polymeric pH-sensitive NCs were used for encapsulation and pH-dependent release studies of Cu-TPMA-Phen. The structure of the Cu complex was monitored with cw-EPR after the release to verify that the conformation, fundamental to the nuclease activity, was retained after the encapsulation/release process. The cytotoxicity of the formulation was also studied in comparison with the free complex by the fellow Ph.D. student M. Louka, CNR (Bologna). Lastly, the CLSM was employed to investigate whether

Cu-TPMA-Phen was released into the nucleus of the cell by the hollow NCs, where it can exert its activity.

5.2 Experimental

5.2.1 Materials and Methods

Dr. A. Kellett's group in DCU, Dublin synthesized and provided Cu-TPMA-Phen and Cu-TPMA-Bipy. DMF and DMSO were purchased from Sigma-Aldrich.

Materials and instruments used for the synthesis and characterization of the pH-sensitive hollow NCs are reported in section 3.2.1.

5.2.2 Electron Paramagnetic Resonance spectroscopy

The samples were measured in frozen solutions with concentrations ranging between 1 and 5 mM. To ensure good glass formation when freezing the samples, toluene was added to samples in organic solvents (equal volume or excess) and for water-containing solutions an equal volume of glycerol was added instead. Continuous-wave (cw) EPR measurements were carried out with a Bruker ESP 380E spectrometer equipped with an EN 4118X-MD4 Bruker resonator. Experimental conditions: microwave (mw) frequency, 9.715 GHz; mw power incident to the cavity, 20 μW; modulation frequency, 100 kHz; modulation amplitude, 0.1 mT; temperature 70 K. Measurements at cryogenic temperatures were performed using a helium cryostat from Oxford Inc. The microwave frequency was measured using a HP 5350B microwave frequency counter and the temperature was stabilized using an Oxford ITC4 temperature controller. Pulse EPR measurements at X-band (mw frequency 9.722 GHz) were performed on a Bruker ESP 380E spectrometer equipped with an EN 4118X-MD4 Bruker resonator. The field-swept EPR spectra were recorded via free induction decay (FID) following a pulse length of 500 ns. Davies Electron Nuclear Double Resonance (ENDOR) experiments were carried out with a pulse sequence of π-*T*-π/2-*τ*-π-*τ*-echo, with a π/2 pulse of length 16 ns, a radio frequency pulse of length 10 μs, and a waiting time *τ* between the pulses of 200 ns. Hyperfine Sublevel Correlation (HYSCORE) spectroscopy with the pulse sequence π/2-*τ*-π/2-t_1-π-t_2-π/2-*τ*-echo was carried out with the following instrumental parameters: $t_{\pi/2}$ = 16 ns; starting values of the two variable times t_1 and t_2, 56 ns; time increment, Δt = 24 ns (data matrix 180 × 180). In order to eliminate blind-spot artifacts, up to four spectra were recorded with τ = 96, 120, 144, and 168 ns. A four-step phase cycle was used to remove undesired echoes. The data were processed with the program MATLAB (The MathWorks, Natick, MA). The HYSCORE time traces were baseline corrected with a second-order exponential, apodized with a Gaussian window, and zero filled. After a two-dimensional Fourier transform the absolute-value spectra were calculated.

The experimental cw EPR, HYSCORE and ENDOR spectra were simulated using the EasySpin package.

5.2.3 pH-sensitive Nanocontainers

The procedure for the synthesis of the pH-sensitive NCs is described in 3.2.2.

Loading experiment

1 mg of NCs were suspended in 950 µl of phosphate buffer saline (PBS) before adding 2 mg of CuNF6 previously solubilized in 50 µl of ACN. The resulting suspension, containing 1 mg of NCs, 2 mg of CuNF6 in 1 ml of mixture PBS:ACN (19:1), was kept under gentle magnetic stirring (ca. 300 rpm) for 24h. The non-encapsulated fraction of Cu-TPMA-Phen was removed with five cycles of centrifugations and resuspensions in fresh mixture PBS:ACN (5 min x 11000 rpm). The amount of encapsulated Cu-TPMA-Phen was determined with UV spectroscopy (λmax 262 nm) and calculated by the difference of Cu-TPMA-Phen concentration between the original Cu-TPMA-Phen solution and the supernatants containing the non-encapsulated drug. The calculations were based on a standard curve in the mixture PBS:ACN. Encapsulation Efficiency (EE%) and Loading Capacity (LC%) were the parameters used to evaluate the process (see 3.2.2, loading of DNR). The experiment was carried out three times for statistical analysis.

In-vitro release experiments

The drug release profile of Cu-TPMA-Phen -loaded NCs was studied with the dialysis bag method (dialysis tube MWCO 140 kDa) in acidic and physiological pH. The release media used were a mixture of citrate buffer pH 4.0, 0.1M and ACN (19:1) for the acidic conditions and a mixture of PBS and ACN (19:1) for pH 7.4. 1 mg of loaded NCs was suspended in distilled water, split into two dialysis bags and incubated in 25 ml of each release medium. At different time points (30 min, 1h, 2h, 5h, 8h, 10h, 24h), 1 ml was collected from each release media and the concentration of the samples was measured with UV-vis. The calculations to were made upon a standard curve of CuNF6 recorded in each buffer (λmax 262 nm). The experiment was carried out three times for statistical analysis.

Structural study of CuNF6 – Election Paramagnetic Resonance

cw-EPR experiments were run to assess whether any structural modification occurred to Cu-TPMA-Phen as a consequence of the encapsulation/release processes. The spectra were recorded at 70 K and the sample concentration was 1-5 mM. Glycerol was added as a glassing agent. The standard release procedure described above needed to be modified to give the required concentration (1- 5 mM) of released complex in the media. 0.5 mg of loaded NCs were suspended in distilled water, put into a dialysis bag and incubated in 0.3

ml of each release medium. After 24 h the resulting media were collected, glycerol was added and the samples were then analyzed.

Intracellular localization - Confocal Laser Scanning Microscopy

The instrument used for the experiment was a Leica TCS SP8 MP, inverted confocal microscope with Acousto-Optical Beam Splitter; for the excitation and multiband spectral detector Argon - excitation at 458, 476, 488, 496 and 514 DPSS 561 - excitation at 561nm (RED). Multiphoton IR laser MaiTai DeepSee from Spectral Physics, excitation at 780nm. Confocal laser scanning microscopy (CLSM) was used to evaluate the uptake of the pH-sensitive NCs and the subsequent release and localization of Cu-TPMA-Phen. MCF-7 cells were inoculated on 22mm cover slips placed into six-well culture plates ($5x10^6$ cells per well) and grown for 24h in 1.5 ml of complete growth medium. Free Cu-TPMA-Phen (10 µM) or Cu-TPMA-Phen -loaded NCs (drug concentration 10 µM) were then added. After 2h incubation, the medium was eliminated and the cover slips were washed twice with PBS, 10% formaldehyde in PBS and PBS again, before placing them onto microscope slides.

5.3 Electron Paramagnetic Resonance

The Ph.D. candidate was involved in the detailed characterization of two complexes of the library by EPR. An in-depth study was performed on Cu-TPMA-Phen and Cu-TPMA- Bipy (Figure 27).

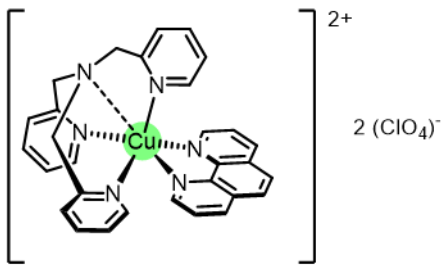

[Cu(TPMA)(Phenanthroline)](ClO$_4$)$_2$
Cu-TPMA-Phen

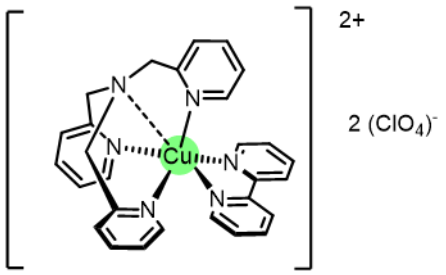

[Cu(TPMA)(Bipyridine)](ClO$_4$)$_2$
Cu-TPMA-Bipy

Figure 27: *Structures of the Cu(II) complexes Cu-TPMA-Phen Cu-TPMA-Bipy.*

5.3.1 Continuous wave EPR (cw-EPR)

Depending on the solvent, the cw-EPR spectra of the two Cu complexes reflected a distorted octahedral geometry (six atoms coordinating the Cu center), a trigonal bipyramidal arrangement (five coordinating atoms) or a mixture of these two species. Figure 28 (bold lines) shows the simulation of the two possible geometries: an almost axial signal with $g_{\text{parallel}} > g_{\text{perpendicular}}$, typical for elongated tetragonal-octahedral or square planar geometry with a d_{x2-y2} ground state (Figure 28A), and a rhombic signal with $g_x > g_y > g_z$ representing

complexes with a d_{z2} ground state and TBP stereochemistry (Figure 28B).[113,114] These simulations were compared with experimental results (dashed lines): Cu-TPMA-Bipy is ascribable to TBP geometry, whereas Cu-TPMA-Phen is not comparable to the two simulated geometries. As evident in Figure 29A, at low field (close to $g_{parallel}$) Cu-TPMA-Phen has a rich structure beyond the typical four-line Cu pattern, which indicates the presence of more than one species in solution. Interestingly, the weighted difference between Cu-TPMA-Phen and Cu-TPMA-Bipy (Figure 28A, dashed line) gave a spectrum typical for tetragonal-octahedral or square planar geometry (six atoms coordinating the Cu center). This is evidence that Cu-TPMA-Phen in solution has two different conformations, where both five and six nitrogen atoms coordinate the Cu center.

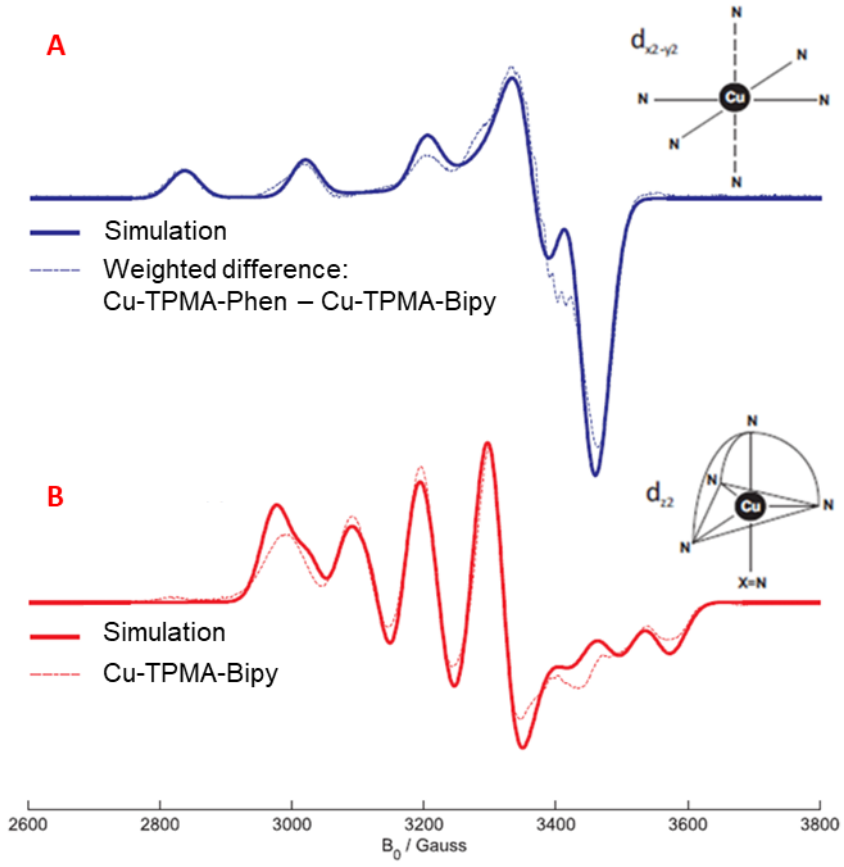

Figure 28: *cw-EPR simulations (bold lines) and experimental results (dotted lines) of distorted octahedral (blue) and trigonal bipyramidal (red) geometries.*

As mentioned above, Cu-TPMA-Phen showed the contribution of two different Cu(II) species when measured in DMSO, ACN and DMF (Figure 29A). This behavior is probably due to the strongly coordinating ligands, which tend to form a six-coordinated structure, and to the rigid construction of TMPA, which results in a preference to a 5-cordination structure. These two opposite tendencies cause the complexes to form an unusual (4 + 1 + 1') structure, where the complexes have 5 strongly coordinated atoms and one semi-

coordinated atom (not always coordinating the Cu center), which causes a mixture of the two species in EPR spectra[115]. Most likely, the TBP geometry is caused by the dissociation of one pyridine nitrogen of TMPA, whose bond with Cu is the longest and weakest.[106]

Upon addition of water in excess (organic solvent 1:19 distilled water), the Cu-TPMA-Phen spectra are dominated by a clean five-coordinated signal. This change in conformation may be due to the solvent and this is in accordance with the previous consideration about the transiently non-coordinating N of TMPA: when the N atom is not coordinating the Cu center its lone pair is available to form a hydrogen bond with the surrounding water molecules, which is a strong hydrogen-bonding donor. In this condition the N is "blocked" outside the first coordination sphere, resulting in a 5-coordiantion structure and a clear trigonal bipyramidal geometry (Figure 29B).

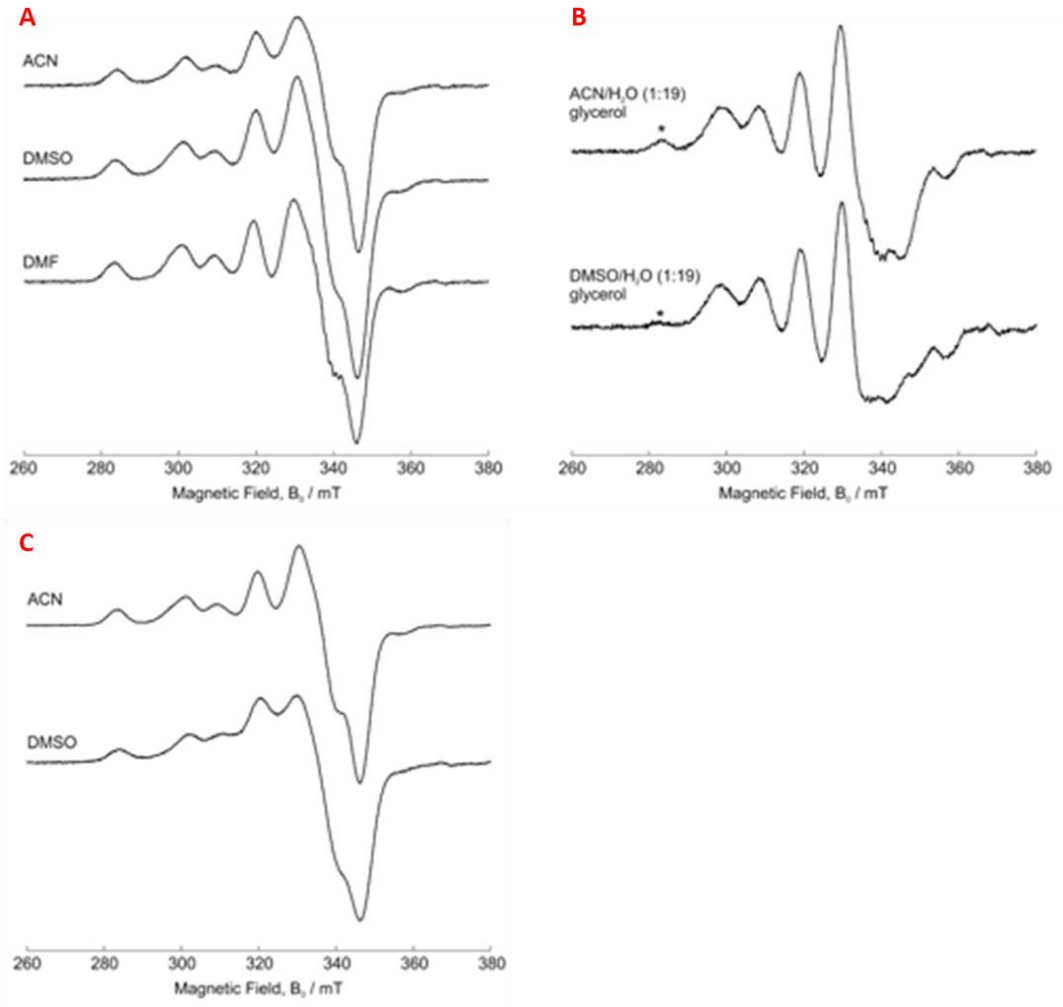

Figure 29: *cw-EPR spectra of Cu-TPMA-Phen: A) mixture of 5- and 6-coordinated structures in DMSO, ACN and DMF; B) 5-coordinated structures in DMSO/H_2O (1:19) and DMF/H_2O (1:19); C) mixture of 5- and 6-coordinated structures obtained by freeze-drying the samples in B and dissolving them again in pure DMSO and ACN.*[106]

To elucidate whether this water-induced modification was a transient solvent-dependent effect, Cu-TPMA-Phen was firstly dissolved in the mixtures of DMSO/toluene (1:19) and

ACN/toluene (1:19), freeze-dried to remove water and then dissolved again in DMSO and ACN respectively. As shown in Figure 29C, in both solvents the initial spectra were reobtained, which is a strong indication that the differences in conformation are due to an interaction with the solvent with no permanent modification of the first coordination sphere.

Analogous results were obtained with Cu-TPMA-Bipy. In particular, the spectrum recorded in ACN shows a mixture of octahedral and trigonal bipyramidal geometry (Figure 30) as for Cu-TPMA-Phen. Interestingly, when Cu-TPMA-Bipy were dissolved in DMF/toluene and DMSO/toluene the results were radically different. In these conditions, the spectra are almost identical one another and reveal a clear TBP geometry. The different behavior of Cu-TPMA-Bipy and Cu-TPMA-Phen can be explained considering the different ligands: 1,10-phenantroline of Cu-TPMA-Phen has a rigid and planar structure, but bipyridine of Cu-TPMA-Bipy is known to be not planar in metal complexes.[116] This behavior of the ligand combined with the steric hindrance of the complex may be the reason for the clear 5-coordinting structure, where a TBP conformation is favored.

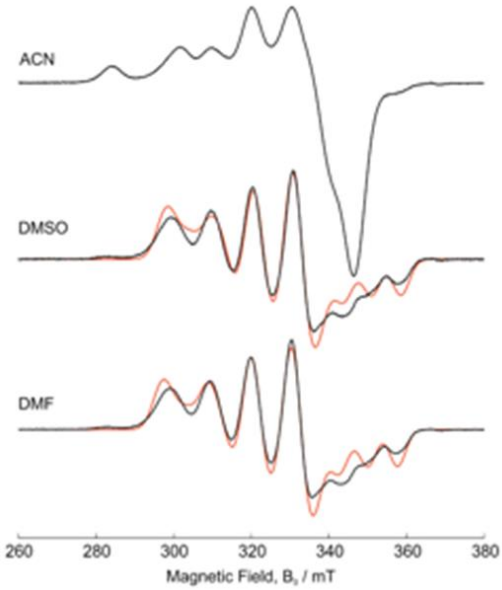

Figure 30: *cw-EPR spectra of Cu-TPMA-Bipy in ACN, DMSO and DMF. The red lines represent the simulation of the structure of a five-coordinated structure.*[106]

5.3.2 Pulse EPR studies

Advanced pulse EPR techniques such as Hyperfine Sublevel Correlation (HYSCORE) and Davies Electron Nuclear Double Resonance (ENDOR) spectroscopies, were run in collaboration with dr. G. Mitrikas, NCSR Demokritos, Athens (GR). More detailed results and the spectra are reported in the paper by the group published in Chemistry – an European journal.[106]

Briefly, ENDOR and HYSCORE were performed to obtain a detailed picture of magnetic interactions between the unpaired Cu(II) electron (d orbital) and the magnetic nuclei of the

ligands, which respectively gave information about the electronic and geometric structure of the complexes. Only compounds with observable electron spin echo (ESE) and no overlapping spectra can be analyzed to have clear results with these techniques. Therefore, the sample of Cu-TPMA-Bipy in DMF/toluene (1:1) and Cu-TPMA-Phen in DMSO/H_2O (1:19), both best described by a dominating d_{z2}, were studied. Both complexes show a penta-coordination structure halfway TBP and square-based pyramidal.[117]

ENDOR measurements highlighted the presence of two axially coordinated nitrogen atoms, that is the TPMA amine and the one of the Phen/Bipy nitrogens. Also, the technique indicated the presence of three additional pyridine nitrogens equatorially coordinated. HYSCORE analysis was used to study the interactions of the Cu atom with atoms outside the first coordination sphere. ^{1}H HYSCORE of Cu-TPMA-Bipy identified a proton with a distance of 3.4 Å, probably belonging to a hydrogen of CH_2 group of TPMA. ^{14}N HYSCORE analysis supports a solution configuration where one of the pyridine N-donor atoms is dissociated to a remote position. However, regarding Cu-TPMA-Phen, spectra are less clear and the remote nitrogen may originate from an axially coordinated DMF solvent; in either case, the remote contact clearly provides solution access to the Cu(II) center which is an important aspect of the catalytic design imposed by the TPMA ligand.

5.4 pH-sensitive Nanocontainers

The pH-sensitive NCs were used for the encapsulation and release of Cu-TPMA-Phen. The system proved able to encapsulate the Cu complex and release different amount of drug depending on the pH. As already seen for DNR and SST, the more acidic the environment, the more drug was released. Since the activity of AMNs relies on the shape and charge of the complex, it was fundamental to confirm that the NCs did not interfere with the structure of the Cu complex.[118,119] The conformation study, aiming at evaluating whether Cu-TMPA-Phen underwent structural modification due to the loading and release processes, was run with cw-EPR. In addition, intracellular localization of the formulation was studied with CLSM. Cell viability of cancer cells treated with free and encapsulated drug was studied with MTS assays by M. Louka, Ph.D. student in the ClickGene network. The following results are part of a manuscript that has been recently published in the journal ACS Omega.[120]

5.4.1 Loading experiment

The loading process depends on the interactions between the pendant functional groups of the suspended NCs and the ones of the dissolved drug.[31,68] In order to reach the complete dissolution of Cu-TPMA-Phen, which is partially water-insoluble, and at the same time allow the formation of an adequate suspension of NCs, the Cu complex was fist dissolved in the

smallest volume of ACN and then mixed with the suspension of NCs in buffer. Specifically, 50 µl of ACN were enough to dissolve 2mg of Cu-TMPA-Phen and the solution was then added to 0.95 ml of PBS containing 1 mg of suspended NCs without causing any problem to the suspension. The encapsulation conditions chosen for the Cu complex were: 2 mg of Cu-TPMA-Phen, 1 mg of NCs in 1 mL of a mixture of ACN: PBS (1:19). The results of the procedure are reported in Table 7.

Table 7: *Results of the drug loading experiments.*

EE%	LC%	mg Cu-TPMA-Phen/mg NCs	µmol Cu-TPMA-Phen/mg NCs
36.4 ± 5.2	42.0 ± 3.3	0.724	0.988

In solution Cu-TPMA-Phen loses its perchlorate counter ion, which leaves the Cu center with a 2+ positive charge. The electrostatic interactions between the 2+ Cu center and the negatively charged carboxylate anions of the pH-sensitive NCs is probably the most relevant driving force for the encapsulation of the Cu complex. Also, as already reported above, a distal pyridine nitrogen of TMPA was identified within the coordination complex and it may therefore interact with the NCs via hydrogen-bonding.

5.4.2 In-vitro release experiments

The release profile of the Cu-TPMA –loaded NCs was tested in acidic (4.0) and physiological pH (7.4). The released media were prepared adding a 1:19 of ACN to avoid any solubility issues of the drug after the release. The acidic release medium was a mixture of 0.1 M citrate buffer pH 4.0 and ACN (19:1), whereas the physiological pH was mimicked with a mixture of PBS and ACN (19:1). The results are reported in Figure 31.

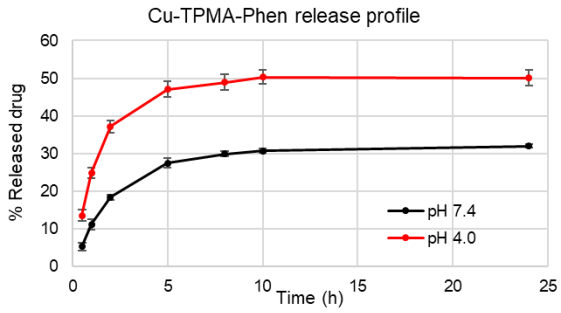

Figure 31: *Drug release profiles of Cu-TPMA-Phen -loaded pH-sensitive NCs in pH 7.4 (black) and pH 4.0 (red).*[120]

The amount of released drug after 24h was 50% in acidic pH (red line) and 30% in slightly basic pH (black line). The concentration of drug in the release media reached a plateau (no more drug was released) after 8-10 h in both conditions. The release profile of Cu-TPMA-Phen is ruled by the same mechanism described for DNR and SST, PMAA carboxylic

groups are the key for the interpretation of these results. They are mostly protonated at pH 4.0, where they cannot interact with the positively charged Cu center of complex, favoring the drug release. On the contrary, in pH 7.4 they are mostly deprotonated and negatively charged, which allows the interaction with and retention of the complex.

The pH-dependent release experiment was also carried out by increasing the amount of ACN in the mixtures up to 9:1. This was carried out to assess whether the amount of ACN affected anyhow the release profile of the systems. The drug release profiles obtained in these conditions were statistically identical to the ones reported in Figure 31.

5.4.3 Structural study of CuNF6 – Election Paramagnetic Resonance

The conformation of synthetic chemical nucleases such as Cu-TPMA-Phen is fundamental for their activity. cw-EPR was used to study the structure of the Cu complex in solution after the release in comparison to the fresh molecule, in order to highlight any possible variation in conformation due to the encapsulation/release processes.

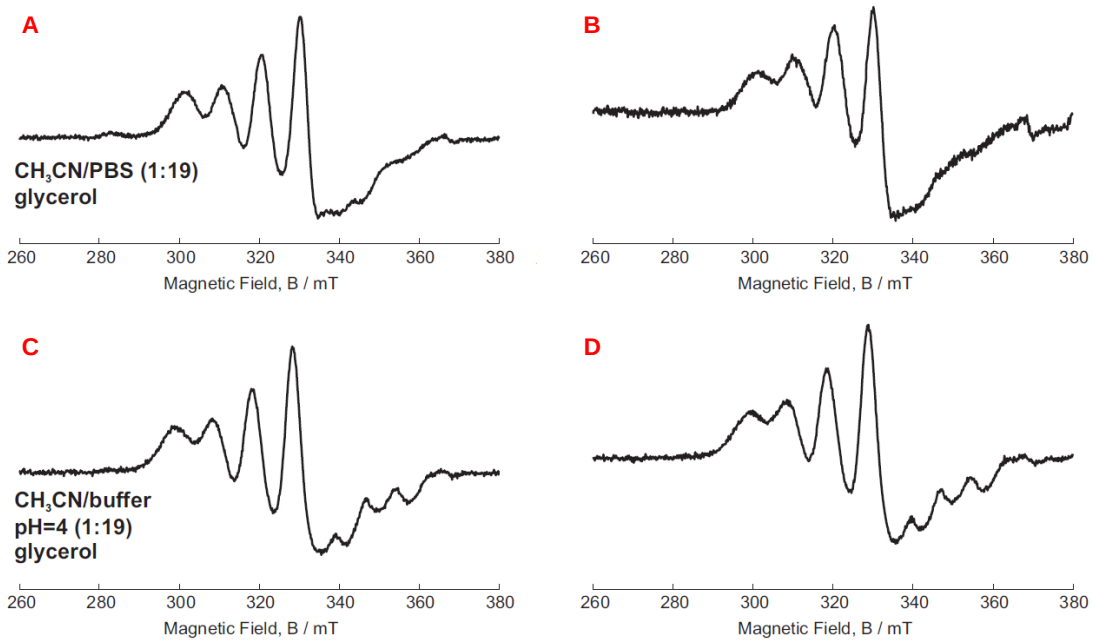

Figure 32: *cw EPR of free and released Cu-TPMA-Phen: A) Free Cu-TPMA-Phen in ACN/PBS (1:19); B) Released Cu-TPMA-Phen in ACN/PBS (1:19); C) Free Cu-TPMA-Phen in ACN/citrate buffer pH 4.0 0.1M (1:19); C) Released Cu-TPMA-Phen in ACN/citrate buffer pH 4.0 0.1M (1:19).*[120]

The spectra of free Cu-TPMA-Phen dissolved in the release media in ACN/PBS (1:19) and ACN/0.1M citrate buffer pH 4.0 (1:19) are reported in Figure 32A and 32C respectively. These spectra were used as references with which to compare the released Cu complex. The spectra show that Cu-TPMA-Phen has a clear TBP conformation, with 5 atoms coordinating the Cu(II) center. This structure is due to interactions between water and the distal nitrogen atom outlined above. When this nitrogen does not coordinate the Cu(II)

center its lone pair is available to form a hydrogen bond with a vicinal water molecule. In such conditions the N is ligated outside the first coordination sphere, which results in a 5-coordination structure and a clear trigonal bipyramidal spectrum.[117,121,122] Figure 32B and 32D show the EPR spectra of released Cu-TPMA-Phen in ACN/PBS (1:19) and ACN/0.1M citrate buffer pH 4.0 (1:19), respectively. The spectra are almost identical to the ones belonging to the free complex in Figure 32A and 32C, which is a strong indication that the encapsulation and release processes did not affect the structure of the complex.

5.4.4 In vitro cytotoxicity

The following experiments were performed by the Ph.D. fellow of the ClickGene network M. Louka, based at Lipinutragen, Bologna, and are here reported as a proof of concept for the release experiments results in Figure 31. MTS assays were run to compare the cell viability of NB100 cells treated with different concentration of free and released Cu-TPMA-Phen. As shown in Figure 33, significant differences in cell viability resulted after 24h treatment in the two described conditions. These difference can be attributed to the smaller amount of bioavailable drug available released form the NCs. Only 30% of the loaded drug is actually released in pH 7.4 (as shown by the black line in Figure 31), which is similar to the cell culture conditions.

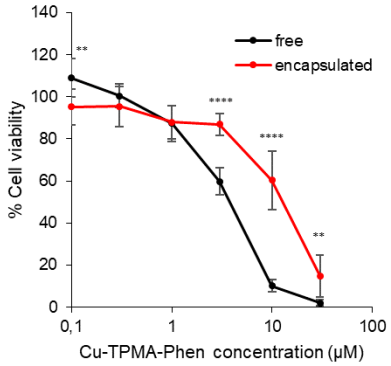

Figure 33: *Dose-dependent response of NB100 cells treated with free or encapsulated CuNF6 for 24 h. Values represent mean ± SD (n=9). Statistical analysis was performed with unpaired t test * ($p < 0.05$), ** ($p < 0.01$), *** ($p < 0.001$), **** ($p < 0.0001$).*[120]

5.4.5 Intracellular localization - Confocal Laser Scanning Microscopy

The intrinsic fluorescence of Cu-TPMA-Phen allowed the CLSM experiments to study intra- and subcellular localization of free and loaded Cu-TPMA-Phen in MCF-7 cancer cells. Both the formulations were tested to investigate any possible difference in behavior due to the encapsulation/release processes. Figure 34 shows that, independently of the formulation, Cu-TPMA-Phen localized mainly in the nuclei of the cells. pH-sensitive NCs do not affect the intracellular localization and the DDS act only as a carrier, delivering the drug without affecting its activity.

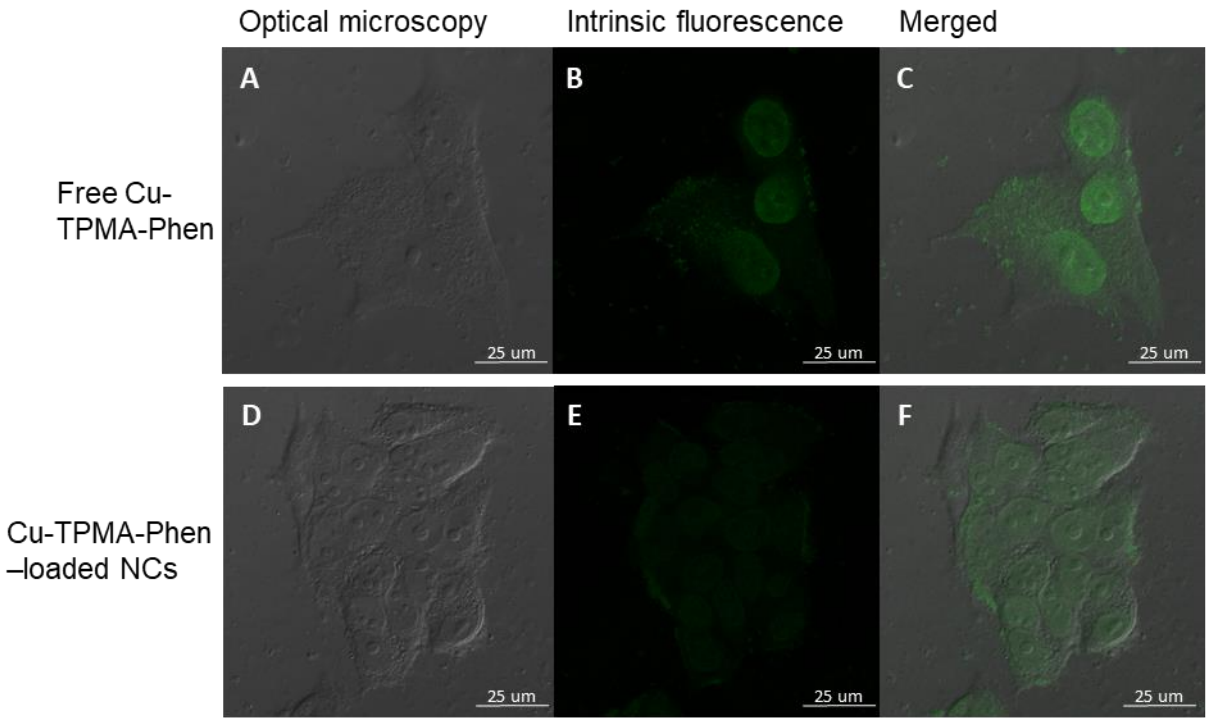

Figure 34: *Confocal laser canning microscopy (CLSM) images of MCF-7 ells for 2h treated with: A,C) free Cu-TPMA-Phen (concentration 10 μM); B,D) Cu-TPMA-Phen –loaded NCs (concentration of the drug 10 μM).*[120]

5.5 Conclusion

The use of copper complexes for gene editing and new therapies based on oxidative mechanisms is currently a cutting-edge research field. One of the core goals of the ClickGene network was the synthesis of a new class of Cu(II) AMNs, which was successfully carried out by the dr. A. Kellett's group in DCU, Dublin. The student was involved in the EPR characterization of this new library of Cu complexes, the results of which were included in a paper published in Chemistry – A European Journal.[106]

The selective release of these molecules in response to tumor microenvironment was also a fundamental goal of the ClickGene project. Specifically, Cu-TPMA-Phen was loaded in the pH-sensitive NCs, which were able to encapsulate and release the complex in a pH dependent manner and without affecting its structure, activity or intracellular localization. The results obtained are part of a publication which has been recently published in ACS Omega.[120]

Oligonucleotide delivery

6.1 Introduction

Nucleic acids play a fundamental role in biology and are essential to all known forms of life. Their function is to store, encode, transmit and express all the information we need for living. Due to the enormous importance of their functions, nucleic acids also have unique potential as therapeutic agents. While conventional small drugs usually target protein-binding sites, short sequences of DNA or RNA (oligonucleotides, ONs) can directly target and interfere with the genetic expression of these protein themselves. Thanks to this new approach previously-unexplored targets can now be reached, and applications such as genomic engineering, protein replacement therapy and cancer immunotherapy are currently under the spotlight, with a special emphasis on rare disorders for which no therapy currently exists.[123,124]

Oligonucleotides (ONs) for gene therapy can be divided in three broad categories depending on their mechanism of action: (i) decreased gene expression, (ii) altered (or new) products of expression and (iii) increased gene expression.[125] Gene expression inhibition (i) (knock-down) can be achieved by using classic single strand DNA ONs (ASOs). These molecules hybrid mRNAs and the resulting hetero-duplexes (DNA-RNA) are degraded by RNAse H. Another mechanism is based on the exploitation of the endogenous mechanism of RNA interference (RNAi), used by cells to control of gene expression.[126] Endogenous miRNAs and properly-designed artificial siRNAs can regulate gene expression through this pathway, resulting in selective message degradation, translation arrest or modulation of transcription.[127] It is also possible to alter the normal gene expression by interfering with the genome splicing (ii). Steric-blocking oligonucleotides block splice sites in pre-mRNA and splice-switching oligonucleotides (SSOs) can either activate splicing (exon skipping) or inactivate splicing (exon inclusion).[128] Last, gene transcription can be increased by blocking natural miRNAs with artificial ONs (iii). miRNA blocking agents are often referred to as antagomirs and have been designed against several diseases, including various cancers.

Despite the potential, the first generation of oligonucleotide therapy did not live up to the expectations in a number of clinical trials.[124] After more than 30 years of research, substantial improvements have been made and there are currently five FDA-approved nucleic acid therapeutics. Such advancements have been possible because of the recent developments of improved chemistries, better understanding of the basic biology of

oligonucleotides and more sophisticated delivery systems, which together have led to an increasing success in the clinic.[125]

In particular, the employment of DDS has been a fundamental step to improve the bioavailability of ONs, which can now be delivered directly to the target site and protected from nuclease degradation. So far several different polymeric DDSs have been used for releasing ON in the cytoplasm or nucleus.[123] Typically, these systems are made of cationic polymer capable of electrostatically interact with polianionic ONs and form complexes. They could be divided into four main categories: (i) nanoparticles made of polymeric matrix (usually amino-modified PLGA solid nanoparticles, obtained with the emulsion polymerization techniques), (ii) micelles (amphiphilic polymers that self-assembly in water), (iii) dendrimers (macromolecules with tree-like architecture) and (iv) nanohydrogels (or polyplex, where ONs and a cationic branched polymer form a complex).[129] Polyplex-forming poly ethylenimine (PEI) is the most studied DSS for ONs and it is still considered the golden standard to which systems are usually compared in terms of cytotoxicity and transfection efficiency.[40]

When approaching the study of ON DDSs, there are some features that have to be taken into consideration. Generally speaking, DDSs with high cationic density condense nucleic acids more efficiently and form more stable complexes, theoretically resulting in high transfection efficacy. However, strongly-binding polycations may limit the intracellular unpacking of the ON-DNA complex, which is necessary for an efficient transfection as well. Therefore, a proper balance has to be sought, since a too-low or too-high binding affinity is translated into poor transfection. The transfection efficiency/unpacking problem is usually solved by employing biodegradable polycations. Although hydrolysable polycations based on ester and amide bonds have been widely used, reduction-sensitive polyplexes are considered to be superior degradable candidates.[130] Also, very strongly charged polycations are often cytotoxic, which is a critical point that needs to be considered before starting the transfection efficiency studies on tumoral cells.[131]

During the Ph.D. period, two main strategies were proposed and tested for the synthesis of DDS for ONs. All the proposed options aimed at the development of positively-chargeable and redox-responsive hollow NCs, in an effort to balance encapsulation and release properties. To date, none of the examined options resulted in the successful synthesis of the designed NCs for the release of ONs. The different approaches are reported below.

6.2 Experimental

6.2.1 Materials and Method

Materials

NH_3 solution 30%, absolute ethanol (EtOH), Tetraethyl orthosilicate (TEOS), 3-(trimethoxysilyl)propyl methacrylate (MPS), Methyl Methacrylate (MMA), Poly(ethylene glycol) methacrylate (average Mn 500) (PEGMA), Divinylbenzene (DVB), Potasium peroxodisulfate (KPS), 2-(Dimethylamino)ethyl methacrylate (DMAEMA) were purchased from Sigma-Aldrich. Methacrylic acid (MAA, 99%) was bought from Sigma-Aldrich and distilled prior use. N,N'-Bis(acryloyl)cystamine (BAC) were purchased from Alfa Aesar and used without further purification. N,N′- methylenebisacrylamide (MBA, 96%) and 2,2′-Azobisisobutyronitrile (AIBN, 98%) were purchased from Acros. The HF/ NH_4F etching buffer (pH 4) was prepared with 5 ml of HF 48% (Sigma-Aldrich), 95 ml of water and 10 g of NH_4F (Sigma-Aldrich) (1.4 M HF / 2.7 M NH_4F).

Scanning Electron Microscopy (SEM)

SEM images of the NPs were taken with ZEISS Leo 1530 microscope. The dried NPs (powders) were placed on a thin layer of carbon tape holder on the specimen stub. The samples were sputter coated before the analysis with a thin layer of gold to prevent charging of a specimen with the electron beam in conventional SEM mode.

The instrumentation used for the characterization of the NPs is the one reported for anthracyclines (3.2.1).

6.2.2 Hollow Nanocontainers via Emulsion Polymerization

The synthesis of positively-chargeable and redox-responsive hollow NCs via emulsion polymerization was designed to be a four-step process.

Synthesis of silica cores

NH_3 (1.35 g, 480 mmol) and distilled water (2.72 g, in total 330 mmol) were added to 92 ml of EtOH. The solution was stirred vigorously at 55°C before and during the addition of TEOS, then the rate of stir was decreased. The reaction was stopped after 2 h and the product was collected by means of three cycles of centrifugation/resuspension in EtOH (5 min x 20000 rpm). After drying in an oven at 50°C overnight, the product was collected as a white powder.

Modification of SiO_2 cores with MPS - SiO_2@MPS

750 mg of silica spheres were suspended in 22.5 ml of EtOH. Afterwards, distilled water (1.5 g, in total 0.082 mol), MPS (3.72 g, 15 mmol) and NH3 (1.2 g, 0.072 mmol) were added

and the reaction was stirred overnight. The product was collected with three cycles of centrifugation/resuspension in EtOH (5 min x 18000 rpm). After drying in an oven at 50°C overnight, the product was collected as a white powder.

Synthesis of the shell - SiO_2@P(DMAEMA-co-MMA-co-PEGMA-co-BAC-co-DVB)

Although several different conditions were tested, no satisfactory shell was obtained with emulsion polymerization. Below is described the procedure that gave the best results.

75 mg of SiO_2@MPS were suspended in 27 ml of distilled water and the medium was stirred vigorously at 80°C for 30 minutes under Ar. Then MMA (30 mg, 0.3 mmol), PEGMA (156 mg, 0.075 mmol), DVB (137 mg, 1.05 mmol), BAC (137 mg, 0.525 mmol) and DMAEMA (295 mg, 1.875 mmol) were added. After 15 minutes, KPS (27 mg, 0.1 mmol) was added as well. The reaction medium was stirred 6h and the product was collected with three cycles of centrifugation/resuspension in distilled water (5 min x 15000 rpm). After drying in an oven at 50°C overnight, the product was collected as a white/reddish powder.

Core removal procedure – Hollow P(DMAEMA-co-MMA-co-PEGMA-co-BAC-co-DVB)

20 mg of core/shell structures were suspended in 2 ml of a mixture of distilled water and HF/NH_4F buffer pH 4 (1:1). After 15 minutes of sonication the medium was stirred for 2 hours at room temperature. The product was collected with four cycles of centrifugation/resuspension (5 min x 18000 rpm) in distilled water. The reaction yielded the product as a brown/transparent powder, after drying at 50°C in the oven overnight.

6.2.3 Hollow Nanocontainer via Distillation-Precipitation Polymerization

The synthesis of positively-chargeable and redox-responsive hollow NCs via distillation-precipitation polymerization was designed as a four-step process. The procedures for the synthesis of the silica cores, their modification with MPS and the attempts to remove the cores are identical to the ones reported for the hollow NCs obtained via emulsion polymerization and can be found above (6.2.3). Therefore, below is reported the synthesis of the shell via DPP only.

Synthesis of the shell - SiO_2@P(DMAEMA-co-MAA-co-PEGMA-co-BAC-co-DVB)

Although the considerable amount of attempts, no satisfactory shell was obtained with distillation-precipitation polymerization.

50 mg of SiO_2@MPS were suspended in 100 ml of ACN with the aid of sonication. The suspension was stirred for 30 min at 75-80°C under nitrogen bubbling before adding MAA (0.21 mmol, 18 µl), BAC (0.26 mmol, 68 mg), PEGMA (0.32 mmol, 141 µl) and MBA (0.14 mmol, 22 mg). After 15 min AIBN (0.16 mmol, 26 mg) was added and then DMAEMA (2.1 mmol, 350 µl) dropwise over 30 min. Afterwards, the temperature was increased to 100°C

to start the distillation. Once distilled 30 ml the reaction was stopped and the product was purified by three cycles of centrifugation/resuspension in ACN (5 min x 10000 rpm). The reaction yielded the product as a white/yellow powder, after drying at 50°C in the oven overnight.

6.3 Hollow Nanocontainers obtained via Emulsion Polymerization

Recently, Poly(dimethylaminoethyl methacrylate) (PDMAEMA), reported also as a temperature-responsive polymer for the three-stimuli-sensitive NCs, has received increasing attention as a non-viral gene delivery system, due to the promising results in terms of transfection efficiency and low cytotoxicity.[40] DMAEMA has been used as main monomer for polyplex-forming DDSs, for the formation of core-shell particles and as block-copolymer for micelles employed for the release of ONs.[129,132]

A new hollow NC for the delivery of ONs was designed by using DMAEMA as the main monomer for the shell formation and BAC as a cross-linking agent. The most important characteristic for ON DDSs is the capability of interacting with the negative charges of DNA, and therefore it needs to be positively charged. DMAEMA bears a tertiary amino group, which can interact with the negatively charged DNA in physiologic conditions. As a co-monomer MMA was used, which is reported to increase the transfection efficiency when co-polymerized with DMAEMA.[133] BAC is the redox-sensitive cross-linking agent and it was used to facilitate the release of DNA inside the cells and to improve the biodegradability of the system.[46] In order to avoid immediate disassembly of the nanocontainer in the cell, also a second cross-linking agent, divinylbenzene (DVB), was used.

6.3.1 Synthesis

The synthesis of the hollow NCs implied four separate steps (Figure 35).

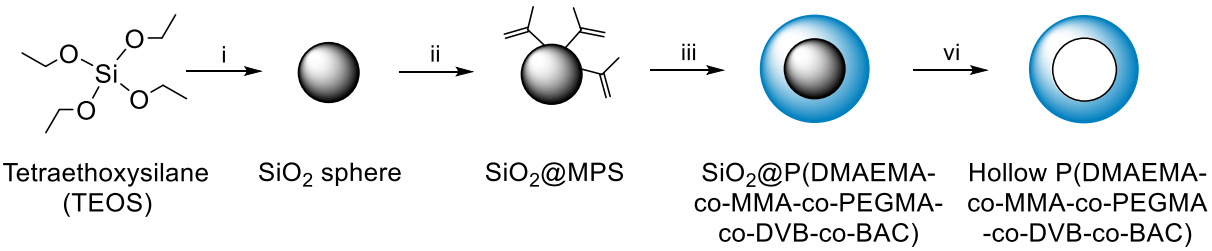

Figure 35: *Scheme of the synthesis of the hollow NCs for ON release: i) Stöber method: NH_3, EtOH, H_2O. ii) Synthesis of SiO_2@MPS: MPS, NH_3, EtOH, H_2O. iii) Emulsion polymerization: DMAEMA, MMA, PEGMA, BAC, DVB, KPS, N_2 bubbling in water at 80°C. ii) Core removal: HF/NH_4F pH 4 buffer and water (1:1).*

The first step was the formation of the silica cores obtained with the Stöber method. The surface of the sacrificial SiO_2 NPs was then modified with 3-(trimethoxysilyl)propyl methacrylate (MPS), which inserted the double bonds necessary for the NPs to participate

in the synthesis of the shell. Emulsion polymerization was then used to form the shell. The last step was the selective SiO_2 core removal, achievable by stirring the NPs in a mixture of HF/ NH_4F etching buffer (pH 4.0) and water for 1h.

The choice of using silica NPs as sacrificial template was due to their inherent advantages. Specifically, several papers have been published on size-tunable monodisperse silica spheres,[134,135] which allowed to prepare NPs below the 200 nm threshold needed for the EPR effect without much optimization. Secondly, the removal of the core can be achieved very easily and in very short time (from minutes to few hours).

The formation of the SiO_2 spheres relies on the sol-gel method, which consists of a series of hydrolysis and condensation reactions that eventually form the monodisperse NPs (Figure 36).

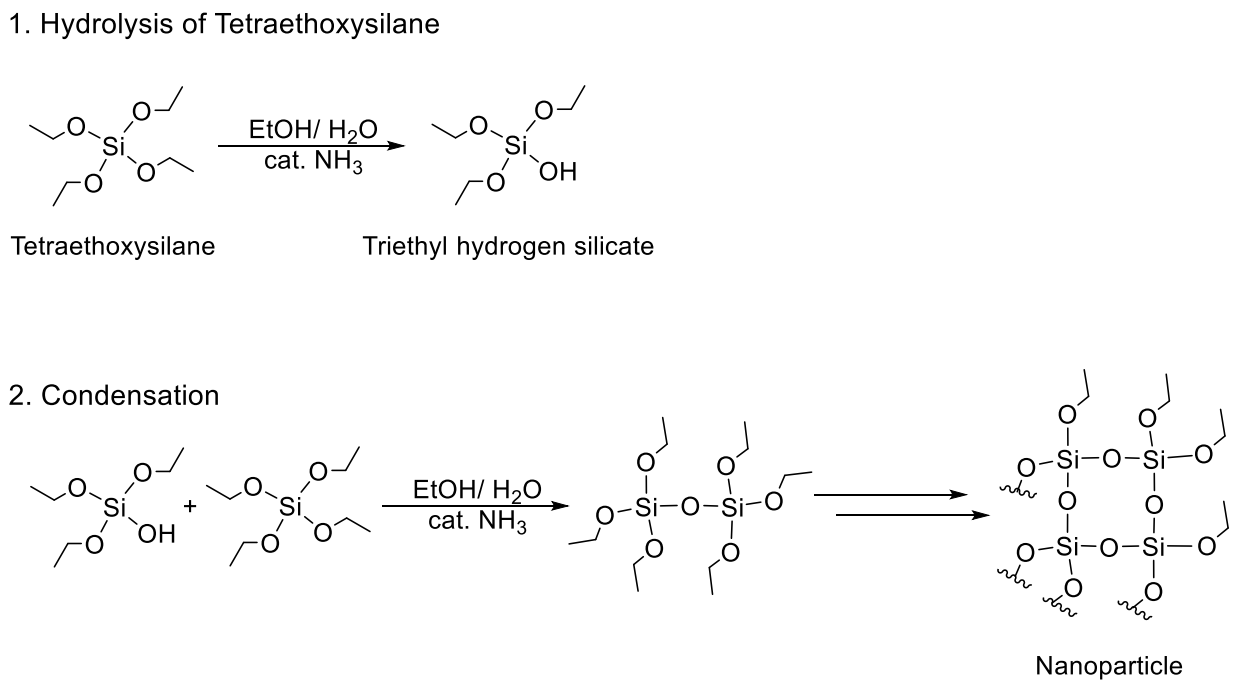

Figure 36: *Mechanism of formation of silica NPs. 1. Hydrolysis of tetraalkoxysilanes in alcohol solution to yield silanols; B. Condensation of silanols to give final NPs (alcohol condensation).*

Tetraethyl orthosilicate (TEOS) or other silicates are dissolved in water, alcohol in presence of ammonia as a catalyst. The concentration of the components is crucial to the determination of final size of the silica NPs. During the hydrolysis reaction, the ethoxy group of TEOS reacts with a water molecule to form the intermediate silanol. The condensation reaction occurs immediately after and consists in the reaction of the hydroxyl group of the silanol with either the ethoxy group of another molecule of TEOS in the “alcohol condensation” or the hydroxyl group of another hydrolysis intermediate in the “water condensation”, forming Si-O-Si bridges. When the products of the hydrolysis and

condensation reactions reach the saturation of the solution, the primary particles are generated by precipitation. These rapidly aggregate to form the mature particles, which grow with the further aggregation of primary particles.[136–139]

The outer surface of the SiO_2 NPs can be further modified by restarting the process. After the hydrolysis on the surface of the NPs to give the silanols, condensation takes place with the MPS molecules in solution, allowing the modification of the silica NP surface with polymerizable double bonds (Figure 37).[139]

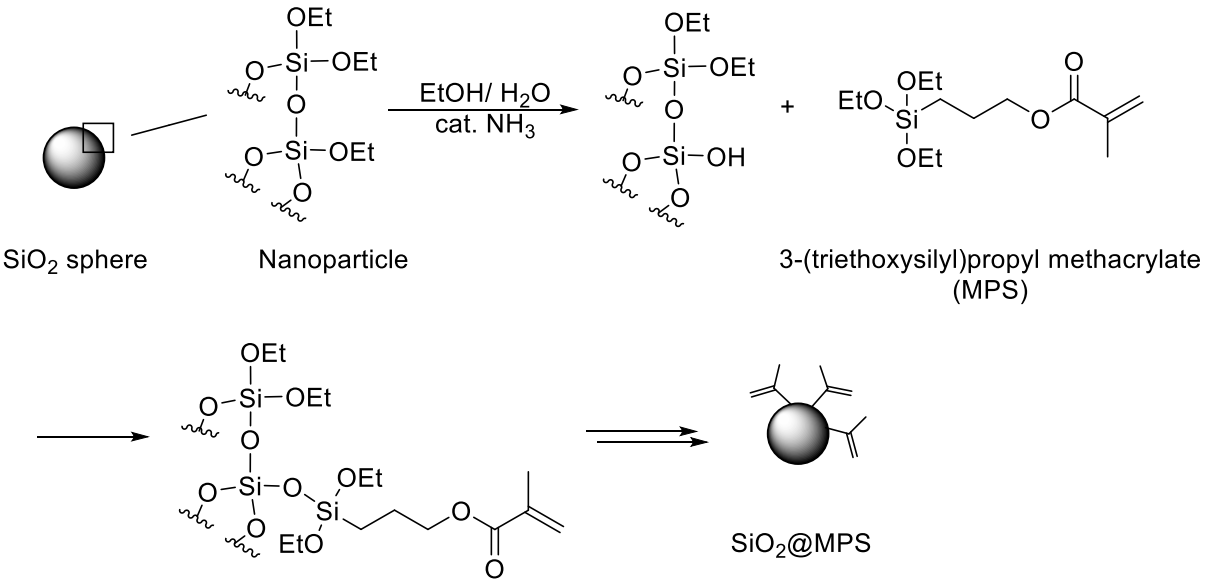

Figure 37: *Modification of the silica NP surface with 3-(trimethoxysilyl)propyl methacrylate (MPS).*

The third step was the synthesis of the shell, which was carried out by emulsion polymerization. DMAEMA, already used for the temperature-responsive shell of the three-stimuli-sensitive drug delivery system in DPP, has also been reported as a useful monomer for the emulsion polymerization.[140–142]

Emulsion polymerization techniques are widely used methods to produce NPs for drug delivery.[143,144] These are heterogeneous free radical polymerization involving the emulsification of hydrophobic monomers in water, followed by the initiation reaction with and initiator (e.g. sodium persulfate, KPS, or AIBN).

A typical emulsion polymerization is characterized by the emulsified monomer droplets dispersed in the continuous aqueous phase with the aid of an oil-in-water surfactant. If the concentration of the surfactant is above its critical micelle concentration (CMC), monomer-containing micelles may be present in the polymerization system. Only a small fraction of the hydrophobic monomer is present in the micelles or dissolved in the aqueous phase: most of the monomer molecules are in the monomer droplets. The polymerization is initiated by the addition of the initiator and the consequent polymerization of its radicals with the

monomers dissolved in the continuous phase. The resulting oligomers radicals, due to the increased hydrophobicity, enter the micelles where they continue to propagate by reacting with the monomer molecules therein. Micelles are eventually transformed into nuclei and nucleation stage (*Interval I*) ends immediately after their exhaustion. The propagation reaction of free radicals with monomer molecules takes place primarily in new formed particles. Monomer droplets only serve as reservoirs to supply the growing particles with monomers and surfactant. The particle growth stage (*Interval II*) ends when monomer droplets disappear from the polymerization system. In *Interval III* the concentration of monomer in the reaction environment continues to decrease toward the end of polymerization.[145]

The surfactant-free emulsion polymerization is a different process where no surfactant is needed. It starts when the initiator radicals are generated by decomposition of initiator. The radical chains grow in size via the propagation reaction with the monomers in the aqueous phase. The oligomer radicals, after reaching a critical chain length, become insoluble and coil up to form nuclei in the aqueous phase. The interaction of these nuclei with one another results in the formation of stable primary particles. The growth is due to the capture of the monomer in solution by the primary particles. This process is ruled by the molecular diffusion of monomers from the oil droplets into the aqueous phase.[145–148]

Most of the experiments of the student were run with the technique of surfactant-free emulsion polymerization. Although several different conditions were tested, this procedure did not give satisfactory results. The standard emulsion polymerization was also tried by using sodium dodecyl sulfate (SDS) as a surfactant, but no improvements were observed.

6.3.2 Characterization

The characterization below shows the samples obtained with the procedures that eventually led to the best results, assessed in terms of percentage and cleanliness of the final hollow NCs. However, the best sample as a whole cannot be considered sufficiently pure and cannot be used for further experiments such as loading and release of ONs.

Scanning electron microscopy

The synthesis of the silica cores and their functionalization with MPS was straightforward. The size of the cores used for the synthesis of the hollow NCs was roughly 85 nm and the NPs were uniform in size and spherical, as shown in Figure 38A. The MPS@SiO_2 NPs, in Figure 38B, were slightly bigger and the homogeneity was retained. In Figure 38C is shown the core/shell sample, most of which is homogenous in size (roughly 90 nm) but some bigger NPs are present (149 nm). The bimodal size distribution of DMAEMA-containing NPs in known in literature.[149] Figure 38D and 38E show the sample containing the hollow NCs.

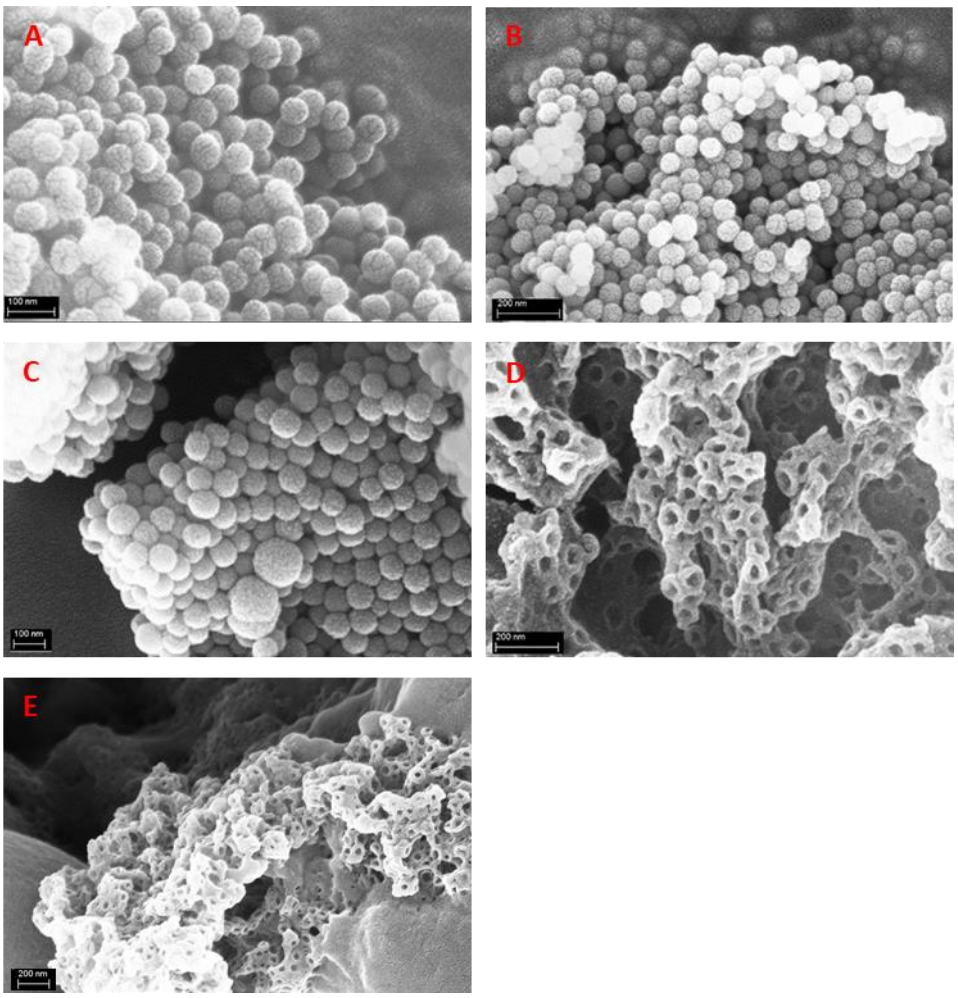

Figure 38: *SEM images of:* ***A.*** *SiO_2 cores;* ***B.*** *SiO_2@MPS NPs;* ***C.*** *SiO_2@P(DMAEMA-co-MMA-co-PEGMA-co-DVB-co-BAC);* ***D.*** *Sample containing Hollow P(DMAEMA-co-MMA-co-PEGMA-co-DVB-co-BAC);* ***E.*** *Detail of the sample in Figure 30E containing Hollow NCs and amorphous material.*

Although in Figure 38D only hollow NCs are present, in other areas of the samples amorphous material is present as well, as shown in Figure 38E.

Table 8 reports the sizes and the standard deviations of the NPs measured with SEM.

Table 8: *SEM measured diameter of the intermediates for the synthesis of hollow NCs for ON delivery via emulsion polymerization. The values represent mean ± standard deviation (n=50).*

Synthesis step	**Size standard ± deviation**
SiO_2 cores	84.7±6.2 nm
SiO_2@MPS	87.9±7.1 nm
SiO_2@P(DMAEMA-co-MMA-co-PEGMA-co-DVB-co-BAC)	89.0±7.2 nm
Hollow P(DMAEMA-co-MMA-co-PEGMA-co -DVB-co-BAC)	n.d.

Dynamic Light Scattering

DLS experiments were run in order to measure the hydrodynamic diameter and the ζ-potential of each synthesis intermediate, in Table 9 are reported the values.

Table 9: *Hydrodynamic diameter (D_h), polydispersity index (PDI) and ζ-potential of the synthesis intermediates of the hollow NCs for ON delivery.*

	D_h	PDI	ζ-potential
Silica cores	131.14 ± 1.00	0.118 ± 0.006	-44.32 ± 0.84
SiO2@MPS	122.05 ± 2.37	0.102 ± 0.017	-46.83 ± 1.46
Core/shell structures	178.21 ± 5.37	0.149 ± 0.020	-13.40 ± 1.63
Hollow NCs	n.d.		

Unlike the intermediates for the synthesis of the pH-sensitive and three-stimuli-sensitive hollow NCs, the intermediates of this DDS are not susceptible to dissolution in water and can therefore be analyzed with DLS. The polydispersity index (PDI) confirmed that the all the samples were monodisperse, which is a crucial parameter for drug delivery applications. The hydrodynamic diameter was below 200 nm as required for the EPR effect. Interestingly, the size of the silica cores is slightly bigger than the SiO_2@MPS NPs, which contradicts SEM results. This behavior can be justified considering that the SiO_2 spheres are probably more aggregation-prone than SiO_2@MPS, due to the functional groups of the surface, and even few aggregates can cause a clear increase in hydrodynamic diameter. The ζ-potential of the silica cores and the SiO_2@MPS was expected to be strongly negative as found. In regard to the core/shell NPs, the ζ-potential increased to -13.40 ± 1.63. This can be explained by considering that the shell monomers were chosen to be positively charged in water and the formation of the shell resulted in a partial quench of the negative ζ-potential of silica. After the removal of the cores, the ζ-potential was expected to become positive. Nevertheless, the DLS experiments were not run on the hollow NC containing sample (Figure 38D and 38E) because the presence of amorphous material did not allow reliable DLS measurement.

FT-IR

FT-IR was used for the structural characterization of NPs. In Figure 39A are presented the spectra of SiO_2 cores (a. black line), SiO_2@MPS (b. red line) and core/shell NPs (c. blue line). When the whole spectra are considered, no significant differences can be seen because of the strong peaks at 1055 and 752 cm^{-1}, which were respectively assigned to the Si–O–Si and Si–C stretching vibrations of the silica cores.[150] In Figure 39B the diagnostic areas are zoomed and the peaks to assess the success of the modifications are more evident. In particular, the peak at 1073 cm^{-1} of SiO2@MPS (b. red line) is assigned to the

C=O stretching absorption of MPS, confirming the functionalization of the cores. After the polymerization (c. blue line), the peak at 1703 cm^{-1} shifted to 1725 and became stronger: this effect can be explained by the overlap of the ester peaks of DMAEMA, PEGMA and MMA. In addition, the peaks at 2949 and 2906 cm^{-1} were attributed to $–CH_2$ symmetrical and anti-symmetrical stretching vibrations of the components of the shell.[151] The red line in Figure 39C represent the spectrum of the sample after the core removal procedure shown in Figure 39D and 39E. This spectrum was recorded and reported to provide an estimation of the chemical composition of the shell/amorphous material. Briefly, 1725 cm^{-1} was assigned to the ester stretching of DMAEMA, PEGMA and MMA; 1650 cm^{-1} and 1458 cm^{-1} were assigned to amide first band and second band of BAC; 1096 cm^{-1} was assigned to C-O-C ether asymmetrical stretching of PEGMA.

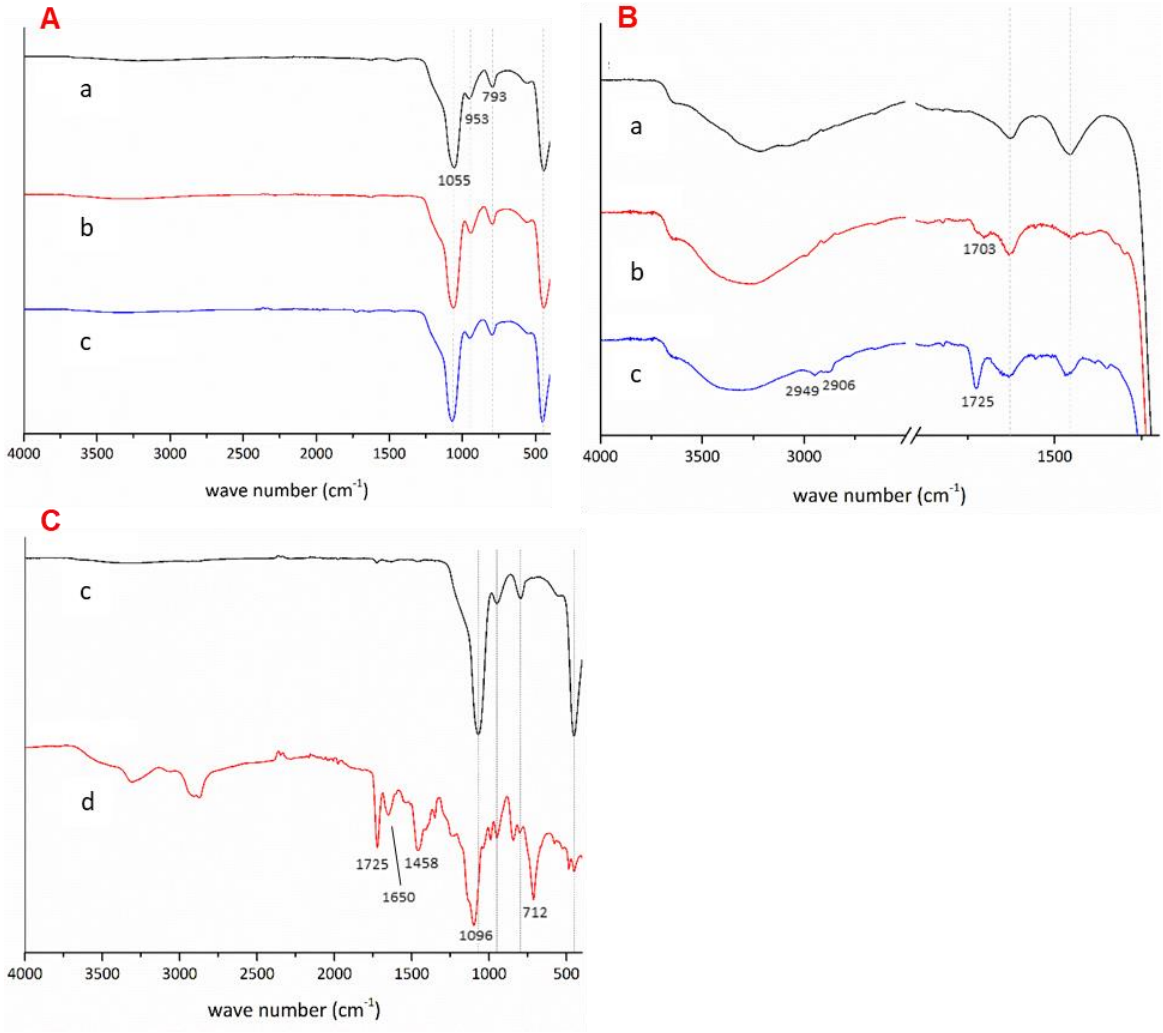

Figure 39: *FT-IR spectra of:* ***a.*** *SiO_2 cores;* ***b.*** *SiO_2@MPS NPs;* ***c.*** *SiO_2@P(DMAEMA-co-MMA-co-PEGMA-co-MBA-BAC);* ***d.*** *Sample containing Hollow P(DMAEMA-co-MMA-co-PEGMA-co-MBA-BAC).* ***A.*** *Full spectra;* ***B.*** *enlargements of the areas of interest of the spectra in Figure 39A (4000-2500 and 1800-1250 cm^{-1});* ***C.*** *comparison between the spectra of SiO_2@P(DMAEMA-co-MMA-co-PEGMA-co-MBA-BAC) (**c**) and the sample containing hollow NCs (**d**).*

EDX spectroscopy

This technique was used to identify all the atoms present in the various synthesis intermediates. When analyzing these images, it has to be considered that this technology gives qualitative results only, and therefore no quantification of the single atoms based on the height of the peaks can be made. In Figure 40A-B are shown the spectra of the silica cores and the MPS-modified silica cores, respectively. In both spectra Si, O and C are present (Au is used to sputter-coat the sample in order to make it conductive and suitable for SEM analysis, it is not part of the sample). Carbon in Figure 40A belong mainly to the to the carbon tape used to fix the sample on the SEM specimen stubs. In Figure 40B the presence of C was expected due to the MPS surface modification of the silica cores. In the core/sell NPs the Si, C and O amounts are so large that the presence of N (due to DMAEMA and BAC) and S (due to BAC) cannot be seen (Figure 40C). When the core was removed the peaks belonging to N and S became visible: N (not labeled) at 0.4 and S at 2.3 and 2.45, confirming that the shell/amorphous material includes these monomers (Figure 40D).

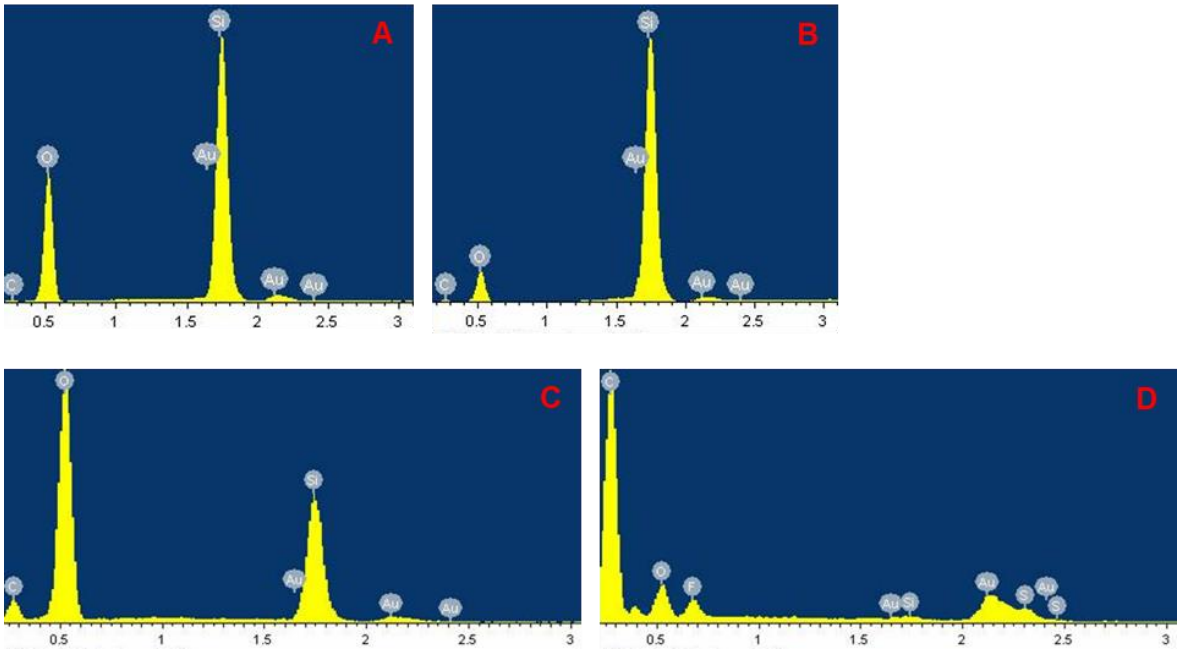

Figure 40: *EDX spectra of* ***A.*** *silica cores;* ***B.*** *SiO_2@MPS NPs;* ***C.*** *SiO_2@P(DMAEMA-co-MMA-co-PEGMA-co-MBA-BAC);* ***D.*** *Sample containing Hollow P(DMAEMA-co-MMA-co-PEGMA-co-MBA-BAC).*

6.3.3 Conclusion

Despite the several conditions tested, the hollow NCs for the delivery of ONs could not be obtained with emulsion polymerization. Firstly, the problem was thought to be in the core removal procedure, therefore some tests were run with different buffer concentrations (buffer 1:3 water, buffer 1:1 water, buffer 3:1 water or pure buffer) and varying the duration of the treatment (30 min, 1 h, 2 h, 4 h and 6 h). Nevertheless, the result can be summarized with two opposite situations: (1) the cores were not removed or (2) the core removal process

mostly destroyed the shells and the samples presented large portions of agglomerates of amorphous material (Figure 38E).

Since no selective core removal was observed, the attention was turned to the formation of the shell: the incapability of removing the cores without breaking the shell could indeed mean that the shell was not properly formed or that it was unstable. When considering the composition of the shell, it has to be pointed out that DMAEMA, on the one hand, tends to give very polydisperse samples when too concentrated. On the other hand, DMAEMA needs to be the main monomer to guarantee that the NCs display enough amino groups to efficiently interact with DNA. According to these limitations, some parameters were changed:

1. Concentration of DMAEMA
2. Ratio DMAEMA: MMA
3. Styrene as a substitute for MMA
4. Ratio BAC: DVB
5. Concentration of the initiator
6. AIBN as a substitute for KPS
7. Rate of addition of monomers
8. Presence of 2-butanone as a second solvent[140]
9. Presence of SDS as a surfactant
10. Duration of the reaction

The best conditions for the formation of the shell were assessed in terms of percentage of hollow NCs in the sample after the core removal procedure. The best results, reported above and described in the experimental section, were obtained with 70mM DMAEMA and with MAA as co-monomer. The ratios DMAEMA: MMA and BAC: DVB were 85:15 and 1:2, respectively. The concentration of the radical initiator potassium peroxide (KPS) was 5.6 mM and the monomers were added all together 15 minutes before adding the initiator. Neither SDS nor 2-propanone were used. In these conditions roughly 50% of the samples consisted of hollow NCs.

6.4 Hollow Nanocontainers obtained via Distillation- Precipitation Polymerization

The second approach to obtain the hollow NCs for the delivery of ONs relies on distillation-precipitation polymerization (DPP) technique. The design of the DDS was based on the employment of the same monomer described above: DMAEMA was used as the amino-bearing monomer and BAC as the redox-sensitive cross-linking agent. These monomers

had been already used for the successful formation of shells in DPP for the three-stimuli-sensitive NCs. Unfortunately, the results have been so far unsatisfactory and can be described with two opposite situations: (1) no shell formation has been observed or it was so thin that it broke under the conditions needed to remove the silica core, or (2) instead of forming the shell, the monomers used for DPP created cross-linked byproducts that were not disassembled with the core removal procedure.

6.4.1 Synthesis

The synthesis approach was very similar to the one reported for the NCs obtained with emulsion polymerization. Firstly, the SiO_2 sacrificial templates were prepared and modified with MPS, then the shell was synthesized on the cores. Lastly, the core removal was tried by stirring the NPs in a mixture of distilled water and HF/NH_4F pH 4.0 buffer. The scheme of the synthesis is shown in Figure 41.

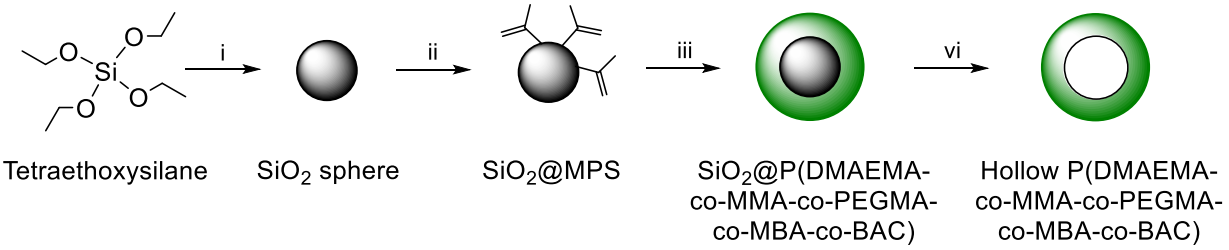

Figure 41: *Scheme of the synthesis of the hollow NCs for ON release: i) Stöber method: NH_3, EtOH, H_2O. ii) Synthesis of SiO_2@MPS: MPS, NH_3, EtOH, H_2O. iii) DPP: DMAEMA, MAA, PEGMA, BAC, MBA, AIBN, nitrogen bubbling in ACN 80°C→ 100°C. ii) Core removal: HF/NH_4F pH 4 buffer and water (1:1).*

1

6.4.2 Characterization

Scanning Electron Microscopy

Figure 42 shows the synthesis intermediates and products of the core removal procedure. Specifically, the silica cores and the SiO_2@MPS images are Figure 42A and 42B. The diameter of these NPs averaged 182 and 188 nm respectively and the samples were fairly monodisperse. Figure 42C and 42D represent the situation where no shell formation was observed and the core removal procedure yielded amorphous material only. On the contrary, Figure 42E shows the presence of byproducts that, after the removal of silica, become the sole species in the sample (Figure 42F). The size of the NPs is reported in Table 10.

Table 10: *SEM measured diameter of the intermediates for the synthesis of hollow NCs for ON delivery via distillation-precipitation polymerization. The values represent mean ± standard deviation (n=50).*

Synthesis step	**Size standard ± deviation**
SiO_2 cores	181.6±8.5 nm
SiO_2@MPS	187.7±10.3 nm
SiO_2@P(DMAEMA-co-MAA-co-PEGMA-co-MBA-co-BAC) in Figure 42C	196.3±9.7 nm
SiO_2@P(DMAEMA-co-MAA-co-PEGMA-co-MBA-co-BAC) in Figure 42E	210.4±12.3 nm

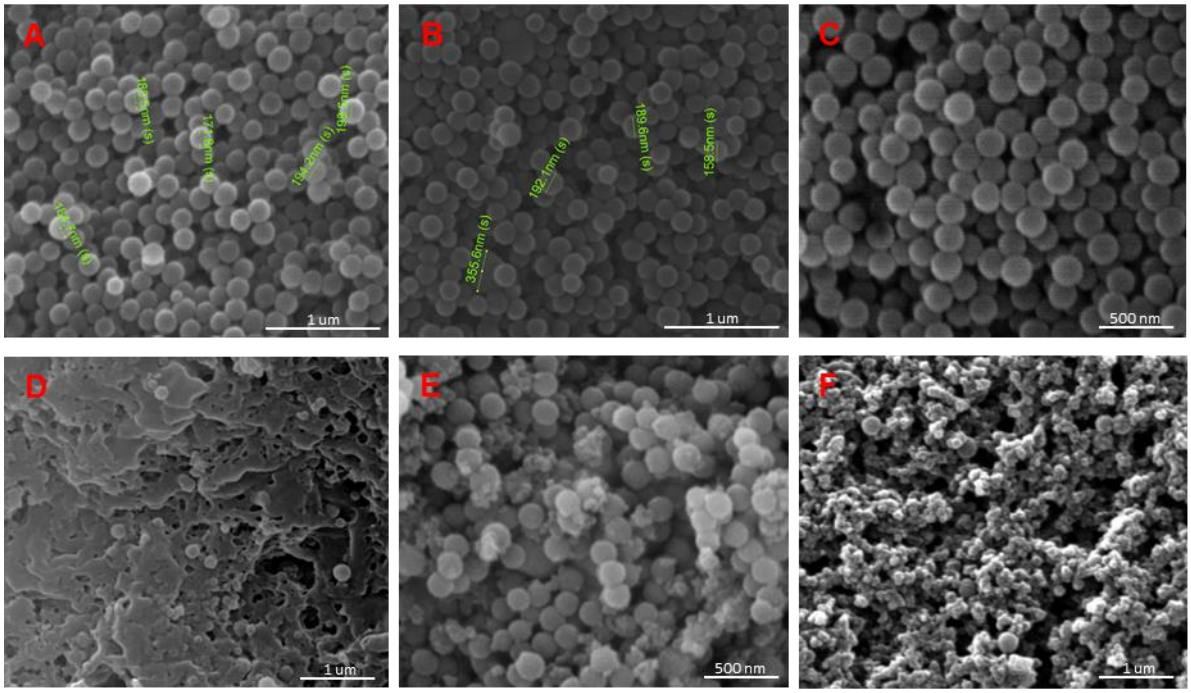

Figure 42: *SEM images of:* ***A.*** *SiO_2 cores;* ***B.*** *SiO_2@MPS NPs;* ***C.*** *SiO_2@P(DMAEMA-co-MAA-co-PEGMA-co-MBA-co-BAC) case 1;* ***D.*** *Core removal product of* ***C****;* ***E.*** *SiO_2@P(DMAEMA-co-MAA-co-PEGMA-co-MBA-co-BAC) case 2;* ***F.*** *Core removal product of* ***E****.*

6.4.3 Conclusion

The formation of the redox-responsive and positively-chargeable hollow NCs was not obtained with DPP. Again, several attempts have been carried out to date, by using different ratios and concentration of monomers. Inevitably, SEM images showed that either amorphous material or large amount of polymerization byproducts were obtained.

6.5 Conclusions and future prospective

Two main different strategies for the synthesis of hollow NCs for ONs have been studied to date. Unfortunately, despite the amount of trials and the considerable amount of variables

taken into account, it was not possible to produce a stable shell to be used for further experiments such as loading and release of ONs.

Nevertheless, a new procedure is being currently studied and will be tested soon. Since the choice of DMAEMA may be responsible for the failure of the previous strategies, the synthesis of another positively-chargeable monomer, N-(2-aminoethyl)methacrylamide, is being considered. This monomer should represent a suitable alternative to DMAEMA, since it bears a primary amino moiety, which will protonate under physiological conditions. Once obtained, it will be used as the main monomer for the formation of the shell via DPP. Except for the replacement of DMAEMA with N-(2-aminoethyl) methacrylamide, the synthesis of the positively charged DDS will follow the procedures described above (Figure 41).
The synthesis pathway for the new monomer is presented in Figure 43, and it consists of two steps: an amidation via acyl chloride, followed by the removal of the tert-butyloxycarbonyl protecting group (BOC). The first reaction is well-known in literature,[152] while the second step can be easily achieved by treating *tert*-butyl (2-mthacrlyamidoethyl) carbamate with trifluoroacetic acid in excess in a suitable solvent.

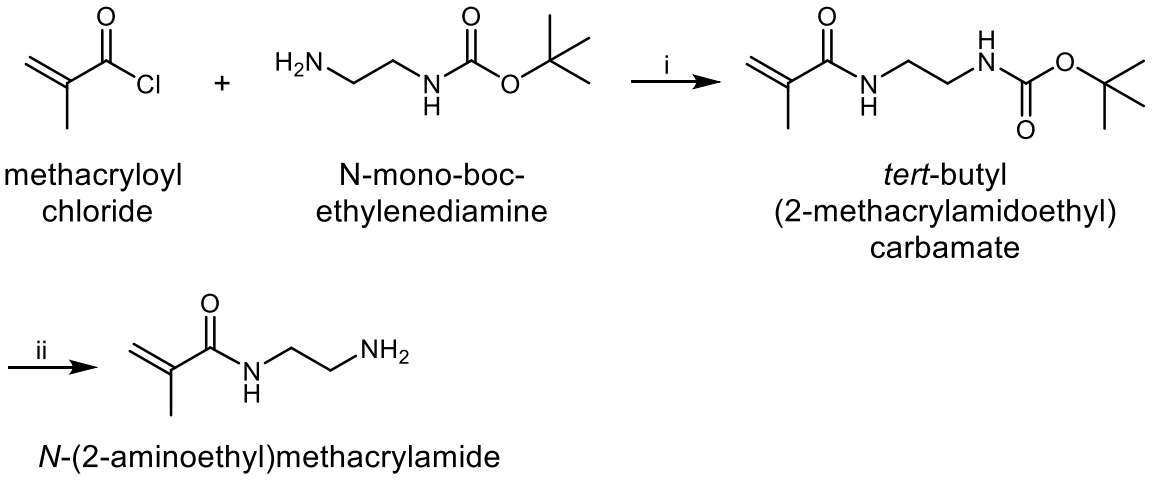

Figure 43: *Synthesis approach for obtaining N-(2-aminoethyl)methacrylamide. i) amidation through acyl chloride and ii) BOC removal.*

Conclusions

The work of the Ph.D. candidate was focused on the study of the properties of DDSs to improve current cancer therapy. Several drugs were tested and encapsulated in the systems to study the release profiles of the resulting formulations.

The first project was the synthesis of two DDSs to encapsulate and release DNR, among the most effective chemotherapy agents available. The first system was a hollow pH-sensitive NC, made of a single shell responsible for the pH sensitivity. The second system, more complex and advanced in its ability to deliver DNR under pre-set tumoral conditions, was a hollow three-stimuli sensitive NCs, responsive to pH, redox condition and temperature variations. Both systems showed promising results in terms of stimuli-dependent and sustained release. The pH-sensitive system showed excellent loading and release ability confirmed with *in vitro* drug release experiments. The release kinetics of this system are being currently analyzed with a mathematical model in collaboration with CNR in Rome. The goal of this part of the project is to give a more detailed insight into the roles of the bounds involved in the drug release under different pH conditions. The three-stimuli-sensitive NCs showed remarkable anti-cancer activity and the results were published in a peer-reviewed journal. The *in vitro* drug release experiments, the cytotoxicity assays on tumoral cells and intracellular localization of the released DNR confirmed the efficacy of the formulation, which can be considered a promising platform for targeted release of anthracyclines.

A second project, run in collaboration with CNR in Bologna and the spin-off company Lipinutragen (Bologna), concerned the release of the cyclic peptide SST. This molecule has enormous therapeutic potential, but its half-life in plasma is too short and would enormously benefit from DDSs capable of prolonging it. In this context of collaboration, two different systems were studied for the encapsulation and release of SST. The first one was the pH-sensitive NC described for DNR, which was able to release the peptide in a pH-dependent manner without affecting the structure. The second DDS was a NE formulation, prepared and characterized in the premises of CNR (Bologna). This formulation was shown, both in buffer and in human plasma, to largely extend the half-life of the peptide by reducing the degradation rate. Also, under certain conditions the NE was shown to release the peptide in a prolonged manner. Both systems gave encouraging results and can be considered as long-circulating depot of SST, capable of improving the short half-life of the peptide.

As a partner of the ClickGene network, one of the core goals of the Ph.D. work was the encapsulation and selective release of the Cu(II)-based AMNs synthesized by the dr. A. Kellett's group in DCU, Dublin. The student was firstly involved in the EPR characterization of the Cu complexes in solution. Cw-EPR and advanced EPR measurements were run in NCSR Demokritos, the results of which were included in a paper recently published. Secondly, the pH-sensitive NCs were used for the encapsulation and release of Cu-TPMA-Phen, one of the Cu(II) complex. The system was able to encapsulate and release the drug efficiently in response to tumor microenvironment without affecting the structure of the molecule, fundamental to the activity, and the intracellular localization. The results obtained have recently been accepted for publication in an international peer-reviewed journal.

Lastly, the synthesis of a novel DDS for the encapsulation and release of ONs were studied. Unfortunately, despite the amount of trials and the considerable number of variables taken into consideration, it was not possible to produce a stable shell to be used for further experiments such as loading and release of ONs. Two different approach were tried, the first based on the emulsion polymerization and the second on distillation precipitation polymerization, but none of them gave the expected results. Nevertheless, a new procedure is being currently studied which involves the synthesis of a suitable monomer to be employed in distillation precipitation polymerization.

As a whole, the Ph.D. work and this thesis concerned the stimuli-sensitive drug delivery of many different kinds of chemotherapeutics. The systems and the resulting drug-loaded forms showed interesting results and can be overall considered as a small step forward in the field of delivery of chemotherapy drugs.

References

[1] F. Bray, J. Ferlay, I. Soerjomataram, R. L. Siegel, L. A. Torre, A. Jemal, *CA. Cancer J. Clin.* **n.d.**, *0*, DOI 10.3322/caac.21492.

[2] C. Moorthi, R. Manavalan, K. Kathiresan, *J. Pharm. Pharm. Sci.* **2011**, *14*, 67–77.

[3] A. A. Stavrovskaya, *Biochem.* **2000**, *65*, 112–126.

[4] S. D. Steichen, M. Caldorera-Moore, N. A. Peppas, *Eur. J. Pharm. Sci.* **2013**, *48*, 416–427.

[5] M. W. Tibbitt, J. E. Dahlman, R. Langer, *J. Am. Chem. Soc.* **2016**, *138*, 704–717.

[6] J. Gautier, E. Munnier, a. Paillard, K. Hervé, L. Douziech-Eyrolles, M. Soucé, P. Dubois, I. Chourpa, *Int. J. Pharm.* **2012**, *423*, 16–25.

[7] D. Peer, J. M. Karp, S. Hong, O. C. Farokhzad, R. Margalit, R. Langer, *Nat. Nanotechnol.* **2007**, *2*, 751–760.

[8] R. Baxter, N. Hastings, A. Law, E. J. . Glass, *Anim. Genet.* **2008**, *39*, 561–563.

[9] W. B. Liechty, N. A. Peppas, *Eur. J. Pharm. Biopharm.* **2012**, *80*, 241–246.

[10] R. Gref, Y. Minamitake, M. T. Peracchia, V. Trubetskoy, V. Torchilin, R. Langer, *Science (80-.).* **1994**, *263*, 1600–1603.

[11] M. L. Immordino, F. Dosio, L. Cattel, *Int. J. Nanomedicine* **2006**, *1*, 297–315.

[12] H. Maeda, *Adv. Enzyme Regul.* **2001**, *41*, 189–207.

[13] T. M. Allen, P. R. Cullis, *Adv. Drug Deliv. Rev.* **2013**, *65*, 36–48.

[14] J. Fang, H. Nakamura, H. Maeda, *Adv. Drug Deliv. Rev.* **2011**, *63*, 136–151.

[15] L. Brannon-Peppas, J. O. Blanchette, *Adv. Drug Deliv. Rev.* **2012**, *64*, 206–212.

[16] R. R. Sawant, V. P. Torchilin, *AAPS J.* **2012**, *14*, 303–315.

[17] J. Nicolas, S. Mura, D. Brambilla, N. Mackiewicz, P. Couvreur, *Chem. Soc. Rev.* **2013**, *42*, 1147–235.

[18] D. Pan, J. L. Turner, K. L. Wooley, **2003**, *1*, 2400–2401.

[19] V. P. Torchilin, *Nat. Rev. Drug Discov.* **2005**, *4*, 145–160.

[20] A. Yaqoob Khan, S. Talegaonkar, Z. Iqbal, F. Jalees Ahmed, R. Krishan Khar, *Curr. Drug Deliv.* **2006**, *3*, 429–443.

[21] T. G. Mason, J. N. Wilking, K. Meleson, C. B. Chang, S. M. Graves, *J. Phys. Condens. Matter* **2006**, *18*, R635.

[22] J. M. Gutiérrez, C. González, A. Maestro, I. Solè, C. M. Pey, J. Nolla, *Curr. Opin. Colloid Interface Sci.* **2008**, *13*, 245–251.

[23] N. Sharma, M. Bansal, S. Visht, P. Sharma, G. Kulkarni, *Chronicles Young Sci.* **2010**, *1*, 2–6.

[24] T. K. Vyas, A. Shahiwala, M. M. Amiji, *Int. J. Pharm.* **2008**, *347*, 93–101.

[25] C. Y. Zhang, Y. Q. Yang, T. X. Huang, B. Zhao, X. D. Guo, J. F. Wang, L. J. Zhang, *Biomaterials* **2012**, *33*, 6273–6283.

[26] A. Gothwal, I. Khan, U. Gupta, *Pharm. Res.* **2016**, *33*, 18–39.

[27] G. S. Kwon, K. Kataoka, *Adv. Drug Deliv. Rev.* **1995**, *16*, 295–309.

[28] V. Mohanraj, Y. Chen, *Trop. J. Pharm. Res.* **2006**, *5*, 561–573.

[29] S. Mura, J. Nicolas, P. Couvreur, *Nat. Mater.* **2013**, *12*, 991–1003.

[30] L. A. Tziveleka, P. Bilalis, A. Chatzipavlidis, N. Boukos, G. Kordas, *Macromol. Biosci.* **2014**, *14*, 131–141.

[31] A.-F. Metaxa, E. K. Efthimiadou, G. Kordas, *Mater. Lett.* **2014**, *132*, 432–435.

[32] R. Cheng, F. Meng, C. Deng, H.-A. Klok, Z. Zhong, *Biomaterials* **2013**, *34*, 3647–3657.

[33] H. Y. Yang, M.-S. Jang, G. H. Gao, J. H. Lee, D. S. Lee, *Construction of Redox/PH Dual Stimuli-Responsive PEGylated Polymeric Micelles for Intracellular Doxorubicin Delivery in Liver Cancer*, **2016**.

[34] L. Liu, P. Du, X. Zhao, J. Zeng, P. Liu, *Eur. Polym. J.* **2015**, *69*, 540–551.

[35] G. Toniolo, E. K. Efthimiadou, G. Kordas, C. Chatgilialoglu, *Sci. Rep.* **2018**, *8*, 14704.

[36] X. Yang, L. Chen, B. Huang, F. Bai, X. Yang, *Polymer (Guildf).* **2009**, *50*, 3556–3563.

[37] X. Zhang, Y. Lin, R. J. Gillies, *J. Nucl. Med.* **2010**, *51*, 1167–70.

[38] C. Tapeinos, E. K. Efthimiadou, N. Boukos, C. A. Charitidis, M. Koklioti, G. Kordas, *J. Mater. Chem. B* **2010**, *4*, 1166–1169.

[39] S. Ganta, H. Devalapally, A. Shahiwala, M. Amiji, *J. Control. Release* **2008**, *126*, 187–204.

[40] Schmaljohann D, *Adv. Drug Deliv. Rev.* **2006**, *58*, 1655–1670.

[41] C. S. S. R. Kumar, F. Mohammad, **2011**, *63*, 789–808.

[42] P. Bilalis, A. Chatzipavlidis, L.-A. Tziveleka, N. Boukos, G. Kordas, *J. Mater. Chem.* **2012**, *22*, 13451–13454.

[43] H. Wei, S. X. Cheng, X. Z. Zhang, R. X. Zhuo, *Prog. Polym. Sci.* **2009**, *34*, 893–910.

[44] G. L. Li, L. Q. Xu, X. Tang, K. G. Neoh, E. T. Kang, *Macromolecules* **2010**, *43*, 5797–5803.

[45] S. H. Cho, M. S. Jhon, S. Hong Yuk, *Eur. Polym. J.* **1999**, *35*, 1841–1845.

[46] F. Meng, W. E. Hennink, Z. Zhong, *Biomaterials* **2009**, *30*, 2180–2198.

[47] M. Huo, J. Yuan, L. Tao, Y. Wei, *Polym. Chem.* **2014**, *5*, 1519.

[48] P. Kuppusamy, M. Afeworki, R. A. Shankar, D. Coffin, M. C. Krishna, S. M. Hahn, J. B. Mitchell, J. L. Zweier, *Cancer Res.* **1998**, *58*, 1562–1568.

[49] P. Kuppusamy, H. Li, G. Ilangovan, A. J. Cardounel, J. L. Zweier, K. Yamada, M. C. Krishna, J. B. Mitchell, *Cancer Res.* **2002**, *62*, 307–312.

[50] E. Fleige, M. a. Quadir, R. Haag, *Adv. Drug Deliv. Rev.* **2012**, *64*, 866–884.

[51] H. Xu, W. Cao, X. Zhang, *Acc. Chem. Res.* **2013**, *46*, 1647–1658.

[52] H. F. Gilbert, *Methods Enzymol.* **1995**, *251*, 8–28.

[53] E. Cabane, X. Zhang, K. Langowska, C. G. Palivan, W. Meier, *Biointerphases* **2012**, *7*, 9.

[54] M. L. Viger, W. Sheng, K. Doré, A. H. Alhasan, C.-J. Carling, J. Lux, C. de Gracia Lux, M. Grossman, R. Malinow, A. Almutairi, *ACS Nano* **2014**, *8*, 4815–4826.

[55] R. Tong, J. Cheng, *Macromolecules* **2012**, *45*, 2225–2232.

[56] J. Babin, M. Lepage, Y. Zhao, *Macromolecules* **2008**, *41*, 1246–1253.

[57] C. Sun, J. S. H. Lee, M. Zhang, *Adv. Drug Deliv. Rev.* **2008**, *60*, 1252–1265.

[58] M. Arruebo, R. Fernández-pacheco, M. R. Ibarra, J. Santamaría, *Rev. Lit. Arts Am.* **2007**, *2*, 22–32.

[59] S. Purushotham, P. E. J. Chang, H. Rumpel, I. H. C. Kee, R. T. H. Ng, P. K. H. Chow, C. K. Tan, R. V Ramanujan, *Nanotechnology* **2009**, *20*, 305101.

[60] A. Wadajkar, J. Menon, T. Kadapure, R. T. Tran, J. Yang, K. T. Nguyen, *Recent Pat Biomed Eng* **2013**, *6*, 47–57.

[61] D. A. Gewirtz, *Biochem. Pharmacol.* **1999**, *57*, 727–741.

[62] G. Minotti, P. Menna, E. Salvatorelli, G. Cairo, L. Gianni, *Pharmacol. Rev.* **2004**, *56*, 185–229.

[63] L. H. Hurley, *Nat. Rev. Cancer* **2002**, *2*, 188–200.

[64] G. Aubel-Sadron, D. Londos-Gagliardi, *Biochimie* **1984**, *66*, 333–352.

[65] A. Di Marco, F. Arcamone, F. Zunino, in *Mech. Action Antimicrob. Antitumor Agents* (Eds.: J.W. Corcoran, F.E. Hahn, J.F. Snell, K.L. Arora), Springer Berlin Heidelberg, Berlin, Heidelberg, **1975**, pp. 101–128.

[66] X. Wei, R. Cohen, Y. Barenholz, *Eur. J. Pharm. Biopharm.* **2016**, *104*, 260–270.

[67] G. L. Li, H. Möhwald, D. G. Shchukin, *Chem. Soc. Rev.* **2013**, *42*, 3628–46.

[68] X. J. Kang, Y. L. Dai, P. A. Ma, D. M. Yang, C. X. Li, Z. Y. Hou, Z. Y. Cheng, J. Lin, *Chem. - A Eur. J.* **2012**, *18*, 15676–15682.

[69] T. Mosmann, *J. Immunol. Methods* **1983**, *65*, 55–63.

[70] Y. Qiu, K. Park, *Adv. Drug Deliv. Rev.* **2012**, *64*, 49–60.

[71] K. Zhang, Y. Luo, Z. Li, *Soft Mater.* **2007**, *5*, 183–195.

[72] P. Bilalis, N. Boukos, G. C. Kordas, *Mater. Lett.* **2012**, *67*, 180–183.

[73] F. Bai, B. Huang, X. Yang, W. Huang, *Eur. Polym. J.* **2007**, *43*, 3923–3932.

[74] D. Qi, F. Bai, X. Yang, W. Huang, *Eur. Polym. J.* **2005**, *41*, 2320–2328.

[75] A. F. Metaxa, E. K. Efthimiadou, N. Boukos, G. Kordas, *J. Colloid Interface Sci.* **2012**, *384*, 198–206.

[76] R. Kiraly, R. B. Martin, *Inorganica Chim. Acta* **1982**, *67*, 13–18.

[77] A. Klaikherd, C. Nagamani, S. Thayumanavan, *J. Am. Chem. Soc.* **2009**, *131*, 4830–4838.

[78] E. K. Efthimiadou, C. Tapeinos, A. Chatzipavlidis, N. Boukos, E. Fragogeorgi, L.

Palamaris, G. Loudos, G. Kordas, *Int. J. Pharm.* **2014**, *461*, 54–63.

[79] H. Cho, J. Bae, V. K. Garripelli, J. M. Anderson, H.-W. Jun, S. Jo, *Chem. Commun.* **2012**, *48*, 6043.

[80] F. Feng, R. Li, Q. Zhang, Y. Wang, X. Yang, H. Duan, X. Yang, *Polym. (United Kingdom)* **2014**, *55*, 110–118.

[81] C. Yanfeng, Y. Min, *Radiat. Phys. Chem.* **2001**, *61*, 65–68.

[82] F. a. Plamper, M. Ruppel, A. Schmalz, O. Borisov, M. Ballauff, A. H. E. Müller, *Macromolecules* **2007**, *40*, 8361–8366.

[83] Y.-J. Pan, Y.-Y. Chen, D.-R. Wang, C. Wei, J. Guo, D.-R. Lu, C.-C. Chu, C.-C. Wang, *Biomaterials* **2012**, *33*, 6570–6579.

[84] M. Ikebuchi, A. Kashiwagi, T. Asahina, Y. Tanaka, Y. Takagi, Y. Nishio, H. Hidaka, R. Kikkawa, Y. Shigeta, *Metabolism* **1993**, *42*, 1121–1126.

[85] G. Weckbecker, F. Raulf, B. Stolz, C. Bruns, *Pharmac. Ther.* **1994**, *60*, 245–264.

[86] Y. C. Patel, *Front. Neuroendocrinol.* **1999**, *20*, 157–198.

[87] K. B. Ain, K. D. Taylor, S. Tofiq, G. Venkataraman, *J Clin Endocrinol Metab* **1997**, *82*, 1857–62.

[88] C. Scarpignato, I. Pelosini, *Chemotherapy* **2001**, *47 Suppl 2*, 1–29.

[89] B. M. Evers, D. Parekh, C. M. Townsend, J. C. Thompson, *Ann. Surg.* **1991**, *213*, 190–8.

[90] M. Körner, J. C. Reubi, *Peptides* **2007**, *28*, 419–425.

[91] H. Reithmeier, J. Herrmann, A. Göpferich, *Int. J. Pharm.* **2001**, *218*, 133–143.

[92] C. Damgé, J. Vonderscher, P. Marbach, M. Pinget, *J. Pharm. Pharmacol.* **1997**, *49*, 949–54.

[93] R. Boöttger, R. Hoffmann, D. Knappe, *PLoS One* **2017**, *12*, 1–15.

[94] N. Greenfield, *Nat Protoc.* **2007**, *1*, 2876–2890.

[95] N. J. Greenfield, *TrAC - Trends Anal. Chem.* **1999**, *18*, 236–244.

[96] W. Wang, *Int. J. Pharm.* **2005**, *289*, 1–30.

[97] B. R. Diel, E. Schneider, H. J. Quabbe, **1977**, *15*, 669–677.

[98] S. M. Kelly, T. J. Jess, N. C. Price, *Biochim. Biophys. Acta - Proteins Proteomics* **2005**, *1751*, 119–139.

[99] Z. Gu, A. Biswas, M. Zhao, Y. Tang, *Chem. Soc. Rev.* **2011**, *40*, 3638–3655.

[100] S. Martins, B. Sarmento, D. C. Ferreira, E. B. Souto, *Int. J. Nanomedicine* **2007**, *2*, 595–607.

[101] B. J. Bruno, G. D. Miller, C. S. Lim, *October* **2008**, *141*, 520–529.

[102] D. S. Pisal, M. P. Kosloski, S. V. Balu-Iyler, *J. Pharm. Sci.* **2010**, *99*, 2557–2575.

[103] C.-K. Kim, Y.-J. Cho, Z.-G. Gao, *J. Control. Release* **2001**, *70*, 149–155.

[104] J. G. Wagner, E. S. Gerard, D. G. Kaiser, *Clin. Pharmacol. Ther.* **n.d.**, *7*, 610–619.

[105] M. Jaiswal, R. Dudhe, P. K. Sharma, *3 Biotech* **2015**, *5*, 123–127.

[106] N. Zuin Fantoni, Z. Molphy, C. Slator, G. Menounou, G. Toniolo, G. Mitrikas, V. McKee, C. Chatgilialoglu, A. Kellett, *Chem. – A Eur. J.* **n.d.**, *0*, DOI 10.1002/chem.201804084.

[107] M. Pitié, G. Pratviel, *Chem. Rev.* **2010**, *110*, 1018–1059.

[108] R. Larragy, J. Fitzgerald, A. Prisecaru, V. McKee, P. Leonard, A. Kellett, *Chem. Commun.* **2015**, *51*, 12908–12911.

[109] A. C. Komor, J. K. Barton, *Chem. Commun.* **2013**, *49*, 3617–3630.

[110] D. S. Sigman, D. R. Graham, V. D. Aurora, A. M. Stern, D. Aurora, *J. Biol. Chem.* **1979**, *254*, 12269–12272.

[111] M. Pitié, B. Sudres, B. Meunier, *Chem. Commun.* **1998**, 2597–2598.

[112] M. Pitié, B. Meunier, *Bioconjug. Chem.* **1998**, *9*, 604–611.

[113] G. Kokoszka, K. D. Karlin, F. Padula, J. Baranowski, C. Goldstein, *Inorg. Chem.* **1984**, *23*, 4378–4380.

[114] F. Jiang, K. D. Karlin, J. Peisach, *Inorg. Chem.* **1993**, *32*, 2576–2582.

[115] Z. Lu, C. Y. Duan, Y. P. Tian, X. Z. You, X. Y. Huang, *Inorg. Chem.* **1996**, *35*, 2253–2258.

[116] A. Hazell, *Polyhedron* **2004**, *23*, 2081–2083.

[117] B. J. Hathaway, D. E. Billing, *Coord. Chem. Rev.* **1970**, *5*, 143–207.

[118] R. A. Peralta, A. J. Bortoluzzi, B. de Souza, R. Jovito, F. R. Xavier, R. A. A. Couto, A. Casellato, F. Nome, A. Dick, L. R. Gahan, et al., *Inorg. Chem.* **2010**, *49*, 11421–11438.

[119] F. R. Xavier, A. Neves, A. Casellato, R. A. Peralta, A. J. Bortoluzzi, B. Szpoganicz, P. C. Severino, H. Terenzi, Z. Tomkowicz, S. Ostrovsky, et al., *Inorg. Chem.* **2009**, *48*, 7905–7921.

[120] G. Toniolo, M. Louka, G. Menounou, N. Z. Fantoni, G. Mitrikas, E. K. Efthimiadou, A. Masi, M. Bortolotti, L. Polito, A. Bolognesi, et al., *ACS Omega* **2018**, *3*, 15952–15965.

[121] F. Jiang, K. D. Karlin, J. Peisach, *Inorg. Chem.* **1993**, *32*, 2576–2582.

[122] T. Fund, **1984**, 4378–4380.

[123] K. J. Kauffman, M. J. Webber, D. G. Anderson, *J. Control. Release* **2016**, *240*, 227–234.

[124] R. L. Juliano, *Nucleic Acids Res.* **2016**, *44*, 6518–6548.

[125] D. B. Rozema, *The Chemistry of Oligonucleotide Delivery*, Elsevier Inc., **2017**.

[126] A. D. Keefe, S. Pai, A. Ellington, *Nat. Rev. Drug Discov.* **2010**, *9*, 537–550.

[127] T. Kaisho, S. Sato, H. Sanjo, K. Takeda, S. Akira, *Nature* **2000**, *408*, 5–10.

[128] M. A. Havens, M. L. Hastings, *Nucleic Acids Res.* **2016**, *44*, 6549–6563.

[129] J. Zhao, S.-S. Feng, *Nanomedicine (Lond).* **2015**, *10*, 2199–228.

[130] F.-S. Du, Y. Wang, R. Zhang, Z.-C. Li, *Soft Matter* **2010**, *6*, 835.

[131] C. J. Bishop, K. L. Kozielski, J. J. Green, *J. Control. Release* **2015**, *219*, 488–499.

[132] S. Agarwal, Y. Zhang, S. Maji, A. Greiner, *Mater. Today* **2012**, *15*, 388–393.

[133] N. Murthy, J. R. Robichaud, D. A. Tirrell, P. S. Stayton, A. S. Hoffman, *J. Control. Release* **1999**, *61*, 137–143.

[134] Y. Huang, J. E. Pemberton, *Colloids Surfaces A Physicochem. Eng. Asp.* **2010**, *360*, 175–183.

[135] S. K. Park, K. Do Kim, H. T. Kim, *Colloids Surfaces A Physicochem. Eng. Asp.* **2002**, *197*, 7–17.

[136] L. L. Hench, J. K. West, *Chem. Rev.* **1990**, *90*, 33–72.

[137] I. a. M. Ibrahim, a. a. F. Zikry, M. a. Sharaf, *J. Am. Sci.* **2010**, *6*, 985–989.

[138] R. J. P. Corriu, D. Leclercq, *Angew. Chemie-International Ed. English* **1996**, *35*, 1420–1436.

[139] A. Liberman, M. Natalie, W. C. Trogler, A. C. Kummel, *Surf Sci Rep.* **2014**, *69*, 132–138.

[140] Y. Hu, J. Wang, H. Zhang, G. Jiang, C. Kan, *Mater. Sci. Eng. C* **2014**, *45*, 1–7.

[141] J. Shen, J. Xu, Y. Hu, J. Sun, L. Li, C. Kan, *Chinese J. Polym. Sci.* **2016**, *34*, 1240–1250.

[142] P. C. Oliveira, A. Guimarães, J.-Y. Cavaillé, L. Chazeau, R. G. Gilbert, A. M. Santos, *Polymer (Guildf).* **2005**, *46*, 1105–1111.

[143] H. Hillaireau, P. Couvreur, *J. Drug Deliv. Sci. Technol.* **2009**, *19*, 385–390.

[144] H. Hu, H. Wang, Q. Du, *Soft Matter* **2012**, *8*, 6816.

[145] C. S. Chern, *Prog. Polym. Sci.* **2006**, *31*, 443–486.

[146] A. R. Goodall, M. C. Wilkinson, J. Hearn, *J. Polym. Sci. Polym. Chem. Ed.* **n.d.**, *15*, 2193–2218.

[147] K. Tauer, R. Deckwer, I. Kühn, C. Schellenberg, *Colloid Polym. Sci.* **1999**, *277*, 607–626.

[148] N. I. Prokopov, I. A. Gritskova, O. P. Kiryutina, M. Khaddazh, K. Tauer, S. Kozempel, *Polym. Sci. Ser. B* **2010**, *52*, 339–345.

[149] L. Deng, Y. Zhai, S. Guo, F. Jin, Z. Xie, X. He, A. Dong, *J. Nanoparticle Res.* **2009**, *11*, 365–374.

[150] A. Beganskiene, V. Sirutkaitis, M. Kurtinaitiene, R. Juskenas, A. Kareiva, *Mater. Sci.* **2004**, *10*, 287–290.

[151] Y. Tang, Y. Yao, T. Zhu, Y. Huang, H. Chen, Y. Wang, H. Mi, *New J. Chem.* **2016**, *40*, 10545–10553.

[152] J. Zou, S. Zhang, R. Shrestha, K. Seetho, C. L. Donley, K. L. Wooley, *Polym. Chem.* **2012**, *3*, 3146–3156.